The Dissertation Committee for Praveenkumar Pasupathy Certifies that this is the approved version of the following dissertation:

Coupled Passive Resonant Circuits as Battery-free Wireless Sensors

Committee:

Dean P. Neikirk, Supervisor

Sharon L. Wood

Aristotle Arapostathis

Arjang Hassibi

Ananth Dodabalapur

Coupled Passive Resonant Circuits as Battery-free Wireless Sensors

by

Praveenkumar Pasupathy, B.E.; M.S.E

Dissertation

Presented to the Faculty of the Graduate School of

The University of Texas at Austin

in Partial Fulfillment

of the Requirements

for the Degree of

Doctor of Philosophy

The University of Texas at Austin

May, 2010

Dedication

for Amma, Appa and Sanath

Acknowledgements

I am indebted to Dr. Dean Neikirk for his guidance and support through graduate school. He has been an excellent advisor and a mentor. I hope to continue enjoying our many discussions on a seemingly endless list of subjects.

I am grateful to Dr. Sharon Wood and her group at the Ferguson Structural Engineering Laboratory. She is highly accommodating my rather erratic schedule. Thanks for providing the concrete answers.

I thank my committee members Dr. Aristotle Arapostathis, Dr. Ananth Dodabalapur and Dr. Arjang Hassibi for having taken the time to serve and guide me through my dissertation which.

I thank the researchers from both groups who worked on this project before and with me. Also thanks to all the members of Team Neikirk for the sharing the time spent in lab and their goodwill.

Thanks to Akshay Prabhu, Erik Pankratz, Shasi Munukutla, and Chris Lombardo for their company and invaluable help.

I am especially thankful to Melissa, for putting up with me and sharing my truly insane life.

I am eternally indebted thank my parents and my brother who have made sacrifices, given me encouragement, the means and the luxury of doing things it in my own way.

.

Coupled Passive Resonant Circuits as Battery-free Wireless Sensor

Publication No._____

Praveenkumar Pasupathy, Ph.D.

The University of Texas at Austin, 2010

Supervisor: Dean P. Neikirk

Detection and monitoring of the damage created by the corrosion of the steel reinforcement in concrete structures is a challenging and multidisciplinary problem. Economical monitoring strategy that is long-term and nondestructive requires low-cost, battery-free, wireless sensors. Our Electronic Structural Surveillance (ESS) platform uses battery-free passive resonant circuit (tag) as a sensor. The tag is magnetically coupled to an external reader coil. It is interrogated/read remotely in a non-contact (wireless) manner and the state of the sensor is determined from a swept frequency impedance measurement. When paired with the correct sensing element (transducer), the tag can be used for a variety of sensing applications for example, chemical & biochemical sensors. A circuit model of the reader and tag for such a universal battery-free wireless sensor platform is developed. The interaction between design and detection limit is examined. The dependence of the measured signal strength and read range on the various reader and tag circuit parameters is analyzed. Since the values of the circuit of the coils are dependent on their geometries, the effect of specific coil geometry is evaluated and design recommendations are made.

Table of Contents

List of Tables

List of Figures

Chapter 1 Introduction

1.1 INTRODUCTION

Civil engineering structures are built for long life times, on the order of multiple decades, making them amongst the few human made objects that have stood the test of time. Bridges and roads, railways and ports, buildings and dams form the infrastructure without which present day lifestyles would be impossible. In addition to being constantly utilized, many of them are subject to harsh corrosive environments and in some cases acute events such as earthquakes. All these could contribute to interruptions in infrastructure availability and in catastrophic cases, loss of life.

Monitoring these structures provides valuable information about its state or "health" [1]. This Structural Health Monitoring (SHM) provides information on the extent of damage and could be used to remedy the afflicted structures. The size, number of structures, and the multiple deterioration mechanisms involved make SHM a complex task. Thus structural health monitoring has developed into a field of its own, borrowing expertise from various disciplines of engineering.

1.2 SCALE OF CORROSION IN INFRASTRUCTURE (ECONOMIC COSTS)

A two year study conducted from 1999-2001, released by the Federal Highway Administration (FHWA), estimates the direct annual costs from metallic corrosion in the U.S. as a 276 billion dollar (USD-$) problem [2]. This cost amounts to 3.15% of the 1998 U.S. Gross Domestic Product (GDP) of $8790 billion. A conservative estimate of the total cost, both direct and indirect, could be as high as 6% of the GDP. The direct costs

were assessed for five industry sectors: infrastructure, utilities, transportation, production, manufacturing, and government.

The infrastructure sector alone has 4 million miles of highways, railroad and waterways, 500,000 miles of oil and gas pipelines, 8.5 million tanks for hazardous materials storage and 18,000 airports. The analysis for this sector puts the estimated direct annual cost at $22.6 billion. Of the 586,000 bridges under this sector, as of 1997, about 15% were deemed to have structural deficiencies stemming from corrosion of steel and steel reinforcement. At $8.3 billion in annual direct costs, it accounts for 36.72% of the corrosion costs for infrastructure sector. Life-cycle analysis estimates the indirect costs from traffic delays and productivity losses at ten times the direct costs or $83 billion. As of December 2006, 73,694 or 12.34% of the total of 596,808 bridges have been deemed structurally deficient [3].

1.3 CONCRETE SENSOR PROBLEM

Much of our civil infrastructure comprises structures constructed with steel-reinforced concrete. The steel reinforcement in concrete structures is subject to corrosion. External factors such as exposure to marine environments and deicing salts aggravate this problem. Corrosion of the steel reinforcement in concrete is one of the major causes of structural damage [2]. Increased internal stresses from corrosion products lead to the deterioration of concrete by causing delamination, cracking and spalling [4]. Figure 1.1 (left) shows spalling on the underside of a bridge deck in Albany, NY and Figure 1.1 (right) shows spalling of concrete bridge bent in Lubbock, TX.

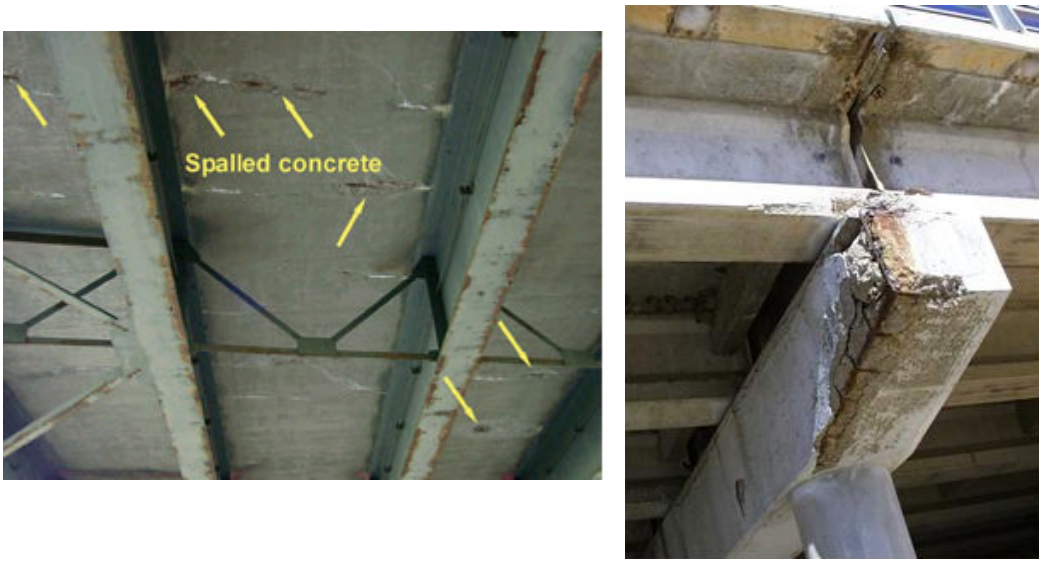

Figure 1.1 (left) Corrosion due to deicer salts causing cracking and spalling on the underside of the bridge deck in Albany, NY [5]. (right) Spalling of concrete bridge bent, Lubbock, TX [6].

While early detection is desirable and in some cases vital to prolonging the life of the structure, monitoring corrosion of rebar embedded in concrete is not easy. Rebar is shielded from plain sight because it is embedded, and by the time its effects are visible on the surface, the extent of the damage is already severe, and the structure may be compromised. Any other form of visual detection involves destructive testing of the suspected area. The use of wired techniques, such as half-cell potential measurements, provides ingress points for chloride ions facilitating corrosion. This problem of potential ingress points necessitates a method of non-destructive evaluation (NDE) of the corrosion damage. Various imaging techniques such as ultrasonic, industrial tomography are complicated and involve huge and bulky measuring equipment infeasible to use in the field. Remote sensing techniques such as acoustic emissions monitoring and electrostatic fields sensing are all highly vulnerable to interference from the environment [6-8].

Embedded sensors are subject to the same environmental effects as the steel reinforcement. These sensors need to be durable to withstand harsh construction environments and concrete curing even before they begin to be used. Corrosion is believed to begin as a localized phenomenon initiated by cracks and ingress points, and progressively gets worse [4]. Sensors, on the other hand, need a global distribution to detect the early onset of localized corrosion. Large structures such as bridges need many sensors in many different places throughout their structure to ensure "coverage." Too high a unit-sensor cost would preclude such a distribution of sensors. An embedded sensor needs both a wire-free method of interrogation from the external world and also power to sustain its operation. Batteries have lifetimes significantly shorter than those of structures they are monitoring. Hence the use of a battery limits the lifetime of the sensors. Thus, in addition to reliability, durability and low cost, the preferred concrete corrosion sensor should be embedded, have wireless interrogation, and have no onboard battery.

1.4 SCOPE OF RESEARCH

The passive wireless Electronic Structural Surveillance (ESS) platform developed at The University of Texas at Austin attempts to address the issues mentioned above. The ESS platform is the result of the work of many researchers [1, 6-16] from the Departments of Civil, Architectural and Environmental Engineering, and Electrical and Computer Engineering. The ESS platform uses two circuits magnetically coupled through the inductive reader and tag coils. The sensors (ESS tags) operate using inductive coupling between an unpowered (battery-free), embedded sensor, and an external reader. The coupled circuits allow for reading the state of the sensor wirelessly. The reader coil is

used to measure impedance response from which information pertaining to the state of the sensor is extracted. The ESS sensor constructed a passive resonant circuit. Since they are battery-free passive resonant circuits interrogated via inductive coupling, extending the read range of these sensors is a challenge. The ability to detect the response of the tags is influenced the method of interrogation, the instrumentation used and the design of the reader and tag coils. The motivation for this work is to explore the interaction between design and detection limits of the ESS system in order to improve the performance of the ESS based sensors.

Chapter 2 introduces and provides a detailed explanation of the Electronic Structural Surveillance platform. ESS sensors that utilize this technology are presented. The functioning of the analog and threshold ESS corrosion sensors developed in the past work at UT-Austin are explained. Universal passive wireless sensors based the circuit models developed for the ESS sensor is discussed.

In Chapter 3 the response of the ESS sensors is presented. Expressions for signal strength of the ESS tag's response are developed. The effect of various tag components on the signal strength is analyzed and their functional relationships are determined. A first set of tag design rules based purely on the circuit behavior of the components can then be developed.

Chapter 4 addresses the ability to detect signal in the presence of finite noise. Expressions for noise and the corresponding uncertainty are developed. The influence of the operating baseline noise is analyzed. An expression for minimum detection limit was developed.

In Chapter 5 pertains to read range analysis. Expressions relating signal strength, minimum detection limit and read range were developed. The influence of tag coil and

reader coil design on read range for size constrained single layer cylindrical solenoids was studied. Recommendations for the design of ESS reader and tag coils are made.

Chapter 6 summarizes the work and presents conclusions enumerates avenues for future work.

Chapter 2: Electronic Structural Surveillance Platform

2.1 ELECTRONIC STRUCTURAL SURVEILLANCE (ESS) SENSOR PLATFORM

As previously discussed, concrete corrosion sensors should be reliable, durable, low cost, wireless, and battery-less. The passive wireless Electronic Structural Surveillance (ESS) platform, developed at the University of Texas at Austin, addresses these requirements. The platform uses two magnetically coupled circuits. Figure 2.1 (Top left) shows a schematic of an embedded battery-free tuned secondary coil (tag) inductively coupled to an external untuned coil (reader). The ESS tags are resonant circuits. The response of the tag, around its resonance, is obtained by performing a swept-frequency impedance measurement at the reader. Figure 2.1 (Top right) is the functional circuit schematic of the ESS platform containing a reader and a tag coil coupled through a mutual inductance (*M*), and Figure 2.1 (Bottom) is the calculated magnitude and phase response of the input impedance Z_{in}. At its resonance frequency, the tag produces a kink in the magnitude and a clear dip in the phase response. The frequency of resonance of the tag is given by

$$f_{0tag} = \frac{1}{2\pi\sqrt{L_{tag}C_{tag}}}, \omega_{0tag} = \frac{1}{\sqrt{L_{tag}C_{tag}}}. \tag{2.1}$$

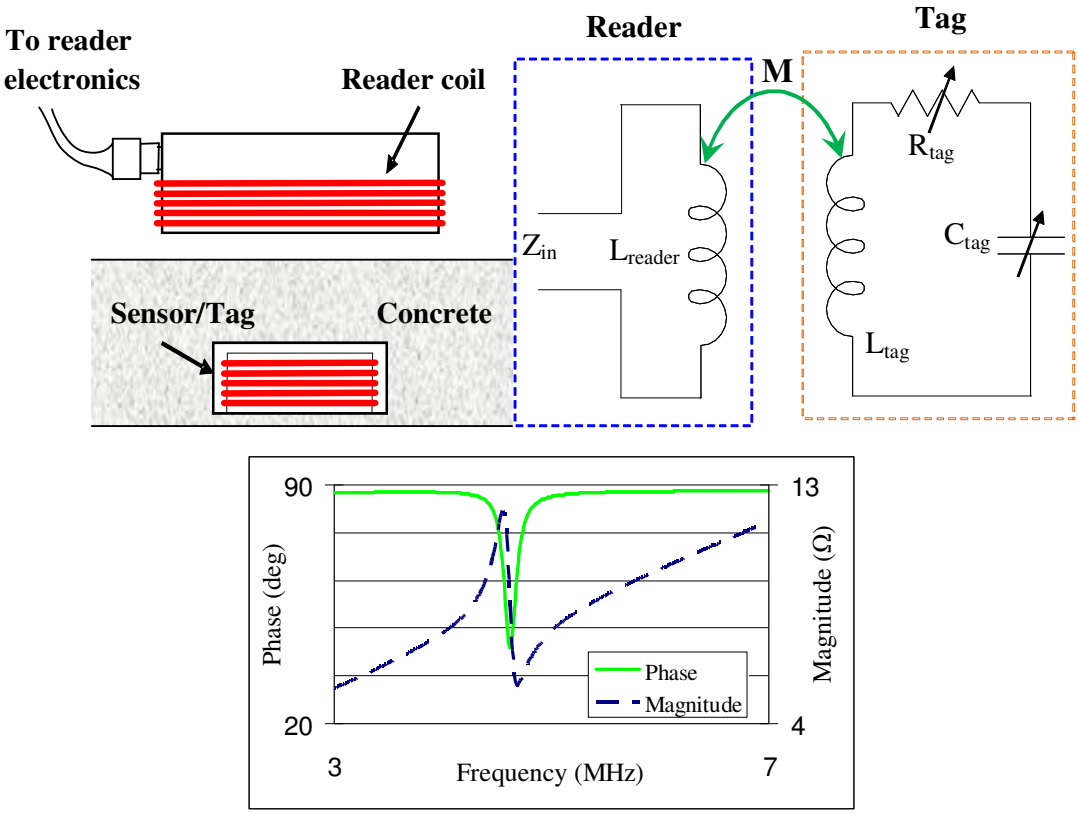

Figure 2.1 Inductively coupled reader and tag forms the basis of the ESS sensor platform (top left) and its equivalent circuit model (top right). The magnitude and phase of input impedance Z_{in} (bottom).

The tag when connected with a transducer forms the sensor. The transducers alter the resonance characteristics of the tag by shifting its resonance frequency, and/or changing the resistive losses which can be detected at the input of the reader. These changes are referred to the input impedance response through the coupled or reflected impedance of the tag.

For the circuit in Figure 2.1, any change in the inductance, capacitance, or the resistance of the tag produces a change in the tag impedance. The series impedance of such a tag is given by

$$Z_{series\_tag} = R_{tag} + j\left(\omega L_{tag} - \frac{1}{\omega C_{tag}}\right). \tag{2.2}$$

The reader impedance by itself is the impedance of the reader inductor:

$$Z_{series\_reader} = j\omega L_{reader}. \tag{2.3}$$

The total the input impedance Z_{in} of the coupled tag and reader as seen from the reader is

$$Z_{in} = Z_{series\_reader} + \left(\frac{(\omega M)^2}{Z_{series\_tag}}\right). \tag{2.4}$$

where the second term in Equation (2.4) is frequently referred to as the reflected or coupled impedance [17]:

$$Z_{coupled} = Z_{reflected} = \frac{(\omega M)^2}{Z_{series\_tag}}. \tag{2.5}$$

Hence, Z_{in} can also be expressed as

$$Z_{in} = Z_{series\_reader} + Z_{coupled}. \tag{2.6}$$

This coupled impedance is a function of frequency (ω), mutual inductance (M), tag inductance (L_{tag}), tag capacitance (C_{tag}) and tag resistance (R_{tag}). $Z_{coupled}$ enables the detection of changes in the tag circuit parameters at a remote reader, effecting its use as a wireless sensor.

2.2 ANALOG AND THRESHOLD SENSORS

The ESS platform is the result of the work of many researchers [1, 6, 8-9, 11, 13-14, 16] from the Departments of Civil, Architectural and Environmental Engineering, and Electrical and Computer Engineering. The ESS sensors developed to date include state sensors, weld crack detection sensors, analog resistance-based corrosion and temperature sensors, corrosion threshold sensors, and concrete conductivity sensors. These sensors can be broadly classified into analog and threshold sensors.

2.2.1 Analog Corrosion Sensor

The analog corrosion sensor is a wireless resistance sensor [9] based on altering the tag resistance (R_{tag}) in the presence of corrosion. The sensor contains a hermetically sealed tag, and an exposed length of bare steel wire (sensor wire), which serves as the transducer. The sensor is embedded in a structure where the sensor wire is exposed to the same environment as the reinforcing steel it is monitoring.

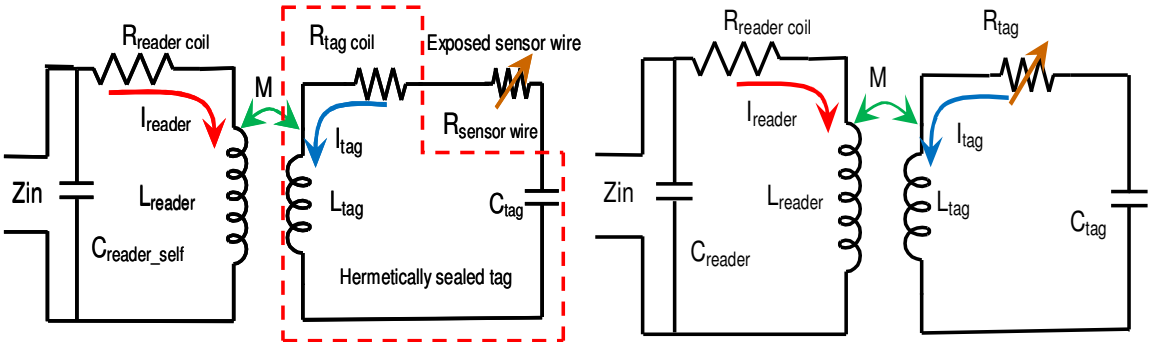

Figure 2.2 Expanded circuit model of the Analog Corrosion Sensor and reader including parasitics (left). A functionally equivalent circuit model that is used in the analysis (right) [1].

An expanded circuit model of the sensor is shown in Figure 2.2 (Left). This model also accounts for the parasitic resistance of both the reader and tag coils and the self capacitance. The sensor wire is modeled as a variable resistor. $R_{tag}=R_{tag\_coil}+R_{sensor\_wire}$, reader resistance and reader and tag capacitances can be lumped as R_{reader} C_{reader} and C_{tag} respectively. The resulting circuit in Figure 2.2 (Right), is functionally equivalent to the expanded circuit model. The input impedance for this model is given by:

$$Z_{in} = \frac{1}{j\omega C_{reader}} \left\| \left\{ \frac{1}{R_{reader} + j\omega L_{reader} + Z_{coupled}} \right\} . \right. \tag{2.7}$$

In the absence of the tag, the impedance Z_{in} is the response of the reader coil, which due to the presence of its self capacitance/resistance behaves as a parallel LC tank with lossy inductor. The magnitude is maximum at resonance. The complex reader impedance is inductive below and capacitive above its self resonance. Figure 2.3 shows the computed magnitude and phase of the input impedance as defined by Equation (2.7) plotted for different values of R_{tag}. The presence of a tag produces a clear dip in the phase of the impedance around the resonance frequency of the tag. As R_{tag} is increased, it damps the impedance response of the tag. This damping is especially visible as the phase dip ($\Delta\theta$) corresponding to the resonance frequency (ω_0) of the tag gets shallower and wider ($\Delta\omega$) with increasing R_{tag}.

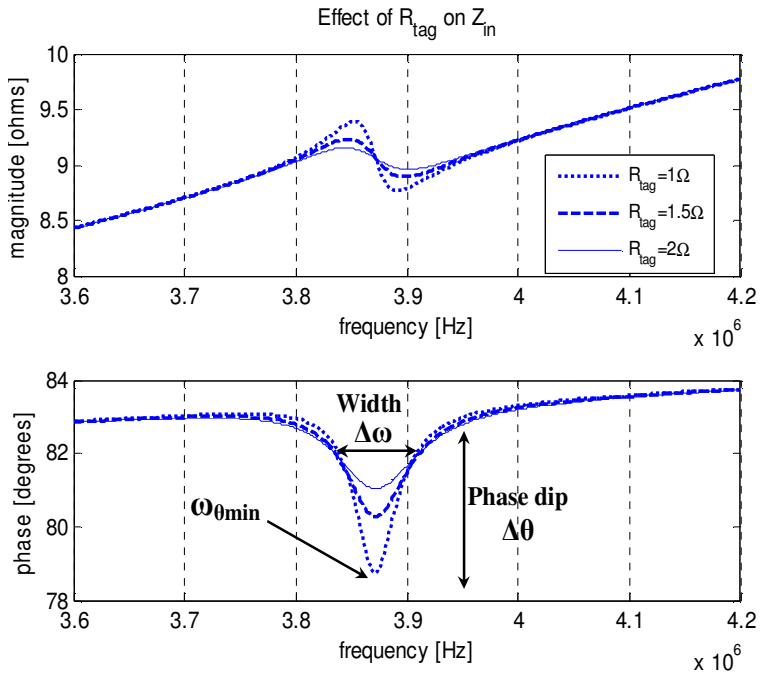

Figure 2.3 The response of Z_{in} to different values of R_{tag} showing that R_{tag} is related to the depth and width of the phase dip

Quality factor is defined as $Q = energy\ stored / energy\ dissipated$. For a series resonant circuit with an inductance *L,* capacitance *C* and a resistance *R*, quality factor $Q = \omega L/R$ [17]. The *Q* at the resonance frequency of the circuit $\omega_0 = 1/\sqrt{LC}$ is given by $Q_0 = \omega_0 L/R = \sqrt{L/C}/R$. We know from circuit theory that quality factor, Q_0, of a circuit, is a measure of its frequency selectivity. Q_0 can be determined from the magnitude of the impedance response curve as the ratio of $\omega_0/\Delta\omega$ where $\Delta\omega$ is the width of the resonance. Since Q_0 is a measure of the sharpness of the resonance, the lower the Q_0 the shallower the response. Although R_{tag} or Q_{0tag} are the ideal quantities to measure[15], since the sensor is embedded, it is not possible to measure them directly. We have to ascertain these from the changes in the input impedance response. The strong correlation between the shape of the dip in the phase curve and R_{tag} promulgates a measurement, termed *pseudoQ* ($\bar{Q}$), similar to Q_0 [10]):

$$pseudoQ = \bar{Q} = \frac{\omega_{\theta\min}}{\Delta\omega} = \frac{\omega_0}{\Delta\omega}. \tag{2.8}$$

where, $\Delta\omega$ is the width of the resonance and is defined as full-width half-max (FWHM) of the phase of the impedance response [9]. For small coupling factors [14] *(K)*, $\bar{Q} \cong Q_0$. Due to the baseline shift [9-10] in measured data, this ratio cannot be easily measured "by hand" from the raw curve. Instead, $\bar{Q}$ is obtained by numerical fitting the measured response. This numerically fitted $\bar{Q}$ is termed $(\bar{Q}_{tag})_{fit}$. It is found from the measured data by windowing the phase dip, and correcting the baseline using a fourth-order inverse polynomial. The interpolated, windowed phase dip is fit with a Lorenztian line shape[10] and the $(\bar{Q}_{tag})_{fit}$, is extracted from its coefficients.

2.2.2 Threshold Corrosion Sensor

The analog corrosion sensor, in its simplest form can serve as a threshold sensor. As the exposed steel wire corrodes, its resistance increases and the size of the phase dip ($\Delta\theta$) decreases. The presence or absence of the phase dip can be used to estimate whether a sensor is corroded or uncorroded. Unlike the width of the resonance $(\Delta\omega)$, the size of the phase dip ($\Delta\theta$) is a strongly dependent on coupling factor *k*, $\left(k = 1/\sqrt{L_{reader}L_{tag}}\right)$ i.e (distance). This distance dependence of $\Delta\theta$ makes it difficult to differentiate between distance and corrosion effects. Additionally if the sensor is corroded, there is no phase dip making it difficult to "locate" the tag. These issues could be addressed by including a second resonant circuit which provides a "reference resonant frequency."

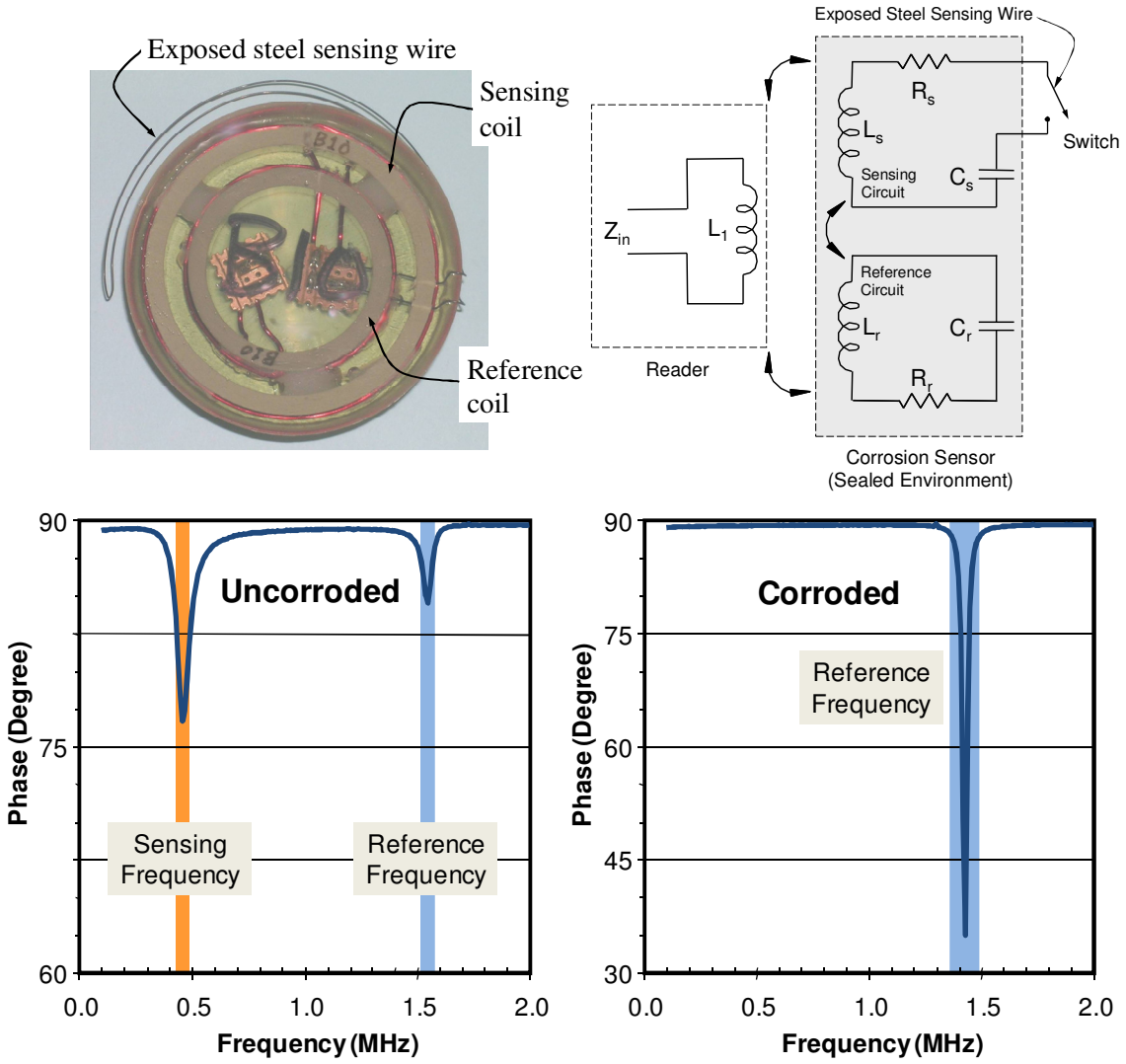

Figure 2.4 (left) shows the concrete corrosion sensor and its circuit model (below) including the reader coil. (right) shows the concrete conductivity sensor and the sensor' circuit equivalent (below)[12].

Various configurations of these coils have been tried resulting in the current-generation sensors. The sensor and its equivalent circuit are Figure 2.4 (top) shows the reference coil and sensing coil which are hermetically sealed. The exposed corroding steel wire (sacrificial transducer) is connected to the sensing coil damping its resonance as it corrodes. In the uncorroded state, the phase response when shows two phase dips

corresponding to the resonant frequencies of the sensing and reference coils and only one phase dip (reference coil) in the corroded state. In this work, we focus on single-coil sensors to understand the factors that affect their design and detection. The lessons learnt from this study can then be extended to dual-coil and other passive wireless sensors.

2.3 UNIVERSAL PASSIVE WIRELESS SENSOR

Although developed with concrete corrosion and structural health monitoring applications in mind, when configured correctly with a sensor/transducer that can alter the resonant characteristics of the tag, the passive wireless sensor can be used for other applications. The tag has been used with a photodiode integrated into a micromachined sensor array as a tag for the detection specific target analytes [18] and with an (IDC) interdigitated capacitor to measure the complex dielectric constant and conductivity of unknown liquids [19]. The collective behavior of resonant tags for use with large area monitoring [20] and the development of new transducers with a non-contact sacrificial layer [21] for corrosion monitoring are also being investigated. Thus the ESS platform has the potential to serve as a tool to develop a range of wireless battery-free sensors.

2.4 BLACK-BOX MODELS

Since the ESS platform is essentially an inductively coupled reader and tag coil, we can make many different sensors by connecting different transducers to the tag coil. The scope of this work covers passive components, so we consider transducers that are either resistors(R), inductors (L), or capacitors (C). The resulting sensor depends not only on the type of transducer used but also on where it is connected to the tag coil. We denote the transducer impedance with Z_x and the resistive, inductive, and capacitive transducers

as R_x L_x & C_x, respectively. The combinations resulting from the series and parallel connection to the tag coil are shown in Figure 2.5.

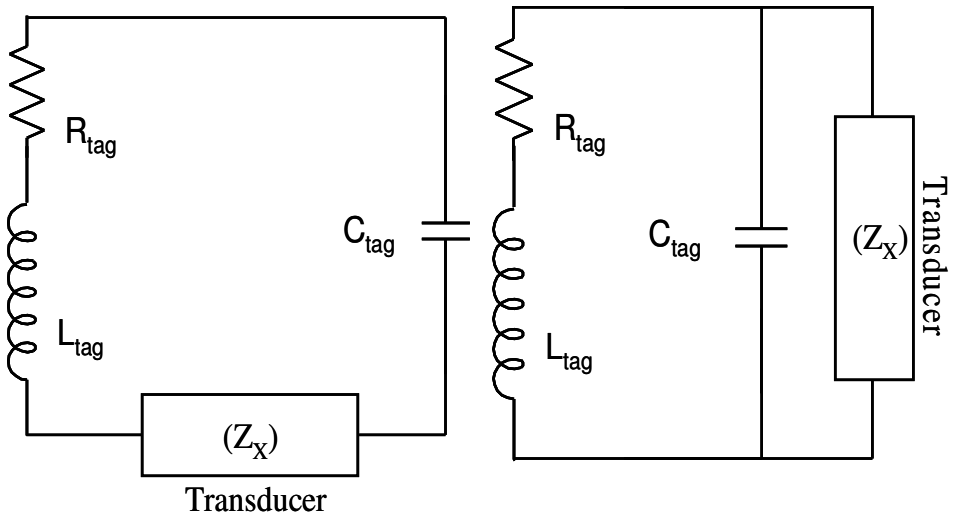

Figure 2.5 The combinations resulting from the series (left) and parallel (right) connection of a passive component (R_x, L_x, C_x) as a transducer for the tag. Z_x is the impedance of the transducer.

Three components ($R_x/L_x/C_x$) and two connections (series/parallel) result in a total of 6 configurations. The components in series only change the effective values of $R_{tag}/L_{tag}/C_{tag}$.. The capacitor in parallel only adds to C_{tag}. Thus, these four configurations can be represented by a simple series RLC circuit, where any one of the three component $R_{tag}/L_{tag}/C_{tag}$ values vary in response to the transducer, as shown in Figure 2.6.

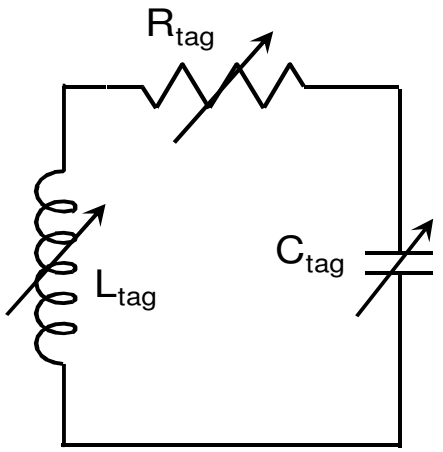

Figure 2.6. Model of the tag (Case 1) for series R_x, L_x, C_x and parallel C_x can be represented as a simple series RLC circuit with variable $R_{tag}/L_{tag}/C_{tag}$.

The model for parallel L_x and R_x change the effective impedance of the nodes across which they are connected. In the absence of R_x, R_{tag} is the essentially parasitic resistance of the tag coil, so parallel L_x and R_x appear across C_{tag}. In fact, in the limiting case where R_{tag} is very small, effective L_{tag} is the parallel combination of L_x and L_{tag}.

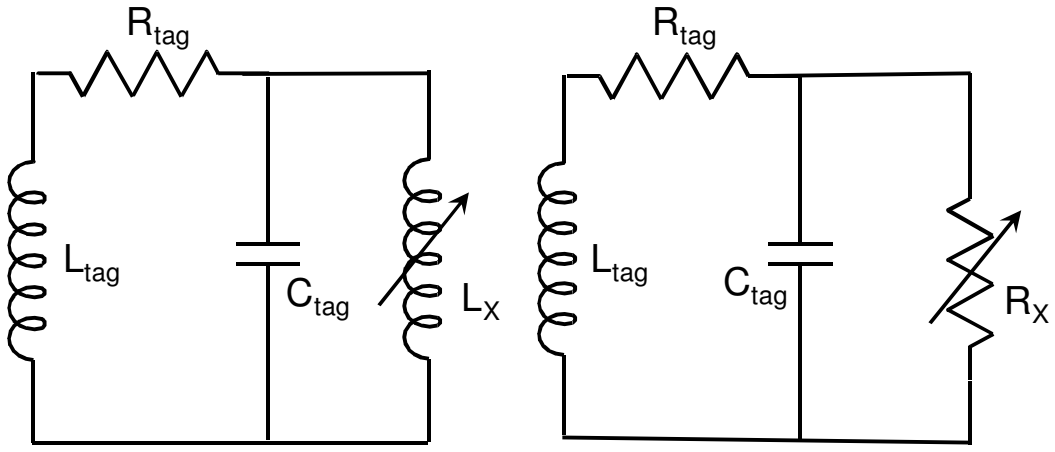

Figure 2.7 Model for parallel inductive transducer L_x (Case 2) (Left), and parallel resistive transducer R_x (Case 3) (Right)

Thus we have three circuit models that cover all six configurations.

- Case 1 (Series R_x, L_x, C_x and Parallel C_x)
- Case 2 (Parallel L_x)
- Case 3 (Parallel R_x)

While case 1 is the circuit model of the resistance-based corrosion sensors, case 2 is the circuit model of the concrete conductivity sensors. The model in case 1 is essentially the circuit model for any passive wireless tag. The phase response of the tag is affected by the value of its parameters (R_{tag}, C_{tag} and L_{tag}). The value of the tag parameters can be set by either changes in the transducer connected to it or by design decisions made in its construction. From the point of view of its circuit response, these are equivalent. Given a passive transducer, we must determine how to use the tag most effectively as a passive wireless sensor. Conversely, given a configuration, we can optimize the design of the transducer (usually more difficult) to improve the overall sensor performance. For both purposes, we need to understand the impedance response of the tag circuit when measured through an inductively coupled reader. Since impedance is usually measured by measuring magnitude and phase response, both are included in the analysis. At this time the effects of the method of and instrumentation for measuring impedance are not considered.

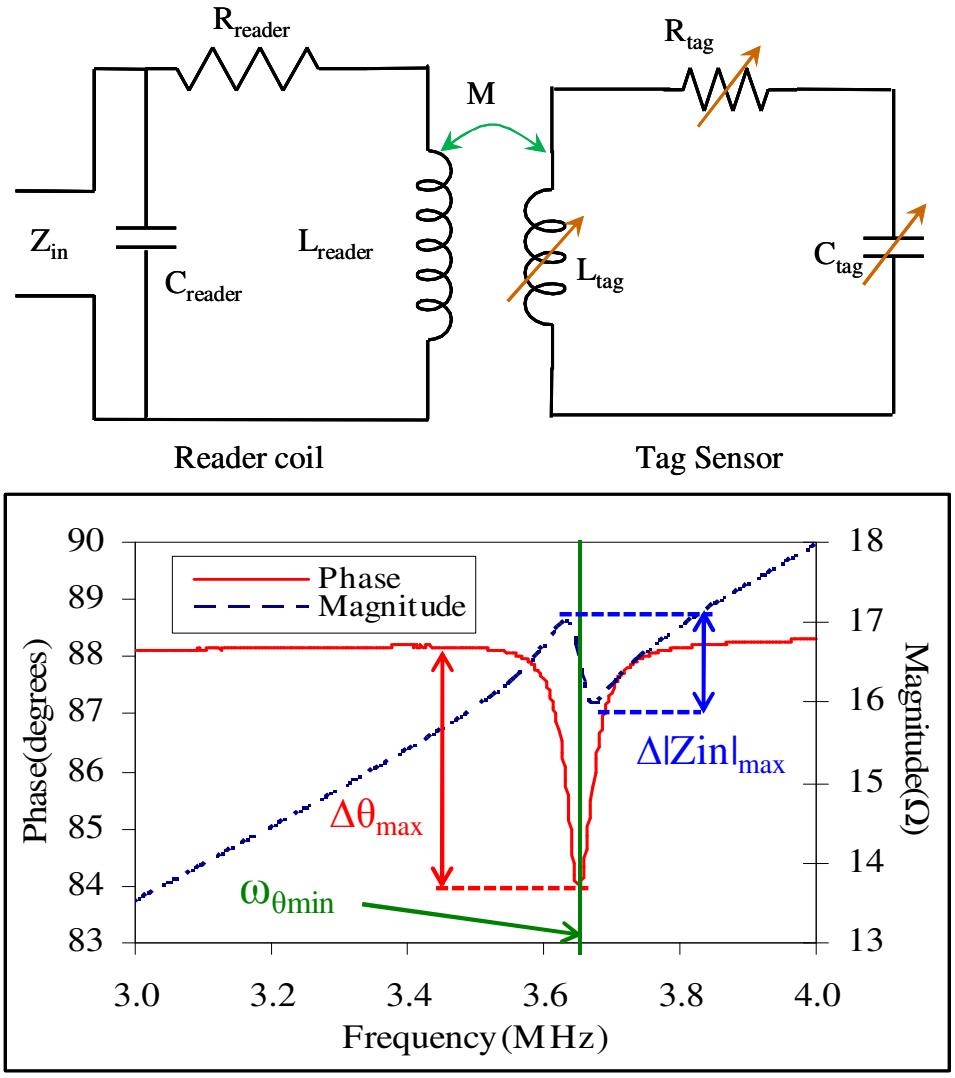

Figure 3.1 (top) Model for a passive wireless tag/sensor can be represented as a simple series RLC circuit with variable $R_{tag}/L_{tag}/C_{tag}$.. The reader coil is modeled as an RLC circuit where R_{reader} and C_{reader} are its parasitic resistance and self capacitance; (bottom) magnitude & phase response of input impedance (Z_{in}).

The reader and tag/sensor are modeled as coupled RLC circuits. With the parasitic resistance and self capacitance of the reader, the circuit behaves as a nonideal tank circuit, i.e. (R+L)||C. When measured through the inductively coupled reader, the series

equivalent RLC circuit response of the tag also exhibits a response similar to that of a non ideal LC tank circuit [15]. The input impedance expressions are given by:

$$Z_{reader} = \frac{1}{j\omega C_{reader}} \Big\| \left(R_{reader} + j\omega L_{reader} \right). \tag{3.1}$$

$$Z_{seriestag} = R_{tag} + j\omega L_{tag} + \frac{1}{j\omega C_{tag}}. \tag{3.2}$$

$$Z_{coupled} = Z_{reflected} = \frac{\omega^2 k^2 L_{reader} L_{tag}}{\underbrace{R_{tag} + j\omega L_{tag} + 1/j\omega C_{tag}}_{Z_{seriestag}}}. \tag{3.3}$$

$$Z_{in} = \frac{1}{j\omega C_{reader}} \Bigg\| \left(R_{reader} + j\omega L_{reader} + \frac{\overbrace{\omega^2 k^2 L_{reader} L_{tag}}^{Z_{refected\ or\ Z_{coupled}}}}{\underbrace{R_{tag} + j\omega L_{tag} + 1/j\omega C_{tag}}_{Z_{seriestag}}} \right). \tag{3.4}$$

A more intuitive view is that the reader (L_{reader}) and tag (L_{tag}) coils form the primary and secondary coils of an air-core transformer. The R_{tag} and C_{tag} are the loads connected to the secondary coil (L_{tag}). Below the resonance frequency ($\omega < \omega_{0tag}$), the tag inductance effectively sees an "open" circuit. Since the reader-tag transformer is driving a high impedance (open circuit), its response is unloaded (unaffected) by the tag transducer. Hence, from Equations 3.1 and 3.4 $Z_{in} = Z_{reader}$. Above the resonance, ($\omega > \omega_{0tag}$), the low impedance of C_{tag} effectively shunts L_{tag}. This shorting of secondary results in smaller effective reader inductance L_{eff} and reduced input impedance (larger primary current). If $R_{tag} \ll 1$, then the value of effective reader inductance, scales with the strength of coupling k as:

$$L_{eff} = L_{reader}(1 - k^2). \tag{3.5}$$

In the limit of weak coupling, $k \ll 1, \Rightarrow L_{eff} = L_{reader}$, and we again have $Z_{in} = Z_{reader}$ similar to the below-resonance case.

At the resonant frequency of the tag ($\omega = \omega_{0tag}$), the inductive and capacitive reactance of the tag cancel and the reader is driving an inductively coupled resistive load R_{tag}. Thus the largest perturbation of the input impedance occurs at the resonant frequency of the tag. Figure 3.1 illustrates this property, as the kink ($\Delta|Z_{in}|$) in the magnitude and a dip ($\Delta\theta_{in}$) in the phase response of the input impedance Z_{in} occur at $\omega_{\theta\min} \approx \omega_{0tag}$ (for "weakly" coupled tag, i.e. k<<1). Since the presence of $\Delta|Z_{in}|$ and $\Delta\theta_{in}$ correspond to the presence of the tag, the larger the deviation, the easier it is to detect the presence of a tag. For any sensor (tag + transducer) including the analog and threshold ESS sensors discussed previously, detection of the tag is the first step in measuring the response of any transducer associated with the tag. Simply put, if we cannot detect the tag, we cannot measure changes in it.

3.1 SIGNAL STRENGTH AND MEASURANDS

The magnitude and phase of input impedance can be the measurands. In the absence of the tag; the reader response sets the baseline. The presence of a tag causes a change/perturbation from the baseline reader response. All tag responses are measured as a deviation from this baseline. This deviation when quantified can be treated as a measure of signal strength of the sensor. We quantify the "signal strength" of this deviation as follows:

for the magnitude response

$$\begin{aligned} \Delta|Z_{in}| &= |Z_{in}|_{tag\ absent} - |Z_{in}|_{tag\ present} \\ \Delta|Z_{in}| &= |Z_{reader}| - |Z_{reader} + Z_{coupled}| \end{aligned}. \qquad (3.6)$$

and similarly, for the phase response:

$$\begin{aligned}\Delta\theta_{in} &= \theta_{in}\big|_{tag\ absent} - \theta_{in}\big|_{tag\ present} \\ \Delta\theta_{in} &= \measuredangle\left[Z_{reader}\right] - \measuredangle\left[Z_{reader} + Z_{coupled}\right]\end{aligned} \tag{3.7}$$

As shown in Figure 3.1,at the frequency $\omega_{\theta\min} \approx \omega_{0tag}$, the magnitude signal strength $\Delta|Z_{in}| = \left(\Delta|Z_{in}|\right)_{\max}$ and the phase signal strength $\Delta\theta_{in} = \left(\Delta\theta_{in}\right)_{\max}$ are maximum. This frequency corresponds to the largest perturbation in the reader baseline due to the presence of the tag, i.e. maximum phase signal strength or the largest phase dip. By using $\left(\Delta|Z_{in}|\right)_{\max}$ and $\left(\Delta\theta_{in}\right)_{\max}$ as a metric we test the effects of both the tag and the reader components on the sensor signal.

To obtain the desired tag response, we can vary a total of 7 circuit parameters : R_{tag}, L_{tag}, C_{tag}, R_{reader}, L_{reader} C_{reader} and mutual inductance *M (or k)*. Instead of arbitrarily selected values, a set of reader and tag parameters typically used in some of our measurements is used. The circuit parameters corresponding to the geometry of the reader and tag coils must first be determined. The following section relates geometry of the tag to these 7 circuit values and includes numerical examples from some of our measured prototypes.

3.2 GEOMETRY → CIRCUIT VALUES

The reader and the tag coil and by extension the components used to model them are dependent on the geometry of the coils which includes shape and size. The values of the L_{reader}, L_{tag} and M are calculated from the geometry of the coils. The formulae used in the calculation of circuit parameters have been used [maa, prn, pkp] extensively during

the course of the development of ESS sensors. For reference, the following sections briefly review the component formulae.

3.2.1 Self and Mutual Inductance

All coils used in this work are single-layer cylindrical short solenoids (Figure 3.2). This means that the length of the coil is much smaller than the diameter of the coil [Grover].

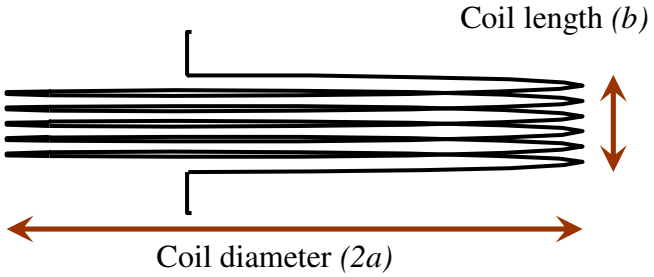

Figure 3.2 Dimensions of a single-layer coil used to determine the solenoid factor (β), which is the ratio of coil length to coil diameter. For a short solenoid 2a>>b.

The formula for computing inductance of such coils is by applying a geometry correction factor given by Nagaoka [22] to the standard formula of inductance.

$$L = 0.002\pi^2 a\left(\frac{2a}{b}\right)N^2 K \quad . \tag{3.8}$$

Where, L is the calculated self inductance in (μH) and a, b are the radius and the coil length respectively, both measured in (cm). K is Nagaoka's geometry correction factor given by

$$K = \frac{2\beta}{\pi}\left[\left(\ln(\frac{4}{\beta}-\frac{1}{2}\right)+\frac{\beta^2}{8}\left(\ln\frac{4}{\beta}+\frac{1}{8}\right)-\frac{\beta^4}{64}\left(\ln\frac{4}{\beta}-\frac{2}{3}\right)+\frac{5\beta^6}{1024}\left(\ln\frac{4}{\beta}-\frac{109}{120}\right)-...\right]. \quad (3.9)$$

β is the ratio of coil length to coil diameter. For a short solenoid $2a>>b$ and

$$\beta = \frac{b}{2a}.$$

Mutual inductance highly depends on the geometry of the two coils and their orientation relative to each other. The mutual inductance between the reader and the tag coil is computed based on the Neumann form as applied to two coaxial circular loops. This is given by [10, 23]:

$$M = N_{reader}N_{tag}\mu\sqrt{r_{reader}r_{tag}}\left[\left(\frac{2}{t}-t\right)\mathrm{K}(t)-\frac{2}{t}\mathrm{E}(t)\right]. \quad (3.10)$$

Equation 3.10 is obtained from the Neumann form by substituting $t^2 = \frac{4r_{reader}r_{tag}}{d^2+\left(r_{reader}+r_{tag}\right)^2}$. K ($t$) and E ($t$) are complete elliptic integrals of the first and second kinds, respectively: $E(t) = \int_0^{\pi/2}\sqrt{1-t^2\sin^2\phi}\,d\phi$ and $K(t) = \int_0^{\pi/2}\frac{d\phi}{\sqrt{1-t^2\sin^2\phi}}$.

N_{reader}, $N_{tag,}$ r_{reader} and r_{tag} are the number of turns and radii of the reader and tag, respectively.

3.2.2 Resistance

The resistance of the reader and the tag are affected by the intrinsic d.c. and skin resistance of their respective coils in addition to any parasitic (connectors) or added resistances (sensor wire). For the tag R_{tag}= R_{sensor_wire} + R_{tag_coil} where, R_{tag_coil} is the parasitic resistance associated with of the tag inductor, and similarly R_{reader}= R_{reader_coil}.

For a given inductor coil, R_{coil} = R_{dc_coil} + R_{skin_coil} which is the sum of the dc resistance of the wire and the ac resistance due to skin effect at high frequencies of

operation. Thus R_{coil} is a frequency-dependent resistor. In this work, wherever applicable, the formula to compute this frequency dependent resistor is assumed to be given by the formula for the impedance of round wires [14-15, 23]:

$$R_{wire} = \Re\left\{ \frac{j}{2\pi r_{wire}} \sqrt{\frac{j\omega\mu_0}{\sigma} \frac{J_0(jx)}{J_1(jx)}} \right\} \quad (\Omega/\text{m}) . \tag{3.11}$$

where $x = r_{wire}\sqrt{j\omega\mu_0\sigma}$ and J_0 and J_1 are the Bessel functions of the first kind, 0th and 1st order respectively, σ is the conductivity of the wire, and r_{wire} is the cross-sectional radius of the wire.

The frequency-dependent resistance R_{coil} for a given coil is then given by:

$$R_{coil} = R_{wire} \cdot l_{wire} \quad (\Omega), \textit{where } l_{wire} = 2 \cdot \pi \cdot r_{coil} \cdot N_{coil} . \tag{3.12}$$

Thus
$$R_{coil} = R_{wire} \cdot 2 \cdot \pi \cdot r_{coil} \cdot N_{coil} , \tag{3.13}$$

where, l_{wire} is the total length of wire used to wind a given coil and , r_{coil} and N_{coil} are the radius and number of turns of the coil respectively.

3.2.3 Capacitance

The capacitors in the tag are tuning capacitors. For a given tag coil inductance, the capacitor sets the resonance frequency of that tag. We employ ceramic capacitors, which have tolerance of 10-20%. Also these capacitors have low loss tangent or very high quality factor, Q_{cap}, on the order of $\geq 10^3 \approx 10\ Q_{coil}$. Since total Q_{tag} is a parallel combination of Q_{tag_coil} and Q_{tag_cap} , the effect of the capacitor losses on the tag is negligible.

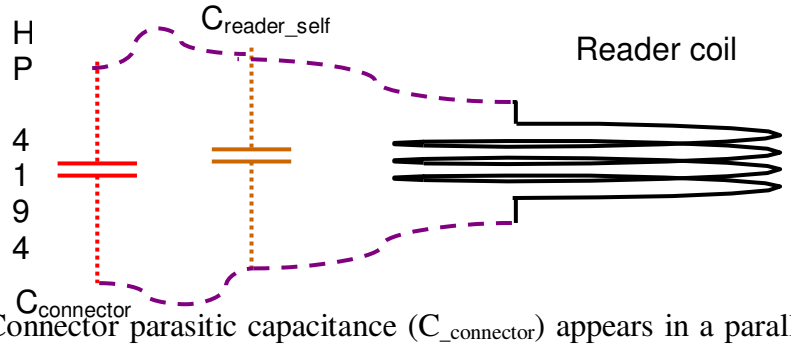

Figure 3.3 Connector parasitic capacitance ($C_{\_connector}$) appears in a parallel combination across the lumped parasitic reader self capacitance (C_{reader_self}).

The reader uses no explicit capacitor, and hence has only its parasitic self capacitance. Our reader coil has an RCA connector and is connected to the HP4194 Impedance Gain-Phase Analyzer (the measurement instrument) through a BNC-RCA adaptor. The connectors themselves have some capacitance which appears in parallel with the reader self capacitance as can be seen in Figure 3.3. Hence $C_{reader} = C_{reader\_self} + C_{conncetor}$. The connector capacitance has a value between 1- 3pF. Since capacitors in parallel are additive, the effect of 3pF is very negligible expect in cases where $C_{reader\_self} \leq C_{conncetor}$ which is true for reader coils with few turns.

The value of this C_{reader} is estimated from the measured impedance response of the reader coil. Since C_{reader} sets the resonant frequency for a give reader coil inductance, its value is calculated using the resonant frequency f_{0_reader} and the value of L_{reader}:

$$C_{reader} = \frac{1}{4 \cdot \pi^2 \cdot f_{0\_reader}^2 \cdot L_{reader}} \tag{3.14}$$

Alternatively, Medhurst's [24] classic empirically determined formula has long been a favourite for determining self capacitance of air-core single layer solenoids especially among amateur radio enthusiasts. The formula is valid only for short solenoid

ratios (β) > 0.05).and is employed where applicable. It is especially not applicable to the single turn coils for which self capacitance is determined experimentally.

As a starting point, we employ a 1 turn reader coil with a diameter of 10cm wound with 18 AWG magnet wire (L_{reader}=344nH). The tag has 5 turns of 22AWG magnet wire with a diameter of 4 cm (L_{tag}=2.1μH) and is tuned with a 470pF capacitor to be resonant at 5MHz. Also, a 1Ω resistor is added as the default transducer resistance *Rx*; this helps smooth out the phase dip, reducing numerical errors. The reader and the tag are coaxially separated at a distance of 5cm, corresponding to a mutual *M*=25.7nH which is a coupling factor *k* =2.9%. All coils are air core cylindrical short solenoids. We begin by analyzing the effects of the reader parameters.

3.3 EFFECT OF READER COMPONENTS

The reader sets the operating baseline of the input impedance. The deviations in this baseline around the tag's resonant frequency detect the presence of the tag and changes in the tag parameters caused by any transducer connected to it.

3.3.1 Reader Capacitance (C_{reader})

The combination of L_{reader} and C_{reader} sets the resonant frequency of the reader $\omega_{0reader} = 1/\sqrt{L_{reader}C_{reader}}$. If no additional capacitance is used, the reader is resonant at its self resonant frequency (SRF). The SRF of the 1 turn reader is 74.75MHz which corresponds to the minimum possible C_{reader}. Connectors and cabling use to connect the reader coil to the measurement instrument only increase the effective value of C_{reader} The tag is tuned to be resonant at $\omega_{0tag} = 1/\sqrt{L_{tag}C_{tag}}$ = 5MHz. For the model shown in Figure 3.4, the magnitude (Figure 3.5) and phase (Figure 3.6) response of the input impedance Z_{in} is calculated for three cases of C_{reader} such that $\omega_{0reader}$ = SRF_{reader} (blue curve), $\omega_{0reader} = 5\times\omega_{0tag}$ (red curve) and $\omega_{0reader} = \omega_{0tag}/5$ (black curve).

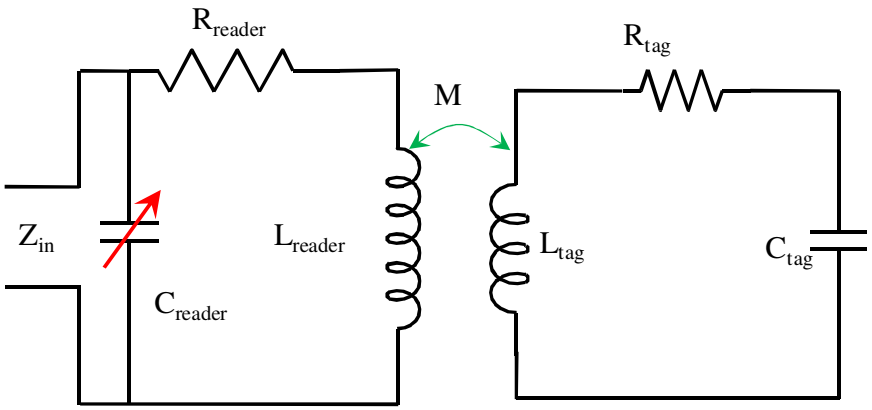

Figure 3.4 Equivalent circuit model of reader and tag used in evaluating the effect of varying reader capacitance C_{reader}

The peaks in the magnitude response (Figure 3.5) correspond to the high impedance, parallel resonance of the reader. The resonant frequency of the self resonant reader (blue) is beyond the frequency axis of the plot. For the red and black curves, the tag is operating below and above the resonant frequency of the tag, respectively. As a result, the tag response is measured either from an inductive $\left(\omega_{0reader} > \omega_{0tag}\right)$ or a capacitive $\left(\omega_{0reader} < \omega_{0tag}\right)$ baseline, which is more apparent from the phase response (Figure 3.6). In either case the axes limits need to be adjusted to make the perturbation due to the tag $\Delta|Z_{in}|$ and $\Delta\theta_{in}$ visible.

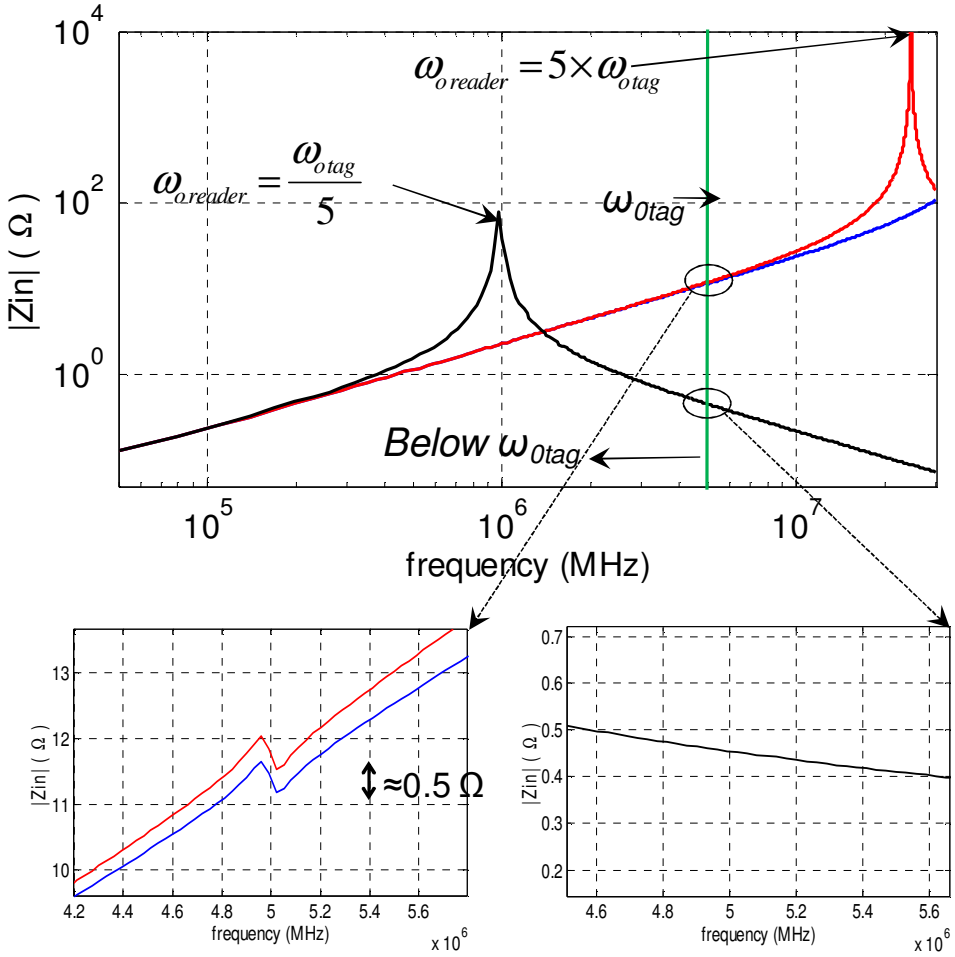

Figure 3.5 Magnitude response of Z_{in} comparing the perturbation produced by the tag as measured above (capacitive baseline) and below (inductive baseline) the resonant frequency of the reader.

At $\omega < \omega_{0reader}$ (i.e. inductive baseline), Z_C presents a high impedance thus $Z_{in} \approx Z_{R+L}$. When measured from an inductive baseline, the tag has a small magnitude signal strength $\left(\Delta|Z_{in}|\right)_{\max}$ =0.5Ω and a measureable phase signal strength $\left(\Delta\theta\right)_{\max}$ =3°. In contrast, the capacitive baseline yields no measureable signal $\left(\Delta|Z_{in}|\right)_{\max}$ and a diminished $\left(\Delta\theta\right)_{\max}$ = 0.15°. In this capacitive-baseline regime, the reader coil impedance (Z_{R+L}) is shunted by impedance (Z_C) of C_{reader}. (Figure 3.7), and $Z_{in} \approx Z_C$ for $\omega > \omega_{0reader}$.

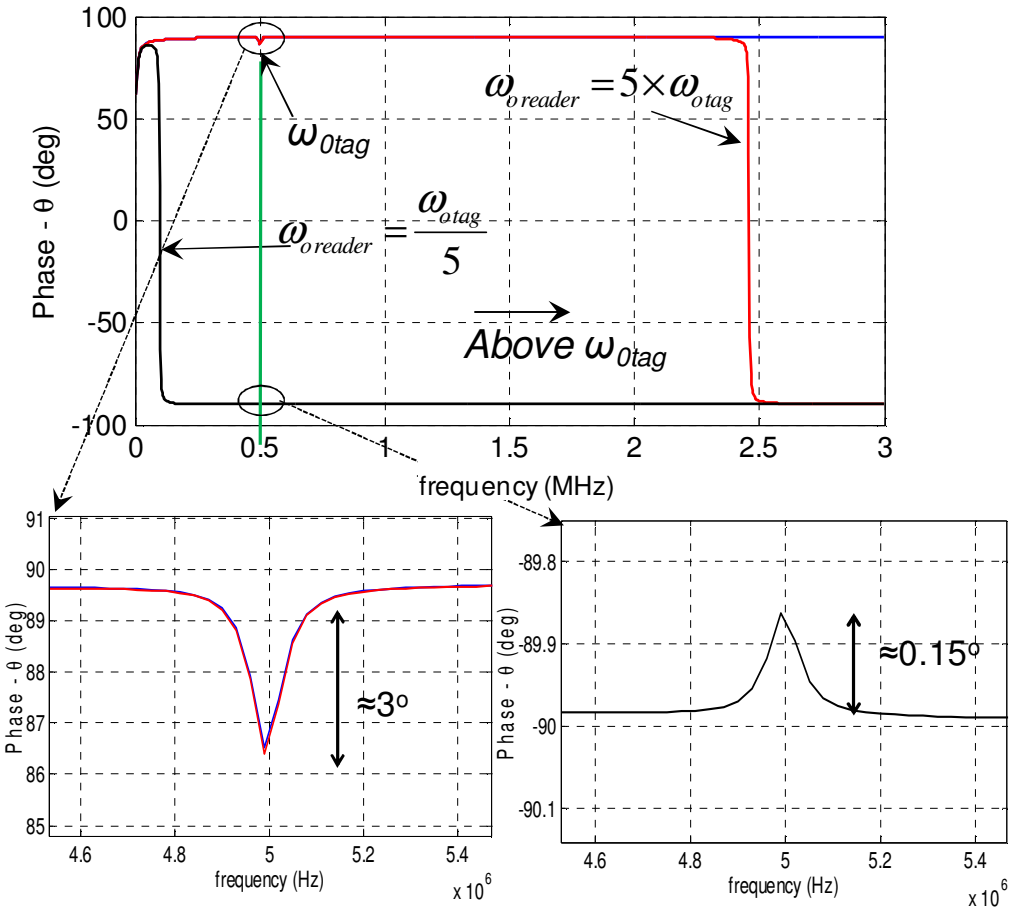

Figure 3.6 Perturbed phase response produced by the tag when measured above (capacitive baseline) and below (inductive baseline) the resonant frequency of the reader.

The reflected impedance of the tag produces a small change in the impedance of the inductive branch (ZR+L) which is shunted by a low impedance, resulting in even smaller changes in Zin. This effect explains the weaker signal strength when the tag is measured through the capacitive baseline. The phase signal performs better since it is measured from a constant baseline (+/-90^{o}).

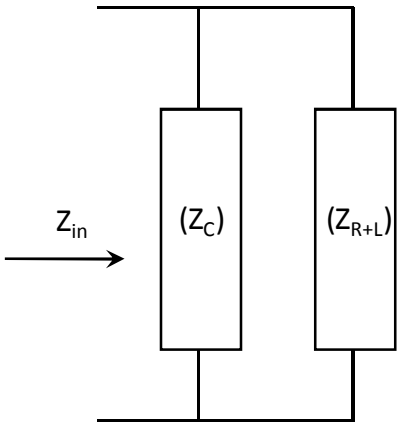

Figure 3.7 Input impedance modeled as a two parallel impedances where $Z_C = 1/j\omega C_{reader}$ and $Z_{(R+L)} = R_{reader} + j\omega L_{reader}$.

Analogous to the Kramers-Kronig relations between real and imaginary parts of complex permittivity, the real and imaginary parts of the impedance/admittance functions for a passive linear network have a well-defined relation [23]. To determine the imaginary part of such a function, it is sufficient to know the real part of a function along the imaginary axis of the complex frequency $(s = \sigma + j\omega)$ plane [23]. The proof for this result is based on the fact that the impedance/admittance functions for a passive linear network must be analytic in one half of the complex frequency plane [23]. This well-known result has been used in rational fitting of network transfer functions from its real part [25].

Since the reader and tag form a passive linear network, the result can be utilized to determine the impedance transfer function uniquely, which can be used to compute the magnitude and phase response. In addition, since the phase signal is bounded and performs better than the magnitude, the analysis is continued using only the phase signal strength $(\Delta\theta)_{\max}$.

3.3.2 Reader Resistance (R_{reader})

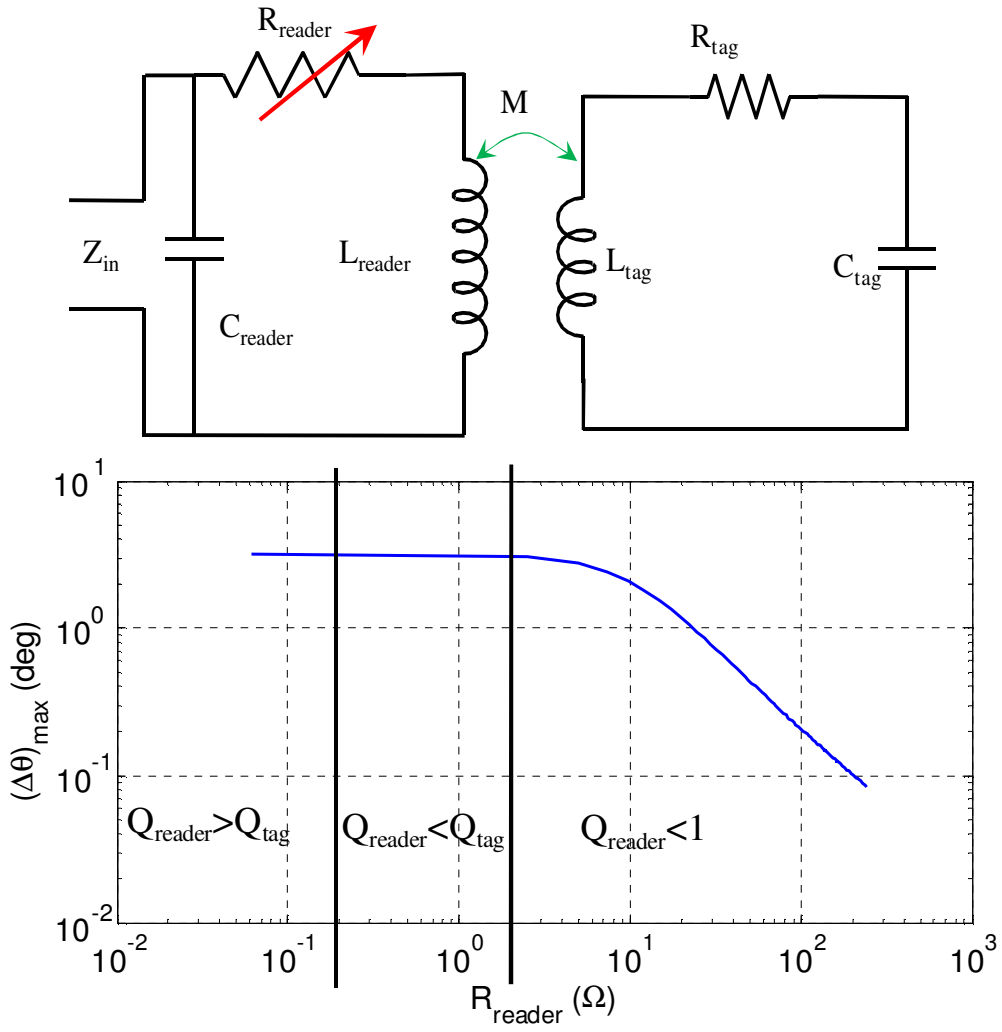

Figure 3.8 (Top) Equivalent circuit model used in evaluating the effect of varying reader resistance R_{reader} & (Bottom) response of the phase signal strength $(\Delta\theta)_{max}$ v. R_{reader}

The reader resistance R_{reader} is the self resistance of the reader coil. Though R_{reader} is typically small, the reader coil can be loaded by external parasitic resistances such as connectors and cabling, increasing the effective R_{reader}. To evaluate the effect of varying R_{reader}, the phase-frequency response $\theta_{in}(\omega)$ is calculated for various values of R_{reader} .

Since $\theta_{in}(\omega)$, is a function of frequency, this yields a surface plot $\theta_{in}(\omega, R_{reader})$. This surface, is first calculated when the tag is absent, i.e. coupling *k* or mutual *M=0*. This graph is the reader's baseline response $\theta_{in}(\omega, R_{reader})|_{tag\ absent}$. A second surface, $\theta_{in}(\omega, R_{reader})|_{tag\ present}$, is generated in the presence of the tag. $\Delta\theta = \theta_{in}(\omega, R_{reader})|_{tag\ absent} - \theta_{in}(\omega, R_{reader})|_{tag\ present}$, the difference between these two surface plots is calculated. $(\Delta\theta)_{\max}$, the locus of the maximum $\Delta\theta$ is then computed. Figure 3.8 (bottom) shows a plot of $(\Delta\theta)_{\max}$ against R_{reader}. A similar approach is used in generating the plot of $(\Delta\theta)_{\max}$ versus circuit parameter under test for all subsequent analysis. As R_{reader} increases from 0.02Ω→ 200Ω, $(\Delta\theta)_{\max}$ = 3° remains constant for R_{reader}< 2Ω. For 2Ω< R_{reader}< 10Ω, $(\Delta\theta)_{\max}$ drops from 3° to 2°, and for R_{reader}> 10Ω, $(\Delta\theta)_{\max}$ falls linearly with increasing R_{reader}. Defining $Q_{reader} = \omega L_{reader}/R_{reader}$, since the measurements of $(\Delta\theta)_{\max}$ occur at $\omega = \omega_{0tag}$, the quality factor of the reader coil at the resonant frequency of the tag is $Q_{reader} = \omega_{0tag} L_{reader}/R_{reader}$. Note that Q_{reader} is not the *Q* of the reader circuit but just that of the reader coil. $Q_{reader\,coil} = Q_{reader}$ is used for notational convenience. As R_{reader} increases, Q_{reader} decreases and as a result, the reader baseline shifts from inductive (+90°) to resistive (0°).When R_{reader}= 2Ω, Q_{reader}=1 and the baseline phase angle at the resonant frequency of the tag $\theta_{baseline}$ = 45°. For R_{reader}> 2Ω, Q_{reader}<1 and $\theta_{baseline}$ < 45°, the reader is more resistive than inductive, as illustrated in the phasor diagram of Figure 3.9. Let $\theta=\theta_{baseline}$ be the phase angle of the baseline at $\omega = \omega_{0tag}$. As R_{reader} increases, Q_{reader} decreases and $\theta_{baseline}$ decreases from 90° to 0° so the ability to measure the phase signal decreases $\Rightarrow (\Delta\theta)_{\max} \downarrow$ (Figure 3.8(bottom)). Thus precaution should be taken so that parasitic resistive loading of Q_{reader} is avoided. This is especially true for readers with small L_{reader} such as single turn coils.

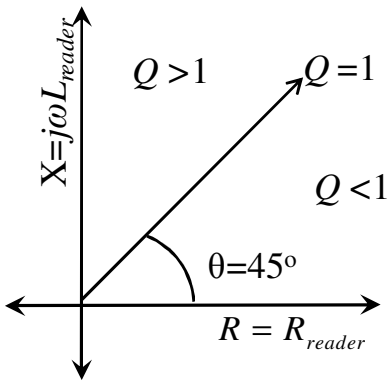

Figure 3.9 Phasor diagram of impedance of the reader showing that for quality factor Q>1 the reader coil is inductive, and for Q<1 it is resistive. θ is the baseline phase angle ($\theta_{baseline}$) of the reader's impedance. Q =1 corresponds to a baseline phase angle of 45°

The requirement that quality factor of the reader coil Q_{reader}>1 at the resonance frequency of the tag sets a lower bound on the operating resonant frequency ω_{0tag} of the tag. Since

$$Q_{reader} = Q_{reader}\big|_{\omega_{0tag}} = \frac{\omega_{0tag} L_{reader}}{R_{reader}}. \tag{3.15}$$

$$Q_{reader} > 1 \Rightarrow \omega_{0tag} > \frac{R_{reader}}{L_{reader}}. \tag{3.16}$$

The analysis of $(\Delta\theta)_{\max}$ versus C_{reader} suggests that $\omega_{0tag} < \omega_{0reader}$. Thus the operating frequency of the tag ω_{0tag} should be chosen such that,

$$\frac{R_{reader}}{L_{reader}} < \omega_{0tag} < \omega_{0reader}, \tag{3.17}$$

or,

$$\frac{R_{reader}}{L_{reader}} < \frac{1}{\sqrt{L_{tag} C_{tag}}} < \frac{1}{\sqrt{L_{reader} C_{reader}}}. \tag{3.18}$$

3.4 EFFECT OF TAG COMPONENTS

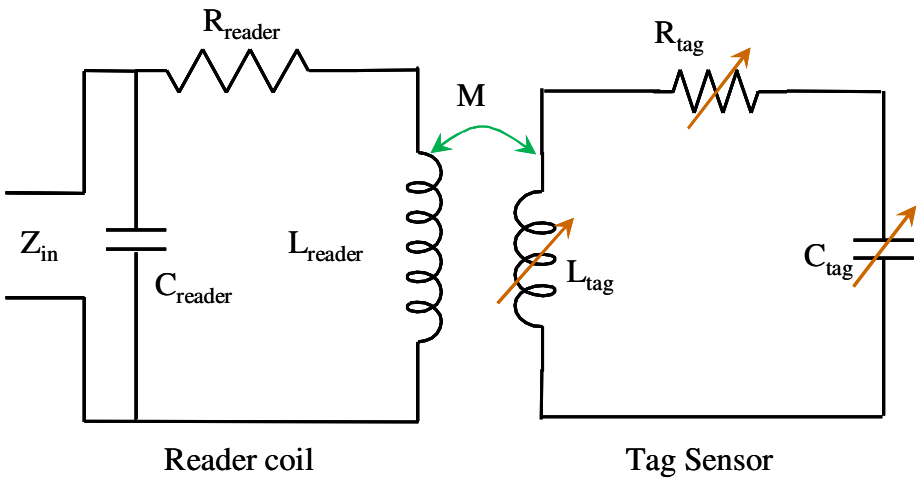

Figure 3.10 Equivalent circuit of a reader and a passive wireless tag/sensor modeled with variable $R_{tag}/L_{tag}/C_{tag}$. The model remains unchanged by connecting a series resistive transducer or series/parallel reactive transducer to the tag. The transducers change the effective values of $R_{tag}/L_{tag}/C_{tag}$.

The sensor is obtained by connected a desired transducer to the tag. As discussed previously, the addition of the transducer does not affect the circuit model (Figure 3.10). The values of R_{tag}, L_{tag}, and C_{tag} can be set by decisions made during the design of the tag. Once a tag is designed and connected to a transducer, barring interference effects, changes in the transducer change effective values of the tag parameters. The following sections study the changes in signal strength $(\Delta\theta)_{max}$, as a result of changes to the effective values of R_{tag}, L_{tag}, and C_{tag}. We keep the magnetically coupled portion of the circuit unaffected. Unless specified otherwise, the values of distance, M and k remain constant and thus all changes in $(\Delta\theta)_{max}$ can be attributed solely to changes in the tag parameter under test.

3.4.1 Tag Inductance (L_{tag})

From Figure 3.10, changing the value of L_{tag} affects the value of mutual inductance M. This is true only if the value of $L_{tag\ coil}$ is changed. The effective value of L_{tag} can be changed by the value of an inductive transducer (L_X) connected in either series or parallel with the tag. If the transducer is fully shielded and lossless it will affect neither the M nor will it add any resistance to the tag, leaving R_{tag} unchanged.

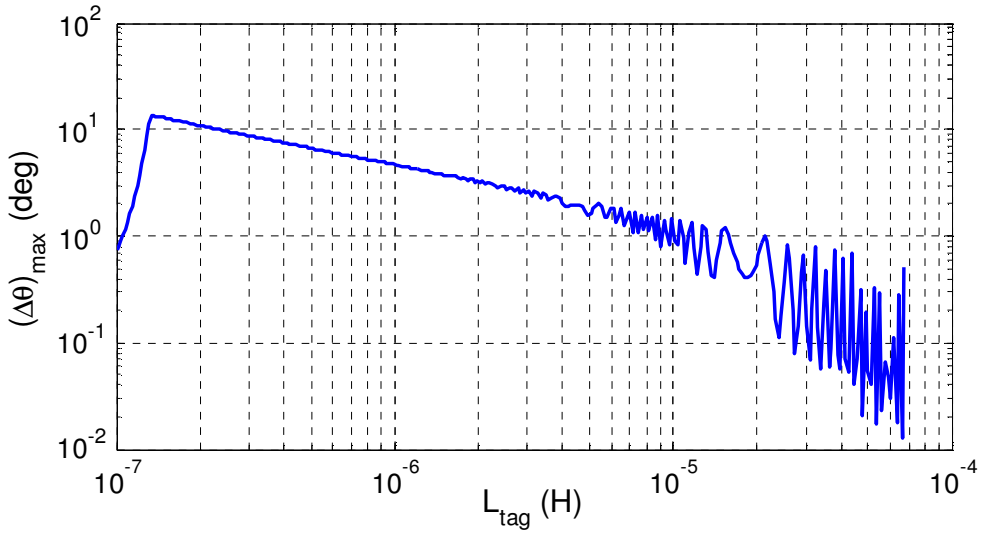

Figure 3.11 Variation of the phase signal strength $(\Delta\theta)_{max}$ in response to changing effective values of L_{tag} caused by a fully shielded lossless inductive transducer (L_X) connected to the tag. The starting value L_{tag}=2.1μH

L_{tag}	f_{0tag}(MHz)	$Q_{reader}\|_{fotag}$
1uH	**7.3**	**15.8**
5uH	**3.2**	**7**
10uH	**2.3**	**5**
20uH	**1.6**	**3**

Table 3.1 As the effective value of L_{tag} increases, both resonant frequency of the tag (f_{0tag}) and quality factor of the reader coil at the resonant frequency of the tag ($Q_{reader}|_{f_{0tag}}$) decrease.

At the resonant frequency of the tag,

$$\omega = \omega_{0tag} = 1/\sqrt{L_{tag}C_{tag}}\ , \tag{3.19}$$

the quality factor of the tag is given by

$$Q_{tag} = \frac{1}{R_{tag}}\sqrt{\frac{L_{tag}}{C_{tag}}}\ , \tag{3.20}$$

the quality factor of the reader coil at this frequency is given by

$$Q_{reader} = \frac{\omega_{0tag}L_{reader}}{R_{reader}} = \frac{1}{\sqrt{L_{tag}C_{tag}}}\left(\frac{L_{reader}}{R_{reader}}\right), \tag{3.21}$$

the reflected impedance is given by:

$$Z_{reflected} = \frac{\omega_{0tag}^2 M^2}{R_{tag}}\ . \tag{3.22}$$

As the effective value of L_{tag} increases,

$$L_{tag}\uparrow \Rightarrow \omega_{0tag} \propto \frac{1}{\sqrt{L_{tag}}}\downarrow$$

$$L_{tag}\uparrow \Rightarrow Q_{tag} \propto \sqrt{L_{tag}}\uparrow$$

$$L_{tag}\uparrow \Rightarrow Q_{reader} \propto \frac{1}{\sqrt{L_{tag}}}\downarrow$$

and since M is constant,

$$L_{tag}\uparrow \Rightarrow Z_{reflected} \propto \frac{1}{L_{tag}}\downarrow .$$

Any gains in signal strength $(\Delta\theta)_{\max}$ by the increase in the quality factor of the tag, Q_{tag}, is over shadowed (Figure 3.11) by the decrease in Q_{reader} and $Z_{reflected}$ due to the reduction in the operating resonant frequency, ω_{0tag}, of the tag. Table 3.1 shows that as $\omega_{0tag}\downarrow Q_{reader}\to 1$ especially for large L_{tag}, pushing the signal into the resistive baseline. This reduction in Q, combined with the reduction in reflected impedance, contributes to the decrease in $(\Delta\theta)_{\max}$ scaling approximately as the inverse $\sqrt{L_{tag}}$.

3.4.2 Tag Resistance (R_{tag})

The variations in the effective value of R_{tag} arises from changes in the resistance of a series connected resistive transducer (R_X) e.g. ESS corrosion sensor. Increasing R_X causes an increase in the effective value of R_{tag}. This increase in resistance reduces the quality factor (Q_{tag}) of the tag. At resonance, $Q_{tag} = \frac{1}{R_{tag}}\sqrt{\frac{L_{tag}}{C_{tag}}}$, since all other variable remain unchanged, $Q_{tag} \propto \frac{1}{R_{tag}}$. The response (Figure 3.12) of the signal strength $(\Delta\theta)_{\max}$ exhibits a similar inverse linear dependence on the value of R_{tag}. The reduction in signal strength is attributed to the damping of the tag's resonance with increased R_{tag}.

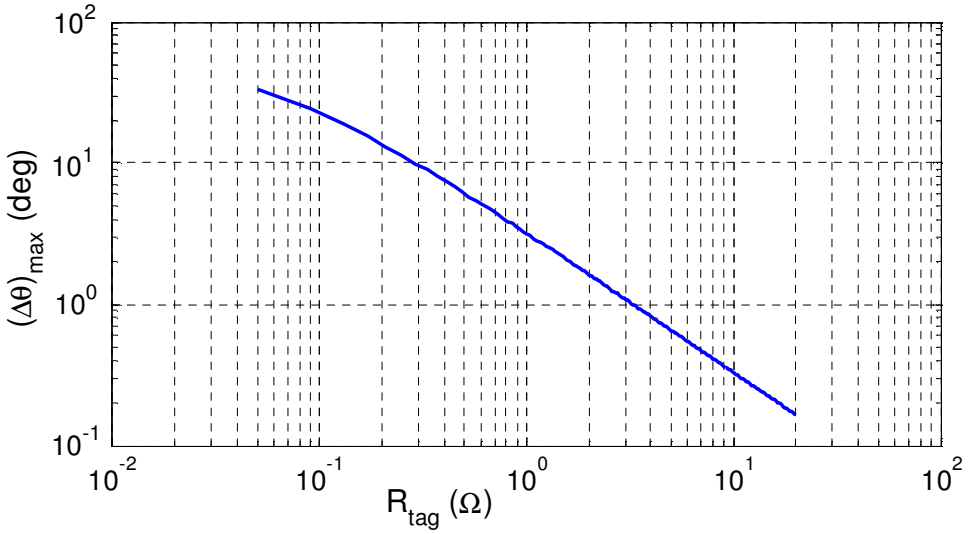

Figure 3.12 Variation of the phase signal strength $(\Delta\theta)_{\max}$ in response to the changing effective values of R_{tag} caused by a resistive transducer (R_X) connected in series with the tag. $R_{tag} \uparrow \Rightarrow Q_{tag} \propto \frac{1}{R_{tag}} \downarrow$ also, $(\Delta\theta)_{\max} \propto \frac{1}{R_{tag}}$

3.4.3 Tag Capacitance (C_{tag})

Changes in the effective value of C_{tag} due to changes in the value of a series- or parallel-connected capacitive transducer C_X, primarily affects only the resonant frequency (ω_{0tag}) of the tag. Reducing ω_{0tag} affects the signal strength $(\Delta\theta)_{\max}$ in a manner similar to L_{tag} except since $Q_{tag} \propto \frac{1}{\sqrt{C_{tag}}}$ and $\omega_{0tag} \propto \frac{1}{\sqrt{C_{tag}}}$ there is no trade off between Q_{tag} and ω_{0tag}. In this case signal strength $(\Delta\theta)_{\max} \propto \frac{1}{\sqrt{C_{tag}}}$, so lower values of C_{tag} provide stronger signal strength. The lower bound on the value of C_{tag} i.e the upper on ω_{0tag} is set by the self resonant frequency of the reader $\omega_{0reader} = \frac{1}{\sqrt{L_{reader}C_{reader}}}$.

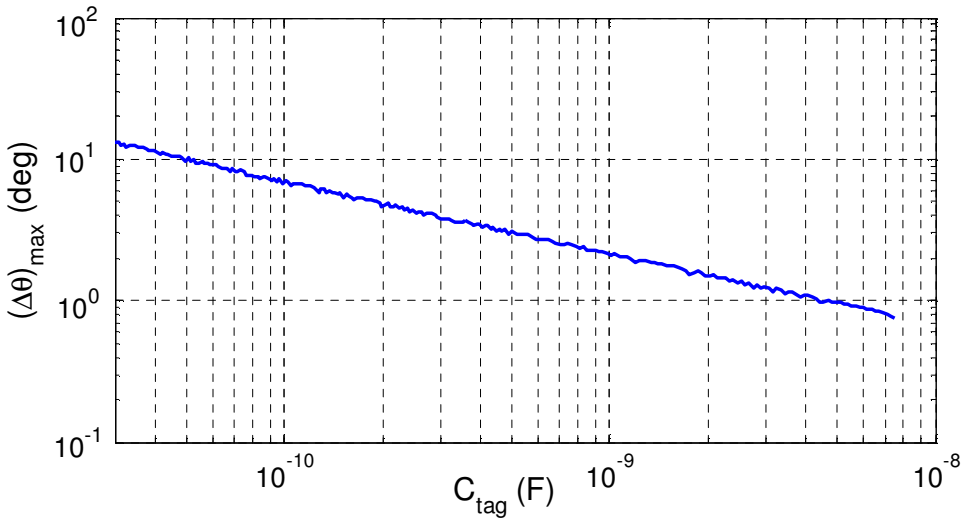

Figure 3.13 Variation of the phase signal strength $(\Delta\theta)_{\max}$ in response to the changing effective values of C_{tag} caused by a capacitive transducer (C_X) connected in series/parallel with the tag. $C_{tag} \uparrow \Rightarrow \omega_{tag} \propto 1/\sqrt{C_{tag}} \downarrow$.Also signal strength, $(\Delta\theta)_{\max} \propto 1/\sqrt{C_{tag}}$.

3.4.4 Mutual Inductance (*M*)/Coupling Factor (*k*)

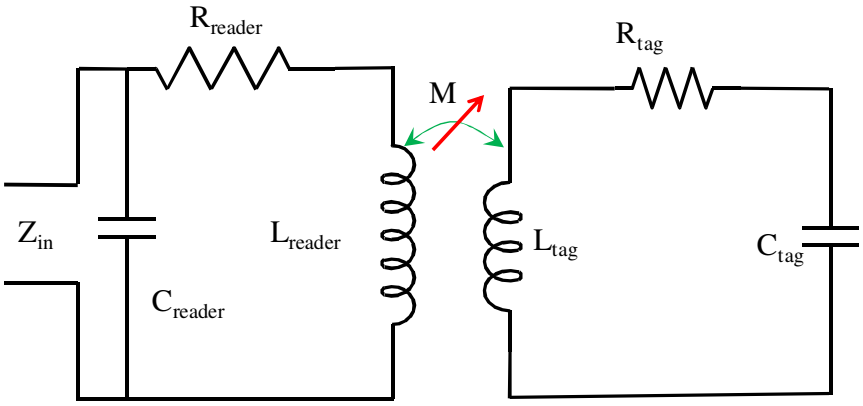

Figure 3.14 Equivalent circuit model used in evaluating the effect of varying mutual inductance *M* keeping all other parameters constant; physically equivalent to changing distance between the reader and tag coil for a fixed orientation.

The mutual inductance *M* or coupling factor *k* between the reader and tag coils is dependent on the shape and size of the coils, the distance between them and their orientation w.r.t each other. It is obvious that these are closely related to the specific geometry of the coils. To evaluate the relationship between *M* and signal strength $(\Delta\theta)_{max}$, the phase response can be calculated for many values of *M*. Changing *M* (Figure 3.14) in this manner by keeping all other reader and tag parameters constant can be physically interpreted as changing distance between the reader and tag coils for a fixed (coaxial) orientation. Since the dimensions and shapes of the coils are known, the *M* values and the corresponding coupling factor (*k*) values can be plotted (Figure 3.15) as a function of distance for a coaxial orientation using Equation. As expected both *M* and *k* decrease with increasing distance (Figure 3.16) and that $M \;\&\; k \propto \frac{1}{dist^3}$.

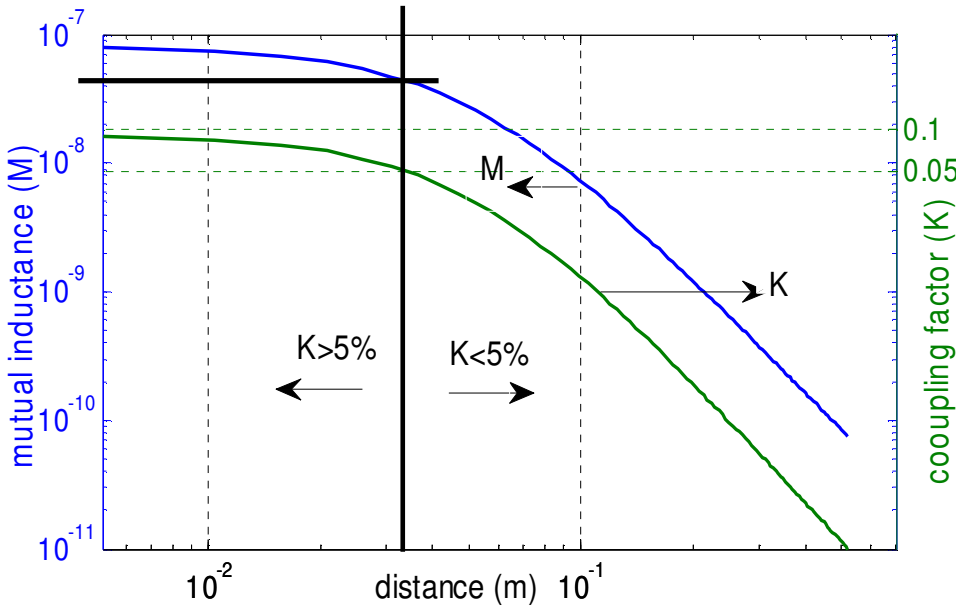

Figure 3.15 Mutual inductance (M) and coupling factor (k) between coaxially separated reader and tag coils as function of the distance of separation, $M \;\&\; k \propto 1/dist^3$.

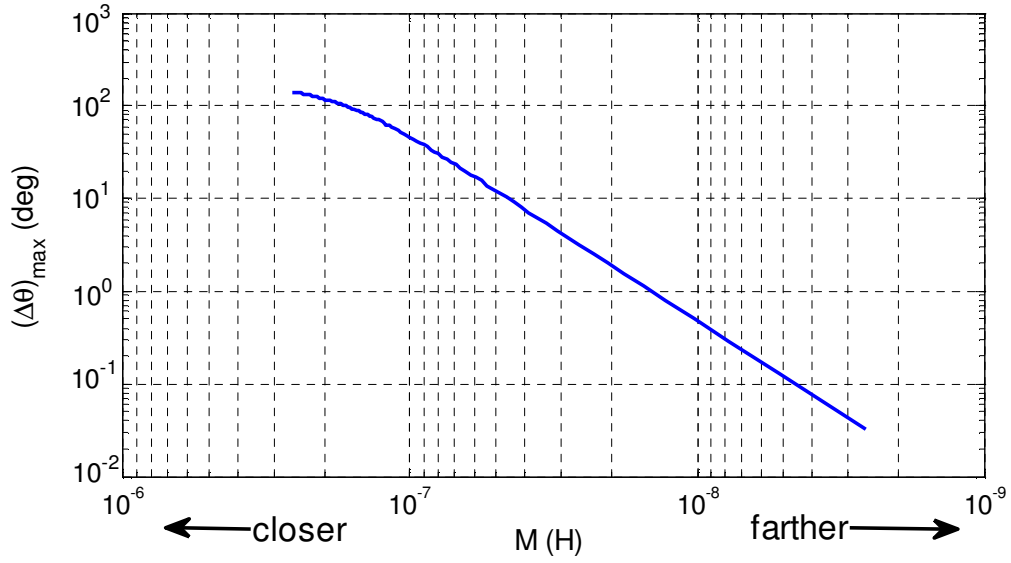

Figure 3.16 Variation of the phase signal strength $(\Delta\theta)_{max}$ in response to the changing mutual inductance (M) solely by changing the distance of separation.

At the resonant frequency of the tag, since reflected impedance is $Z_{reflected} = \frac{\omega_{0tag}^2 M^2}{R_{tag}}$. As mutual inductance increases $M \uparrow \Rightarrow Z_{reflected} \propto M^2 \uparrow$. The signal strength $(\Delta\theta)_{\max}$ exhibits (Figure 3.16) a similar dependence $(\Delta\theta)_{\max} \propto M^2$ on mutual inductance. Since $(\Delta\theta)_{\max} \propto M^2$ and $M \,\&\, k \propto \frac{1}{dist^3}$, it follows that signal strength falls as the sixth power of distance.

$$(\Delta\theta)_{\max} \propto \frac{1}{dist^6}. \tag{3.23}$$

This relationship severely limits tag/sensor detection at larger distances (read range).

Chapter 4: Noise/Detection Limit

4.1 I-Q METHOD FOR MEASURING PHASE:

To measure the phase of an unknown impedance Z, the impedance is driven by a swept frequency sinusoidal source $V_{in} = A_V \cos(\omega t)$, where A_V is the magnitude of the source voltage and ω is the angular frequency in rad/s. It draws a current $I_{in} = A_I \cos(\omega t + \theta)$ where, A_I is the magnitude of the current and θ is its phase shift due to the impedance Z, as shown in Figure 4.1.

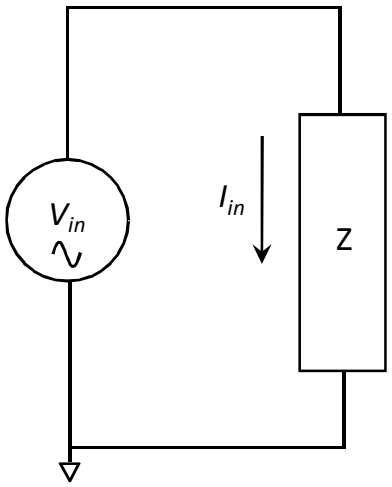

Figure 4.1 Impedance Z driven by a sinusoidal voltage source V_{in} draws a current I_{in}

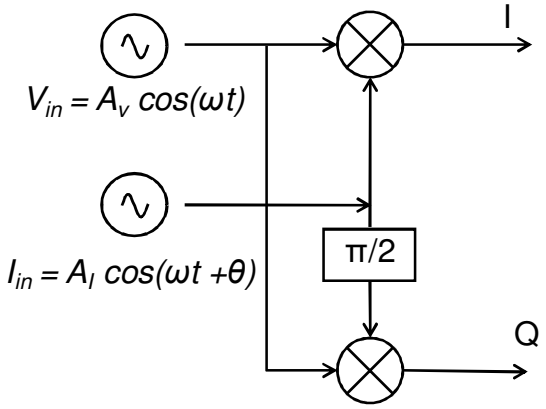

Figure 4.2 Schematic representation of the generation of I and Q components

The current I_{in} is split into $I_{inI} = A_I \cos(\omega t + \theta)$ which is in-phase signal with I_{in} and a 90 degree phase shifted signal $I_{inQ} = A_I \cos\left(\frac{\pi}{2} - (\omega t + \theta)\right) = A_I \sin(\omega t + \theta)$, which is in quadrature to I_{in} . As illustrated in Figure 4.2, V_{in} is mixed with the signals I_{inI} and I_{inQ} separately at the two mixers as follows:

$$
\begin{aligned}
&I_I = I_{inI} \cdot V_{in} \\
&Q_I = I_{inQ} \cdot V_{in} \\
&I_I = A_I \cos(\omega t + \theta) \cdot A_V \cos(\omega t) \\
&I_I = \frac{A_I A_V}{2}\left\{\cos\left((\omega t + \theta) - \omega t\right) + \cos\left((\omega t + \theta) + \omega t\right)\right\} \\
&let\ \frac{A_I A_V}{2} = A; \qquad (4.1) \\
&I_I = \underbrace{A\cos(\theta)}_{DC \propto \theta} + \underbrace{A\cos(2\omega t + \theta)}_{HF - filtered\ out} \\
&Q_I = A_I \sin(\omega t + \theta) \cdot A_V \cos(\omega t) \\
&Q_I = \frac{A_I A_V}{2}\sin\left((\omega t + \theta) - \omega t\right) + \sin\left((\omega t + \theta) + \omega t\right) \\
&Q_I = \underbrace{A\sin(\theta)}_{DC \propto \theta} + \underbrace{A\sin(2\omega t + \theta)}_{HF - filtered\ out}
\end{aligned}
$$

The high frequency component is filtered out, leaving the in-phase d.c. component $I = I_I = \underbrace{A\cos(\theta)}_{DC \propto \theta}$ and the qudrature-phase d.c. component $Q = Q_I = \underbrace{A\sin(\theta)}_{DC \propto \theta}$. The ratio of the two components $\frac{Q}{I} = \frac{A\sin(\theta)}{A\cos(\theta)}$, is used to obtain the phase angle of the current θ_I :

$$\theta = \theta_I = \tan^{-1}\left(\frac{Q}{I}\right) \qquad (4.2)$$

The phase angle *(θ_Z)* of the impedance *Z* is obtained as follows:

$$\theta_Z = \tan^{-1}\left(\frac{V_{in}\angle 0}{I_{in}}\right) \tag{4.3}$$

Now, for V_{in} = 1V, and rewriting I_{in} in terms of I and Q we have,

$$\theta_Z = \tan^{-1}\left(\frac{1}{I + jQ}\right) = \tan^{-1}\left(\frac{-Q}{I}\right). \tag{4.4}$$

$$\theta_Z = \tan^{-1}\left(\frac{-A\sin(\theta)}{A\cos(\theta)}\right). \tag{4.5}$$

4.2 PHASE UNCERTAINTY:

All measurements are affected by the presence of finite noise. At a constant V_{in}, the measured I_{in} is split into its I and Q components. Hence any noise present in the measurement if I_{in} is perfectly correlated i.e. the in-phase and quadrature phase channels are corrupted by identical noise. Also if the instrument is noiseless, and the circuit/component to be measured is passive, the dominant noise is thermal noise.

4.2.1 Thermal Noise of Resistor:

To understand the effects of thermal noise on a phase measurement, consider the phase measurement of a 50Ω non-ideal resistor using the above described I-Q method. Further, let the measurements be performed at room temperature (T=300 K).

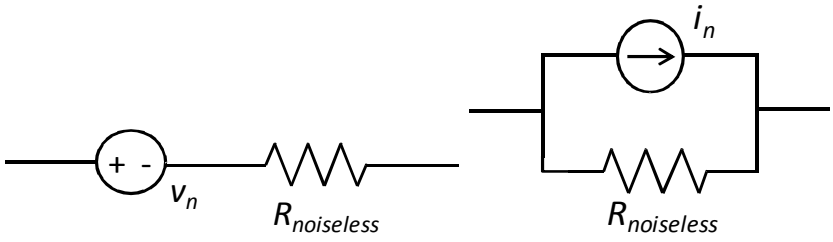

Figure 4.3 Thevinin and Norton equivalent models of a non ideal (noisy) resistor

The non-ideal resistor can be represented by a voltage source in series with an ideal noiseless resistor. The power spectral density- $S_{VV}(f)$ (mean square voltage /Hertz) is given by:

$$S_{VV}(f) = 4k_B TR \quad \left(V^2/Hz\right). \tag{4.6}$$

Where k_B is Boltzmann's constant given by 1.3806504 x 10-23 J/K, T is the absolute temperature in Kelvin (K) and R is the value of the resistor in Ohms (Ω). The mean square voltage is a measure of the variance (σ_v^2) of the noise voltage and is

$$S_{VV} = \sigma_v^2 = v_n^2 = \int_{-\infty}^{\infty} 4k_B TR\, df \quad \left(V^2\right). \tag{4.7}$$

For a given bandwidth Δf, the root mean square (RMS) of the noise voltage which is also a measure of its standard deviation is given by:

$$\sigma_v = v_n = \sqrt{4k_B TR\Delta f} \quad (V).$$

The RMS noise voltage for a 50Ω resistor at 300K is 0.91nV≈1nV. The noise voltage source in series with a noiseless resistor model can be expressed in current noise terms by its Norton equivalent. This is represented by a noise current source in parallel with a noiseless resistor. The RMS value of the noise current (A) source is given by:

$$\sigma_i = i_n = \sqrt{\frac{4k_B T\Delta f}{R}} \quad (A). \tag{4.9}$$

Using the Norton equivalent of the voltage noise, the RMS current noise of the 50Ω resistor at 300K is 0.018nA ≈0.02nA. Since the phase is estimated from a

measurement of the *I & Q* components of current, to be able to compare the measured current to noise, the current noise (i_n) model is used.

We supply a swept-frequency sinusoidal voltage (V_{in}) and measure the current (I_{in}). The *I & Q* components of the measured current yieldtan^{-1}(-*Q/I*), which provides an estimate of the phase of the resistor (impedance).

The expression for computing phase - θ_Z of *Z* can be expressed in terms of the magnitude of current $|I_{in}|$ as:

$$\theta_Z = \tan^{-1}\left(\frac{-|I_{in}|\sin(\theta)}{|I_{in}|\cos(\theta)}\right) \tag{4.10}$$

In the presence of additive random noise, we add random variables r1 and r2 giving:

$$\theta_Z = \tan^{-1}\left(\frac{-|I_{in}|\sin(\theta)+r_1}{|I_{in}|\cos(\theta)+r_2}\right) \tag{4.11}$$

Assuming that the instrument is noiseless then the noise is perfectly correlated i.e. the in-phase and quadrature phase channels are corrupted by roughly identical noise (r1 = r2 = r).

$$\theta_Z = \tan^{-1}\left(\frac{-|I_{in}|\sin(\theta)+r}{|I_{in}|\cos(\theta)+r}\right) \tag{4.12}$$

If the circuit/component to be measured is passive, the noise contribution chiefly arises from thermal noise. Furthermore, we can represent $r = \sigma_i \cdot n$ where σ_i the RMS (standard deviation) of the noise current and *n* is a standard normal distribution.

$$\theta_Z = \tan^{-1}\left(\frac{-|I_{in}|\sin(\theta)+\sigma_i \cdot n}{|I_{in}|\cos(\theta)+\sigma_i \cdot n}\right) \tag{4.13}$$

Rearranging the Equation 4.13 we have:

$$\theta_Z = \tan^{-1}\left(\frac{-\frac{|I_{in}|}{\sigma_i}\sin(\theta)+n}{\frac{|I_{in}|}{\sigma_i}\cos(\theta)+n}\right) \tag{4.14}$$

Here we define signal to noise ratio of current as:

$$SNR_i = \frac{|I_{in}|}{\sigma_i} \tag{4.15}$$

substituting in the Equation 4.14 yields:

$$\theta_Z = \tan^{-1}\left(\frac{-SNR_i\sin(\theta)+n}{SNR_i\cos(\theta)+n}\right) \tag{4.16}$$

The uncertainty (σ_θ) in the measurement of phase of θ_Z , can be estimated from the joint probability density function (PDF) of the Equation 4.16. Alternatively it can be done statistically using MATLAB ®'s randn function to generate n-trials of a standard normal distribution. The latter approach is used here.

For the case of a resistor, the phase angle θ_Z is ideally 0^o, if SNR_i is known, we can estimate σ_θ. Since, for the 50Ω resistor at 300K, the RMS noise current σ_i =0.02nA, if the SNR_i = 100, then |Iin|= 2nA implies that the source voltage Vin= 100nV Figure 4.4(top). The mean value of phase μ_θ =0.01^o, and the uncertainty σ_θ=0.57^o. If a more realistic source voltage of 1V is used, |Iin|= 0.02A, SNR_i = 109, μ_θ =6.6E-11^o and negligible phase uncertainty σ_θ=5.7E-8^o. Figure 4.4 (middle). On scaling the axis, the random variation of the phase becomes visible Figure 4.4(bottom).

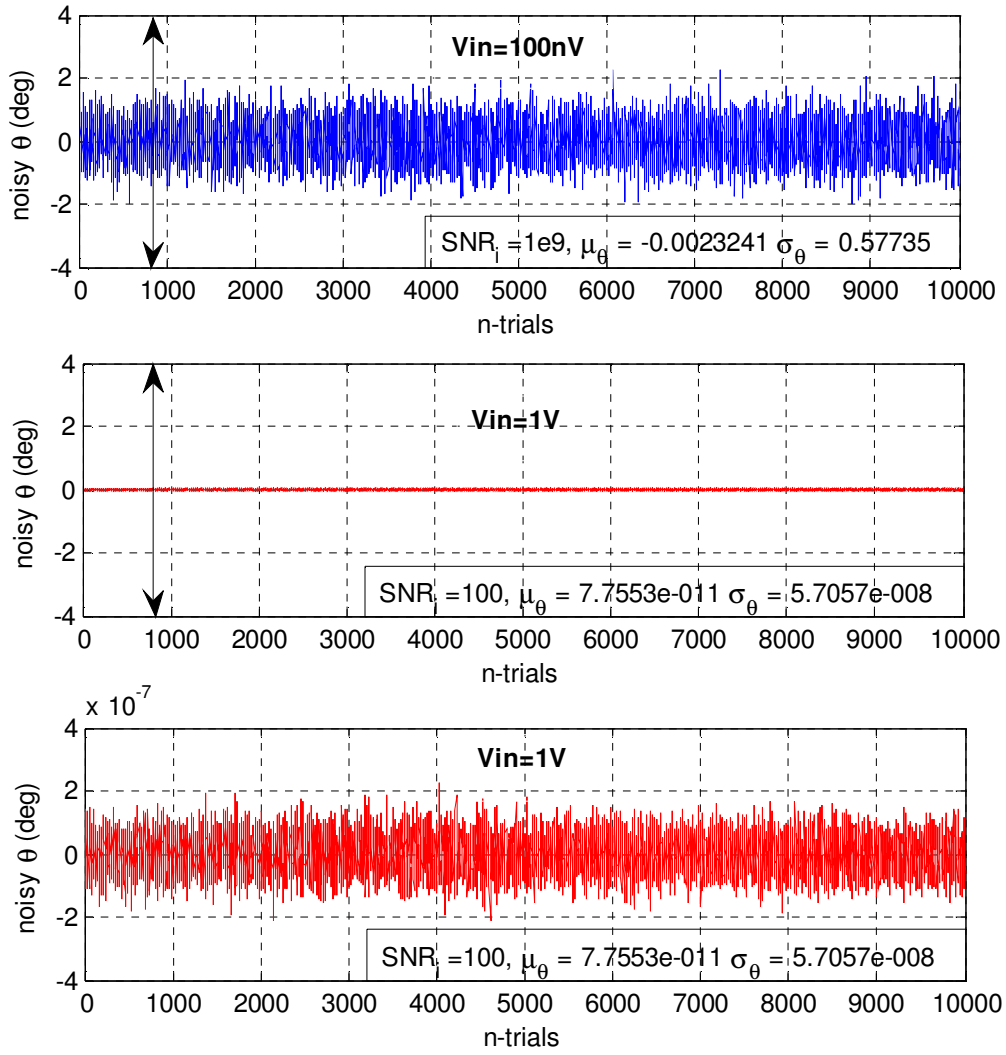

Figure 4.4 Uncertainty in the estimation of the phase of a 50Ω resistor due to its thermal noise for input current measured at three different input voltages (SNRi).

4.2.2 Universal Phase Uncertainty Surface

The above Equation 4.16 in terms of SNR_i, θ and n can be used to generate a surface which describes the variation of phase uncertainty σ_θ for arbitrary SNR_i and θ_i(phase of current). This can be used as a quasi-universal look up table to determine σ_θ if the values of SNR_i and θ are known. The actual values of SNR_i and θ are determined by the circuit/component being tested. Since we are interested in the values of θ between

-90^o and 90^o, such a surface is generated for these values of θ for an arbitrary range of SNR_i between 0.1-10^6 (Figure 4.5).

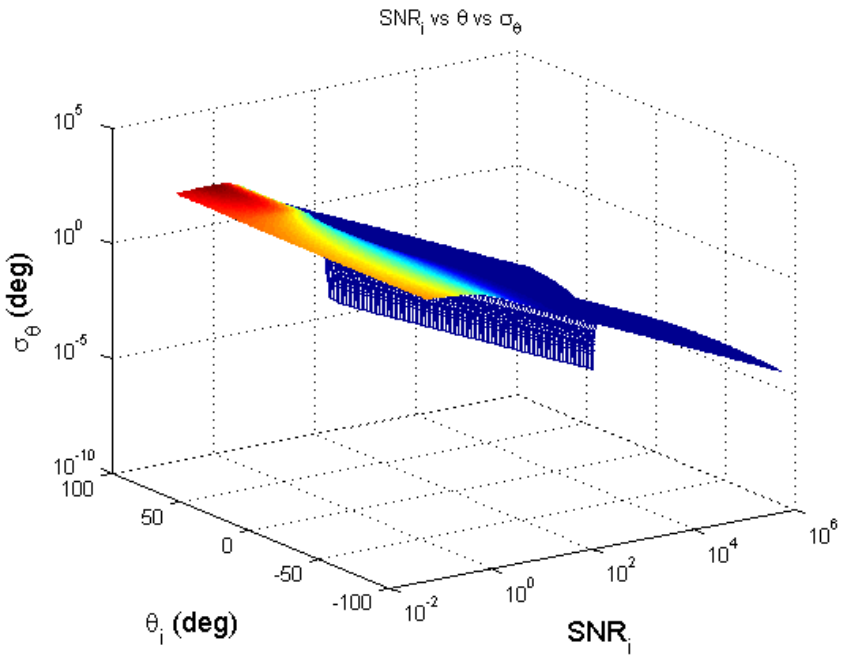

Figure 4.5 A surface of phase uncertainty (σ_θ) values estimated for arbitrary values of signal-to noise-ratio (SNR_i) and phase (θ_i) of current

The Figures 4.6 (top) and (bottom) are projections of the surface along the XZ (SNR_i, σ_θ) and YZ(θ_i, σ_θ) axes respectively. The plots suggest that the uncertainty in measuring the phase of impedance (θ_Z), σ_θ improves (reduces) almost linearly with increasing SNRi for values of SNRi>10 for all values of the phase of the current (θ_i). For SNRi >104, $\sigma_\theta < 0.01^o$ for all values of phase θ_i. The minimum σ_θ occurs at $\theta_i=45^o$ for all SNR_i. This is due to the assumption that the I and Q channels are corrupted by identical noise (completely correlated), so at 45^o I and Q are exactly identical i.e $\theta_Z = \tan^{-1}(1)$ hence $\sigma_\theta \approx 0$.

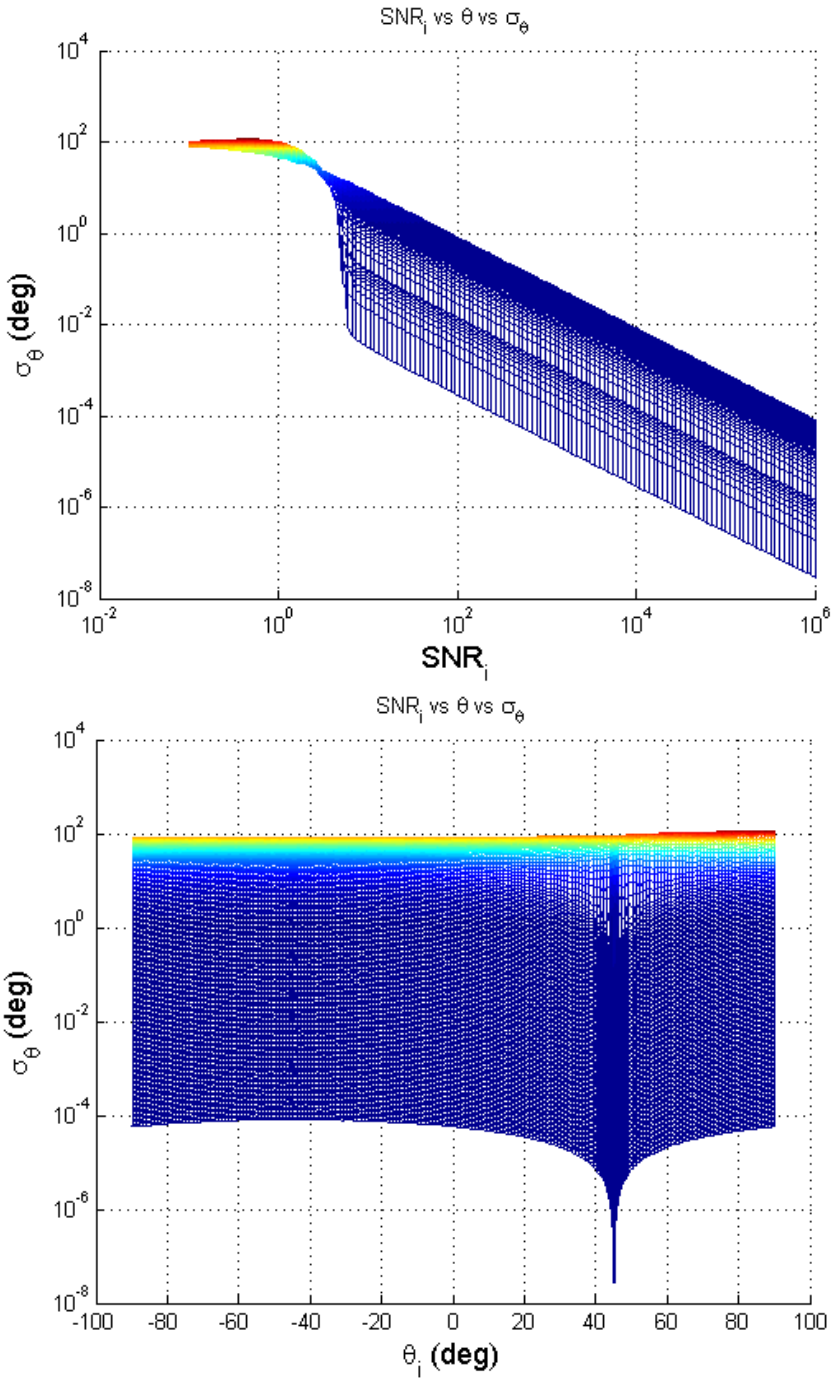

Figure 4.6 (top) and (bottom) are projections of the surface from Figure 4.5 along the XZ (SNR_i, σ_θ) and YZ(θ_i, σ_θ) axes respectively

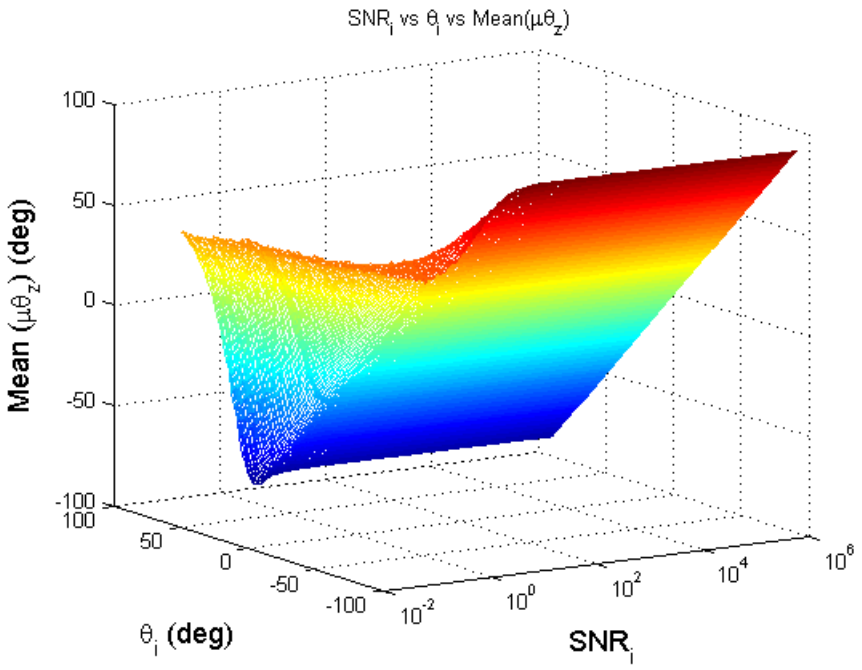

Figure 4.7 A surface of expected values (mean μ) of phase of impedance θ_Z estimated in the presence of noise for arbitrary values of signal-to noise-ratio (SNR_i) and phase (θ_i) of current.

The above Figure 4.7 is a surface that shows the variation of the expected value (mean = $\mu\theta_Z$) of the phase of impedance (θ_Z) for various phase angles of the current (θ_i) and SNR_i. The Figure 4.8 (top) and (bottom) are the projections of the surface along the XZ (SNR_i, $\mu\theta_Z$) and YZ(θ_i, $\mu\theta_Z$) axes respectively. Since σ_θ decreases as SNR_i increases, we observe Figure 4.8 (top) that for $SNR_i > 10$ the expected value $\mu\theta_Z$ begins approaching the actual value of θ_Z. For larger values of SNR_i (>100) the relationship between $\mu\theta_Z$ and θ_i follows the $\theta_Z = -\theta_i$ behavior yielding a straight line with slope -1, as expected Figure 4.8 (bottom)

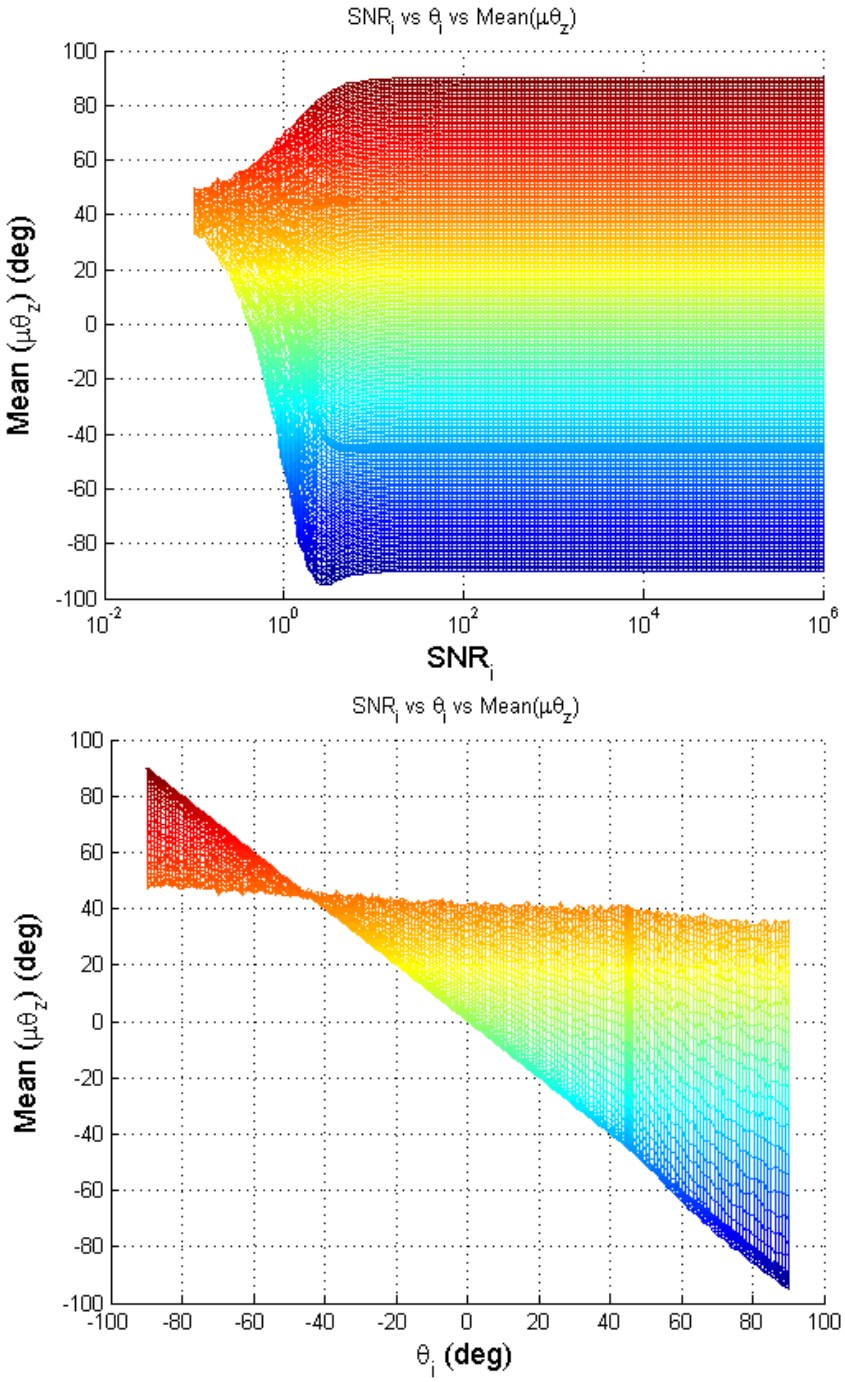

Figure 4.8: (top) and (bottom) are the projections of the surface from Figure 4.7 along the XZ (SNR_i, $\mu\theta_Z$) and YZ(θ_i, $\mu\theta_Z$) axes respectively

4.3 PHASE UNCERTAINTY IN ESS SYSTEMS

Phase uncertainty σ_θ, is a function of SNR_i and θ_i. SNR_i is a function of the value of σ_i and I_{in}. All three quantities θ_i, σ_i and I_{in} depend on the component/circuit under test. Since our coupled reader and tag circuit is comprised entirely of passive components, we consider only the effect of Johnson-Nyquist (thermal) noise. If the impedance at the input of the reader is Z_{in} , the PSD of the voltage noise referred to the input is given by Equation 4.17 where, k_B is Boltzmann's constant in J/K, T is the absolute temperature in *K*, *f* is the frequency in Hz and $\Re\{Z_{in}(f)\}$ is the real part of the frequency dependent complex input impedance Z_{in}.

$$S_{VV}(f) = 4k_B T \,\Re\{Z_{in}(f)\} \quad \left(V^2/Hz\right) \tag{4.17}$$

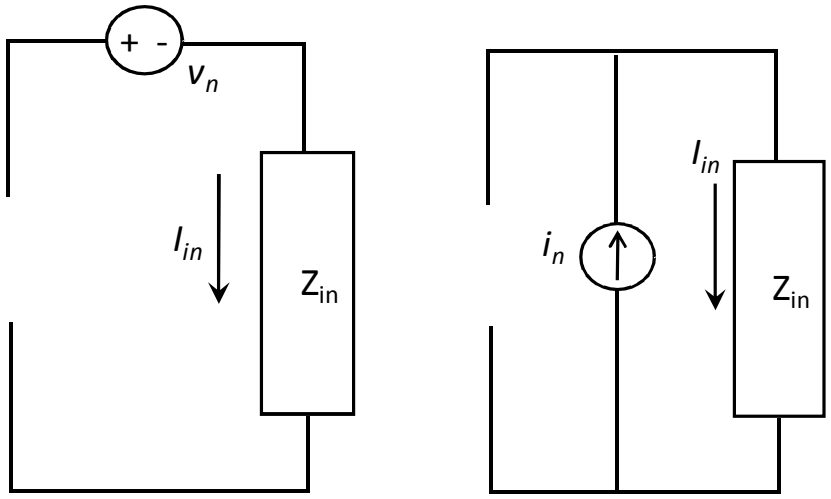

Figure 4.9 Thevinin and Norton equivalent circuits for voltage and current noise referred to the input

In order to obtain the PSD of the noise current $S_{II}(f)$, the voltage noise PSD $S_{vv}(f)$ is:

$$S_{II}(f) = S_{VV}(f)\left|H(f)\right|^2 \tag{4.18}$$

where $\left|H(f)\right|^2$ is the power transfer function[26] . In this case $\left|H(f)\right|^2 = \frac{1}{\left|Z_{in}(f)\right|^2}$, so substituting, and expanding $S_{vv}(f)$ from Equation 4.17 we obtain:

$$S_{II}(f) = S_{VV}(f)\frac{1}{\left|Z_{in}(f)\right|^2} \tag{4.19}$$

$$S_{II}(f) = 4k_B T\,\Re\{Z_{in}(f)\}\frac{\Re\{Z_{in}(f)\}}{\left|Z_{in}(f)\right|^2} \tag{4.20}$$

Since $\Re\{Y_{in}(f)\} = \frac{\Re\{Z_{in}(f)\}}{\left|Z_{in}(f)\right|^2}$ where $\Re\{Y_{in}(f)\}$ is the real part of the frequency dependent complex input admittance $Y_{in}(f)$, we have

$$S_{II}(f) = 4k_B T\,\Re\{Y_{in}(f)\}\ \left(A^2/Hz\right) \tag{4.21}$$

The variance or mean squared current noise σ_i^2 or i_n^2 for a finite bandwidth (Δf) is given by:

$$\sigma_i^2 = S_{II} = 4k_B T\,\Re\{Y_{in}(f)\}\cdot\Delta f\ \left(A^2\right) \tag{4.22}$$

The standard deviation (σ_i) or r.m.s. current noise i_n for a 1Hz bandwidth (Δf =1Hz) is:

$$\sigma_i = i_n = \sqrt{4k_B T\,\Re\{Y_{in}(f)\}}\ (A) \tag{4.23}$$

For known transfer function $Z_{in}(f)$ and $Y_{in}(f)$, σ_i I_{in} & θ_i can be used to determine phase uncertainty σ_θ.

In the coupled reader and tag system we perform two phase measurements:

- Phase (θ_Z) of input impedance Z_{in} when only the reader is present and tag is absent (coupling factor k=0) which provides a baseline i.e. $\theta_z\big|_{k=0}$.
- Phase (θ_Z) of input impedance Z_{in} when both the reader and tag are present (coupling factor $k \neq 0$) i.e. $\theta_z\big|_{k\neq 0}$

Signal strength is a measure of the size of the phase dip and was defined as $\Delta\theta = \theta_z\big|_{tag\ absent} - \theta_z\big|_{tag\ present}$ which is equivalent to $\Delta\theta = \theta_z\big|_{reader\ only} - \theta_z\big|_{reader+tag}$. Using the notation from above,

$$\Delta\theta = \theta_z\big|_{k=0} - \theta_z\big|_{k\neq 0} \tag{4.24}$$

For every measurement of θ, the associated uncertainty is σ_θ. Thus for $\Delta\theta$, we have $\sigma_\theta\big|_{k=0}$, and $\sigma_\theta\big|_{k=0}$ which are the uncertainties of $\theta_z\big|_{k=0}$ and $\theta_z\big|_{k\neq 0}$ respectively. Thus the total uncertainty in the measurement of $\Delta\theta$ denoted by $\sigma_{\Delta\theta}$ is given by:

$$\sigma_{\Delta\theta} = \sqrt{\sigma_\theta^2\big|_{k=0} + \sigma_\theta^2\big|_{k\neq 0}} \tag{4.25}$$

where $\sigma_\theta^2\big|_{k=0}$ and $\sigma_\theta^2\big|_{k\neq 0}$ are the variances of $\sigma_\theta\big|_{k=0}$, and $\sigma_\theta\big|_{k=0}$ respectively. Further we define signal to noise ratio for $\Delta\theta$ i.e. $SNR_{\Delta\theta}$ as:

$$SNR_{\Delta\theta} = \frac{\Delta\theta}{\sigma_{\Delta\theta}} \tag{4.26}$$

Thus for our coupled reader and tag combination, if measured with a perfect instrument (i.e. no instrument noise), driven by a unit source voltage, the component values and thermal noise determine $\sigma_{\Delta\theta}$ which sets the minimum detection limit (MDL).

A surface which shows the variation of $\sigma_{\Delta\theta}$ for arbitrary values of SNR_i and $\Delta\theta$ similar to that of phase uncertainty σ_θ can now be plotted. Although it can be used as a

look up table to estimate $\sigma_{\Delta\theta}$, such a surface has to be specific to the baseline from which Δθ is measured. As an example, he case of an inductive baseline $\theta|_{k=0} = 90^o$ is considered.

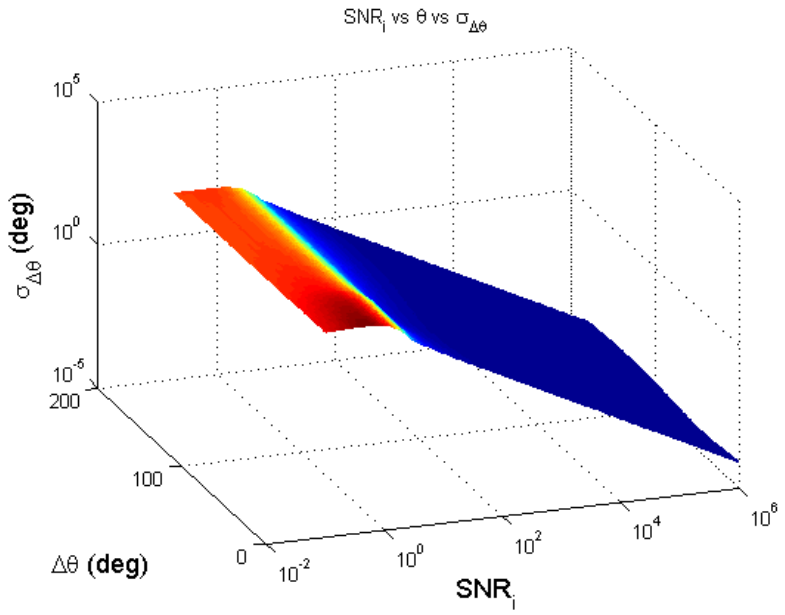

Figure 4.10 A the surface plot for uncertainly $\sigma_{\Delta\theta}$ in estimating signal strength Δθ when measured from an inductive baseline $\theta|_{k=0} = 90^o$ for arbitrary SNR_i

The Figure 4.10 is the surface plot for Δθ measured from an inductive baseline. The value of $\theta|_{k=0} = 90^o$, is fixed but $\theta|_{k\neq 0}$ can take on values between -90° and +90°. Thus as θ_i varies from +90° to -90°, Δθ varies from 0° to 180°. The uncertainty $\sigma_{\Delta\theta}$ reduces as SNR_i increases for all Δθ. For $SNR_i > 10^4$, $\sigma_{\Delta\theta} < 0.01^o$.

A set of reader and tag coils commonly used in our ESS system are now analyzed. The specifications of these coils are provided in Table 4.1. All coils are single-layer cylindrical short solenoids wound on a cylindrical form using enameled magnet wire.

Specification	Reader (RC1N)	Reader (RC5N)	Tag coil
Radius	5 cm	5 cm	3 cm
Wire gauge (AWG)	18	18	18
Turns (N)	1	5	5
Self Inductance (L)	0.35 μH	6 μH	3.2 μH

Table 4.1 Dimensional specifications of the reader and tag coil geometries used in this analysis and their corresponding lumped element component values

The tag coil is tuned using a 470 pF capacitor to a resonant frequency of 4.1MHz. The source voltage V_{in} is set to 1V. The impedance (Z_{in}) at the input of the reader is calculated using Equation 3.4. The input admittance Y_{in}, the current I_{in}, phase angle of impedance θ_{in} (or θ_Z) and the phase angle of the current θ_i are then computed. The PSD $S_{II}(f)$ is estimated, and the r.m.s. noise current σ_i is calculated using a 1Hz bandwidth. Plugging these values into (Equation 4.16), we determine the phase uncertainty as a function of frequency $\sigma_\theta(f)$. Since the presence of the tag is measured as a deviation from the phase response of the reader's input impedance, the uncertainty in this "baseline" phase response of the reader must first be determined. To determine the baseline uncertainty, we set coupling factor $k = 0$ in the expression for input impedance, effectively measuring the phase response $\theta|_{k=0}$ of only the reader. The coupled "reader + tag" response, in the weakly coupled limit, is then calculated by setting $k = 3\%$ ($\theta|_{k=3\%}$). The signal strength $\Delta\theta$ and its uncertainty $\sigma_{\Delta\theta}$ is determined using Equations 4.25, 4.16 and 4.25.

The resonant frequency of the reader ($\omega_{0reader}$) relative to that of the tag (ω_{0tag}) determines the phase angle of the operating baseline. The three cases considered here are:

1. Inductive Baseline: $+90^o$ → occurs when the $\omega_{0reader} > \omega_{0tag}$ –reader is inductive.
2. Capacitive Baseline: -90^o → occurs when the $\omega_{0reader} < \omega_{0tag}$ –reader is capacitive.
3. Resonant Baseline: 0^o → occurs when the $\omega_{0reader} = \omega_{source}$ –reader is tuned to be resonant at the source frequency.

4.3.1 Inductive ($+90^o$) Baseline:

This is the most frequently used during measurement and testing of our sensors. It is also preferred, since the response easily lends itself to the extraction of *pseudoQ,* which has a well-defined relation to the quality factor Q_{tag} [10]. If no additional tuning capacitors are used, the self resonant frequency (SRF) of the reader sets the upper bound on the maximum ω_{0tag} that can be used. The ω_{0tag} =4.1MHz, and the SRFs for RC1 (ω_{01N}) and RC5 (ω_{05N}) are 190MHz and 18MHz respectively. This ensures that $\omega_{0tag} < \omega_{0reader}$ for both readers. The equivalent circuit and phase response of input impedance (θ_Z) as a function of frequency for a 1-turn and 5-turn reader coil both when tag is absent and present are is shown in Figure 4.11(top) and (bottom) respectively. The deviation from the ideal $+90^o$ phase in the baseline is due to presence finite reader coil resistance and its effect is pronounced at lower frequencies.

The frequency axis is adjusted (1-10MHz) to make the tag response more visible - Figure 4.12 (top). When the tag is absent (reader only), the baseline approaches the inductive $+90^o$ value. Since the 5-turn reader has a larger L/R ratio than the 1-turn coil, its phase baseline is closer to $+90^o$. The presence of the tag produces a phase dip in the reader baseline.

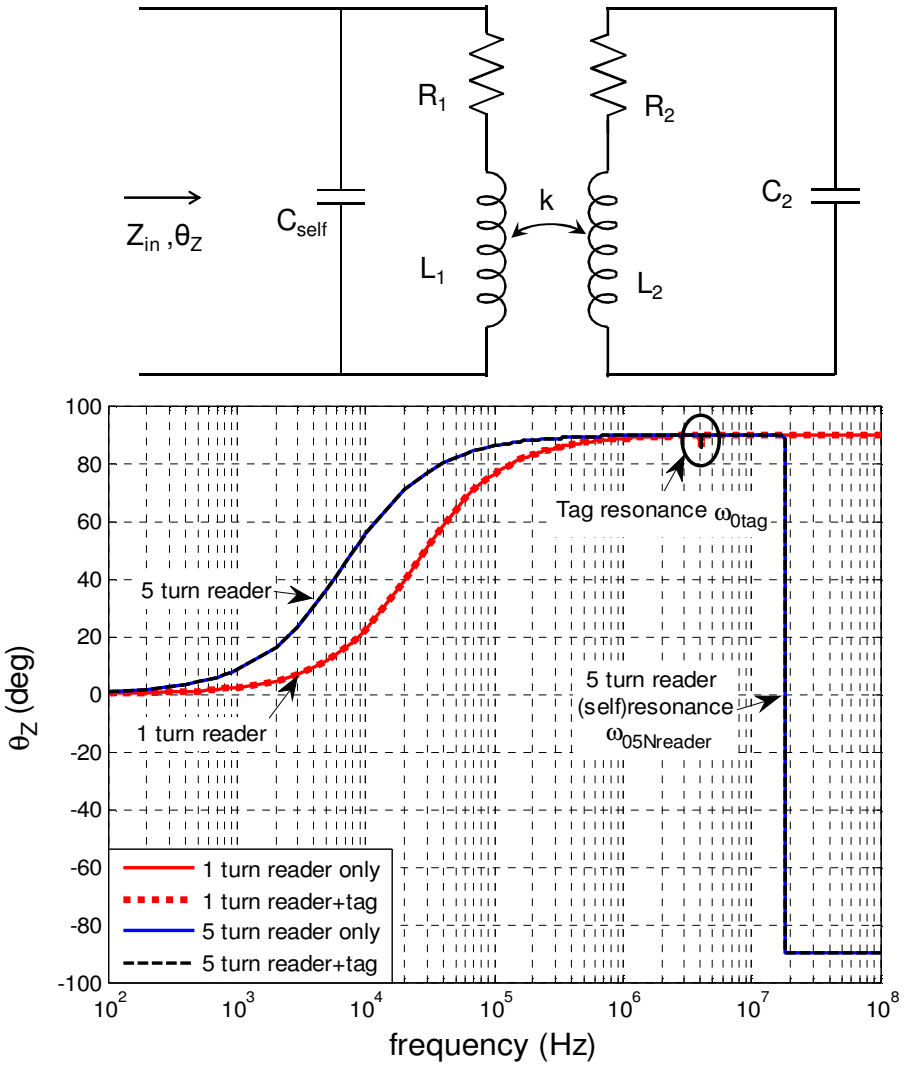

Figure 4.11 (top) Equivalent circuit model used in the analysis, and (bottom) the calculated phase response (θ_Z) of input impedance as measured from the inductive baseline (+90°) of the reader

Since k=3% for RC1 and RC5, the minimum phase θ_{min} occurs at ω_{0tag} (4.1MHz) for both and is ≈85.55° for both cases. In Figure 4.12 (bottom), a small mismatch (0.23°) in signal strength ($\Delta\theta$) is visible. We attribute the deviation of the phase from its baseline for the two cases to the mismatch in their respective baselines (0.24°).

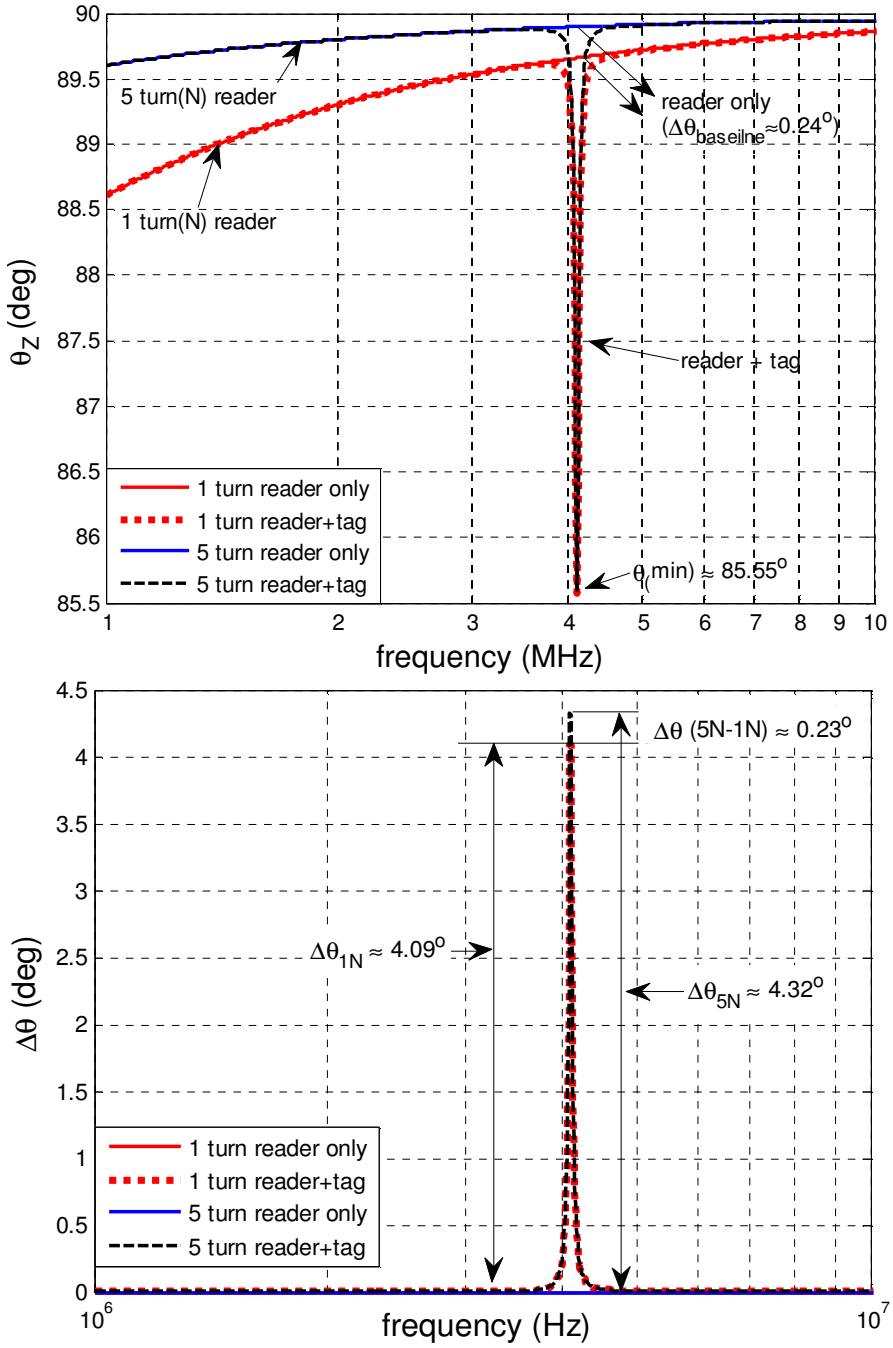

Figure 4.12 (top) The phase response (θ_Z) with the frequency axis is adjusted (1-10MHz) to make the tag response more visible and (bottom) signal strength ($\Delta\theta$) which is the deviation of the phase from its baseline

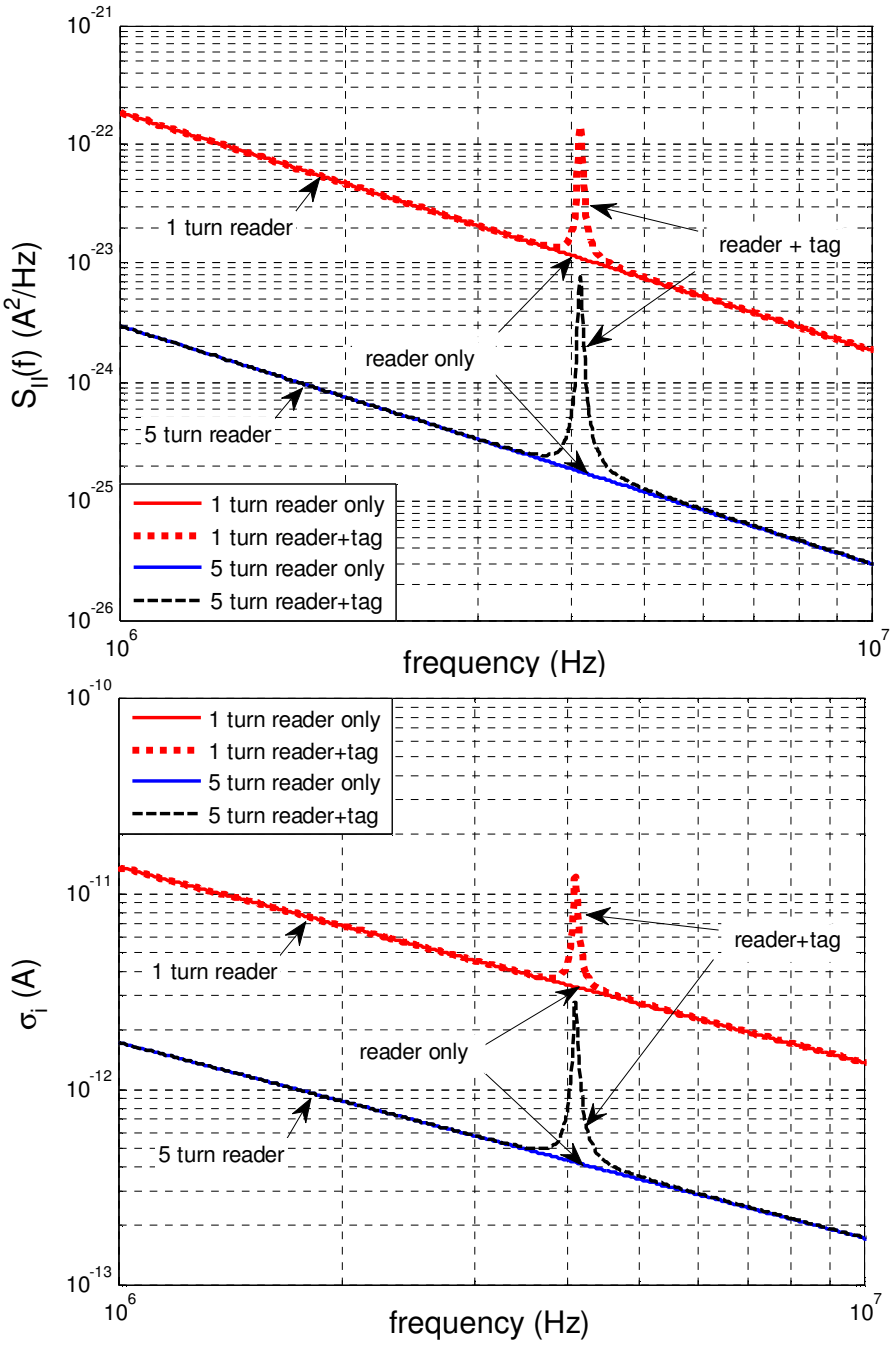

Figure 4.13 (top) Power spectral density ($S_{II}(f)$) of the noise current and (bottom) the r.m.s noise current (σ_i) calculated for a unit bandwidth in the presence and absence (baseline) of the tag when baseline is inductive.

The PSD (Figure 4.13 (top)) of the noise current ($S_{II}(f)$) and the (σ_i) r.m.s noise current (Figure 4.13 (bottom)) (for unit bandwidth) peak at ω_{0tag} when the tag is present. This peaking arises because the noise current is scaled by the resonance response of the tag. The PSD and σ_i are lower for the 5-turn coil than the 1-turn coil. If R_1 and L_1 are the resistance and self inductance of the one turn reader coil, the real part of its input admittance $\Re(Y_{in})$ is given by

$$\Re\left(Y_{in1}\right) = \frac{R_1}{R_1^2 + \omega^2 L_1^2} = \frac{1}{R_1\left(1 + \omega^2 \frac{L_1^2}{R_1^2}\right)} \tag{4.27}$$

Since the number of turns is the only parameter that is changed (N), the resistance (R_5) and self inductance (L_5) of the 5-turn coil is given by $L_5 = N^2 \times L_1$ & $R_5 = N \times R_1$. The real part of the input impedance of the 5-turn coil $\Re\left(Y_{in5}\right)$ can be expressed as:

$$\Re\left(Y_{in5}\right) = \frac{1}{N \cdot R_1\left(1 + N^2 \cdot \omega^2 \frac{L_1^2}{R_1^2}\right)} \tag{4.28}$$

Since the PSD is $S_{II}(f) = 4k_B T \Re(Y_{in})$, it follows that PSD and σ_i are lower for the 5-turn coil than the 1-turn coil. In spite of a lower r.m.s noise current σ_i the signal to noise ratio SNR_i of the 5-turn reader is lower than the 1-turn case (Figure 4.14). The 5-turn reader has a lower magnitude of admittance-$\left|Y_{in}\right|$ (larger magnitude of impedance$\left|Z_{in}\right|$). At a constant source voltage V_{in} it draws a smaller current $I_{in5} < I_{in1}$ which leads to a smaller SNR_i. The "sag" at higher frequencies for the 5-turn reader is the current beginning to roll off due to increase in the impedance near the reader's self resonance which occurs at 18MHz.

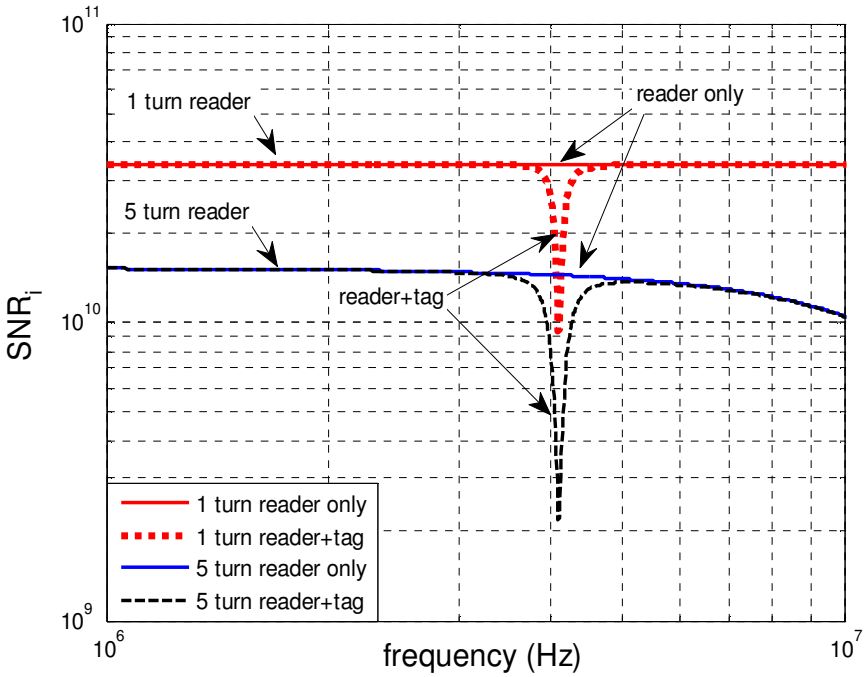

Figure 4.14 Signal-to-noise ratio (SNR_i) of the current I_{in} calculated in the presence and absence (baseline) of the tag when baseline is inductive. Since it draws a smaller current, the SNR_i of 5-turn reader is lower than the 1-turn case.

The lower SNR_i of the 5-turn compared to the 1-turn reader is responsible for the higher phase uncertainty σ_θ in the 5-turn reader (Figure 4.15 (top)), both in the absence (baseline) and presence of the tag. The cumulative effect (since variances add) of the phase uncertainties (σ_θ) in measuring the baseline and when tag present, is the uncertainty ($\sigma_{\Delta\theta}$) in measuring $\Delta\theta$, as shown in Figure 4.15 (bottom). This overall uncertainty describes the ability to measure a phase dip $\Delta\theta$ as the difference between two phase responses in the presence of noise. The maximum uncertainty occurs at the resonant frequency of the tag.

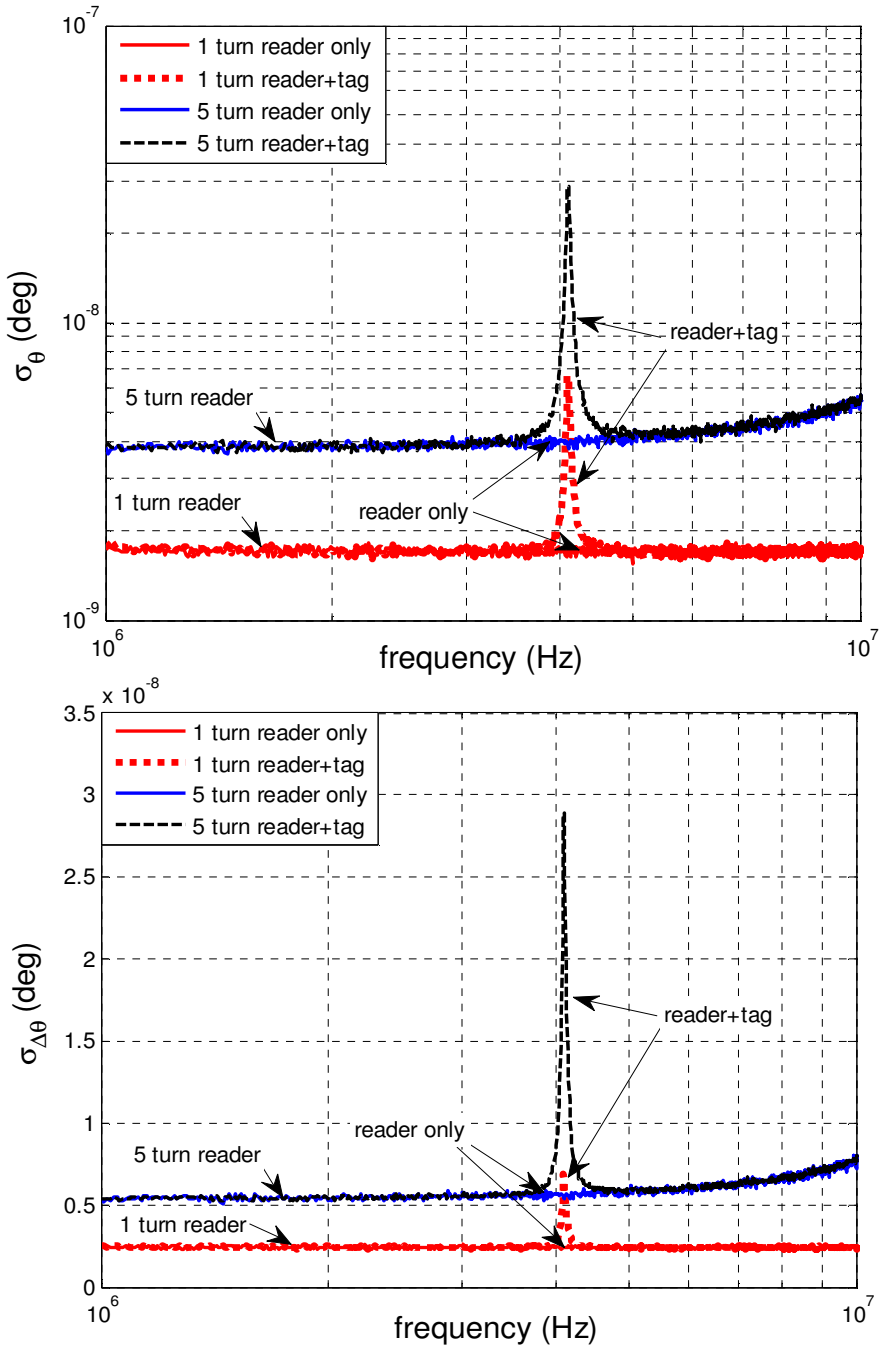

Figure 4.15 (top) The uncertainty (σ_θ) in estimating the phase response in the presence and absence (baseline) of the tag for an inductive baseline. The variances add resulting in the uncertainty ($\sigma_{\Delta\theta}$) in estimation of the signal ($\Delta\theta$) sets the value of the minimum resolvable signal.

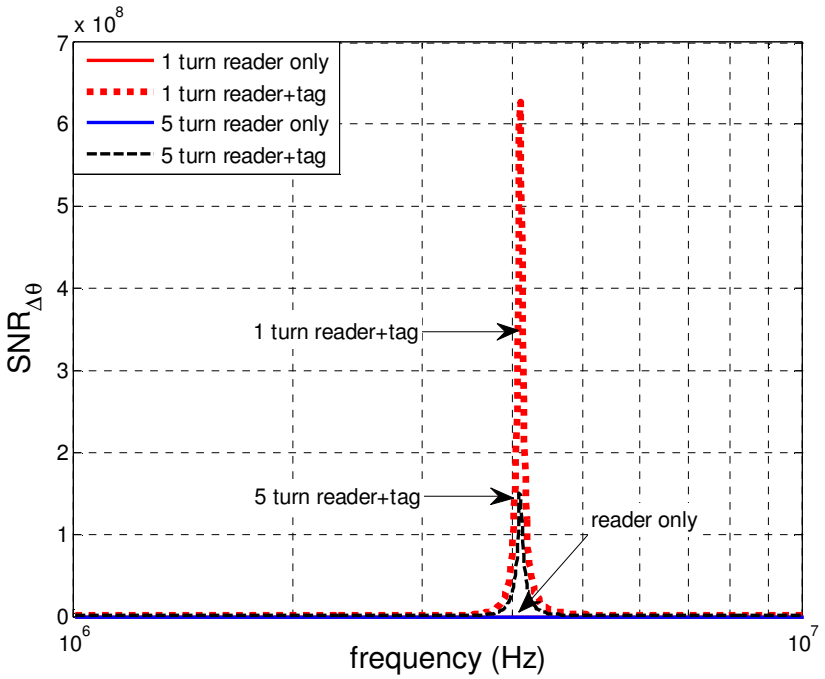

Figure 4.16 Signal-to-noise ratio $SNR_{\Delta\theta}$ is the ratio of phase change ($\Delta\theta$= signal) due to the presence of the tag to the uncertainty in its estimation ($\sigma_{\Delta\theta}$=noise)

Once the value of signal uncertainty $\sigma_{\Delta\theta}$ is determined, it can be compared with the signal strength ($\Delta\theta$) to give a measure of signal to noise ratio $SNR_{\Delta\theta}$ for the ESS system under consideration (Figure 4.16). The extremely large value of $SNR_{\Delta\theta}$ ($\approx 10^8$) in spite of the small signal strength ($\Delta\theta \approx 4^o$) is due to the small value of the noise ($\sigma_{\Delta\theta} \approx 10^{-8}$). The plot suggests that for a given coupling factor, the $SNR_{\Delta\theta}$ decreases with increase in the number of turns, thus the maximum occurring for 1turn reader. It is important to note that this does not necessarily increase read range, since the distance at which k=3% for a 5-turn reader is greater than that for the 1-turn reader.

4.3.2 Capacitive (-90^o) Baseline

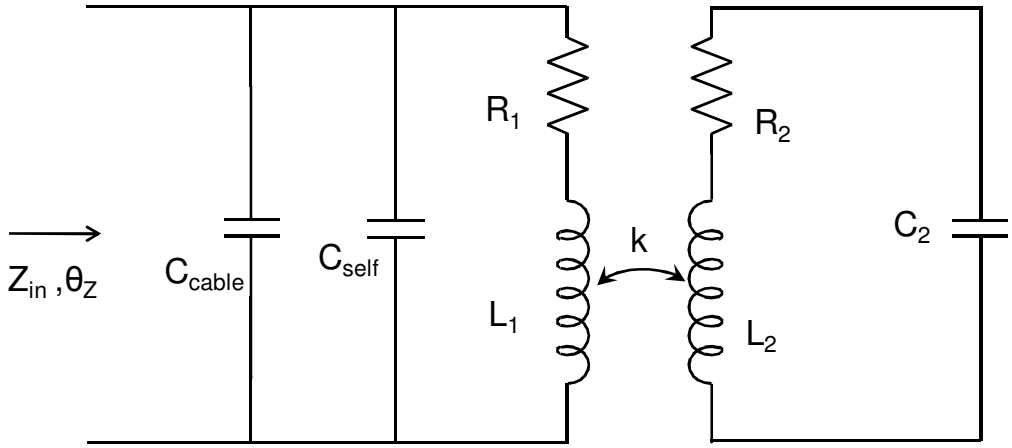

Figure 4.17 Equivalent circuit model used in the analysis of the capacitive baseline case. The increase in reader capacitance is attributed to the parasitic capacitance added by cabling used to connect the reader to the instrument.

The capacitive-baseline case is encountered in the field when, due to limited access, long coaxial cables connect the reader and the impedance analyzer. The increased cabling adds capacitance (C_{cable}) to the reader coil, reducing its resonant frequency ($\omega_{0reader}$). The capacitive baseline can also occur either when a large reader coil (and/or a coil with many turns) is used, and the combination of an increased self inductance (L) and self capacitance (C_{self}) drives down the self-resonant frequency of the reader coil even more. While either excessive cabling or a large reader coil could yield a capacitive baseline ($\omega_{0reader} < \omega_{0tag}$), the large coil increases the coupling factor (*k*), while the cabling does not. To test the effect of measuring from a capacitive baseline without altering the *k*, an additional capacitance C_{cable} is added in parallel across the reader coil such that $\omega_{0reader} < \omega_{0tag}$. This connection mimics the effects of using longer cables. For all calculations when tag is present, k=3% as in the previous case. Figure 4.17 shows the equivalent circuit model used in the calculations.

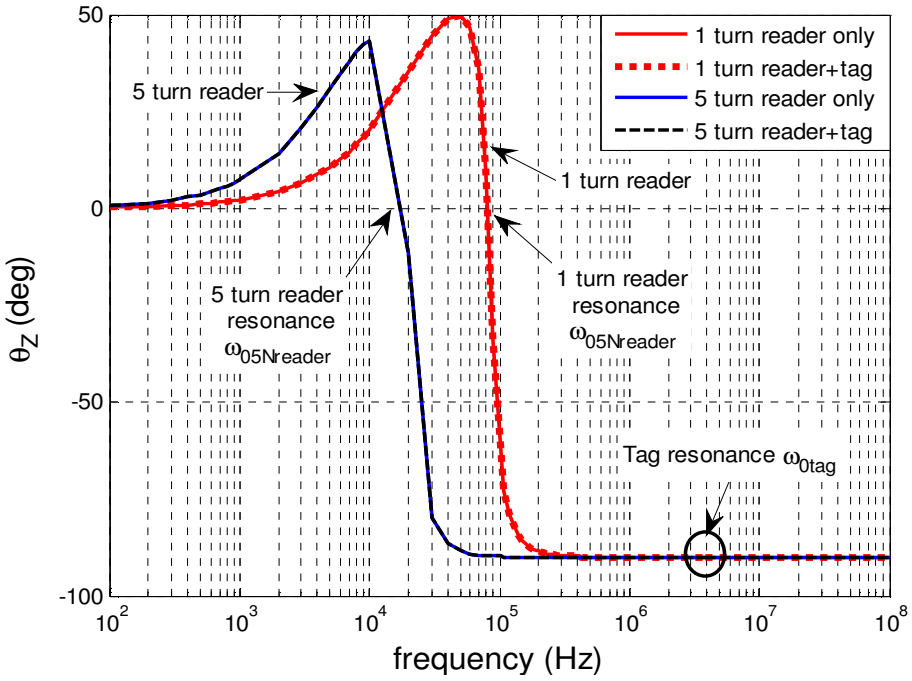

Figure 4.18 The calculated phase response (θ_Z) of input impedance exhibits a series RL circuit behavior until it approaches the resonance frequency of the reader. It is uniformly capacitive (-90^o) at all frequencies above the resonance of the reader.

Figure 4.18 plots the phase response θ_z for the capacitive baseline case. For a fixed reader capacitance C_1 = (C_{cable}+ C_{self}) =10μF the 1- and 5-turn reader coils have $\omega_{0reader}$ =88kHz and $\omega_{0reader}$ =20kHz, respectively. Since $L_{1N} < L_{5N}$, $\omega_{01Nreader} > \omega_{05Nreader}$. At all $\omega < \omega_{0reader}$ we observe, a series RL circuit behaviour. If C_1 were increased further, it will behave like a parallel RC circuit with the phase response beginning at 0 and decreasing motonically to -90^o. While the baseline approaches -90^o, it is never quite reaches -90^o. Finite reader resistance is responsible for both the imperfect baseline and the slow phase transitions at resonance.

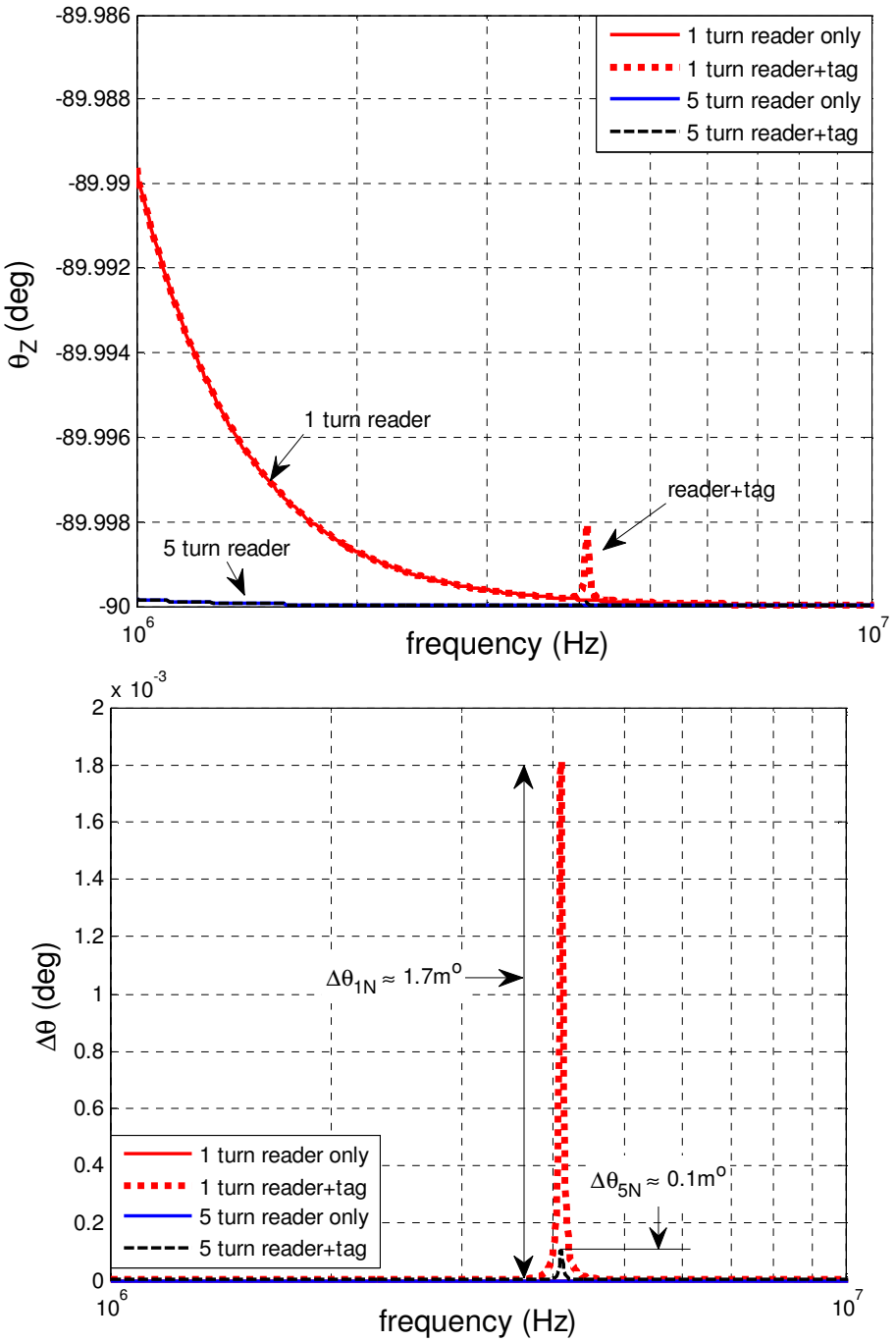

Figure 4.19 (top) The phase response (θ_Z) with the frequency axis is adjusted (1-10MHz) to make the tag response more visible, and (bottom) signal strength ($\Delta\theta$) which is the deviation of the phase from its baseline

For the case when the tag is present, we would expect the tag response to appear at ω_{0tag}= 4.1MHz. In the Figure 4.19 (top), adjusting the frequency axis to 1-10MHz to view the phase response of the tag, we observe that the response for the 1-turn reader is $\approx 2m^{o}$; the response for the 5-turn reader case is barely visible.

In Figure 4.19 (bottom) the signal strength ($\Delta\theta$) estimated from the phase response shows that $\Delta\theta_{1N} \approx 1.7m^{o}$ and $\Delta\theta_{5N} \approx 0.1m^{o}$. Consider the total reader capacitance C_1 with impedance is Z_{C1}. The impedance of the reader coil is the total impedance of the series combination of R_1 and L_1. Now, at $\omega > \omega_{0reader}$, the reader coil is shunted by the extremely low reactance of the reader capacitance $C_1 \approx (4m\Omega|\omega_{0tag})$. Since the input impedance Z_{in} is the parallel combination of the impedance (Z_{C1}) of C_1 and the reader coil, it is dominated by Z_{C1}. In addition, since the impedance of the 1-turn reader coil is much less than that of the 5-turn reader coil ($Z_{1Ncoil} << Z_{5Ncoil}$), a change in Z_{1Ncoil} due to the reflected impedance of the tag has a larger impact on the total Z_{in}, thus producing a larger signal.

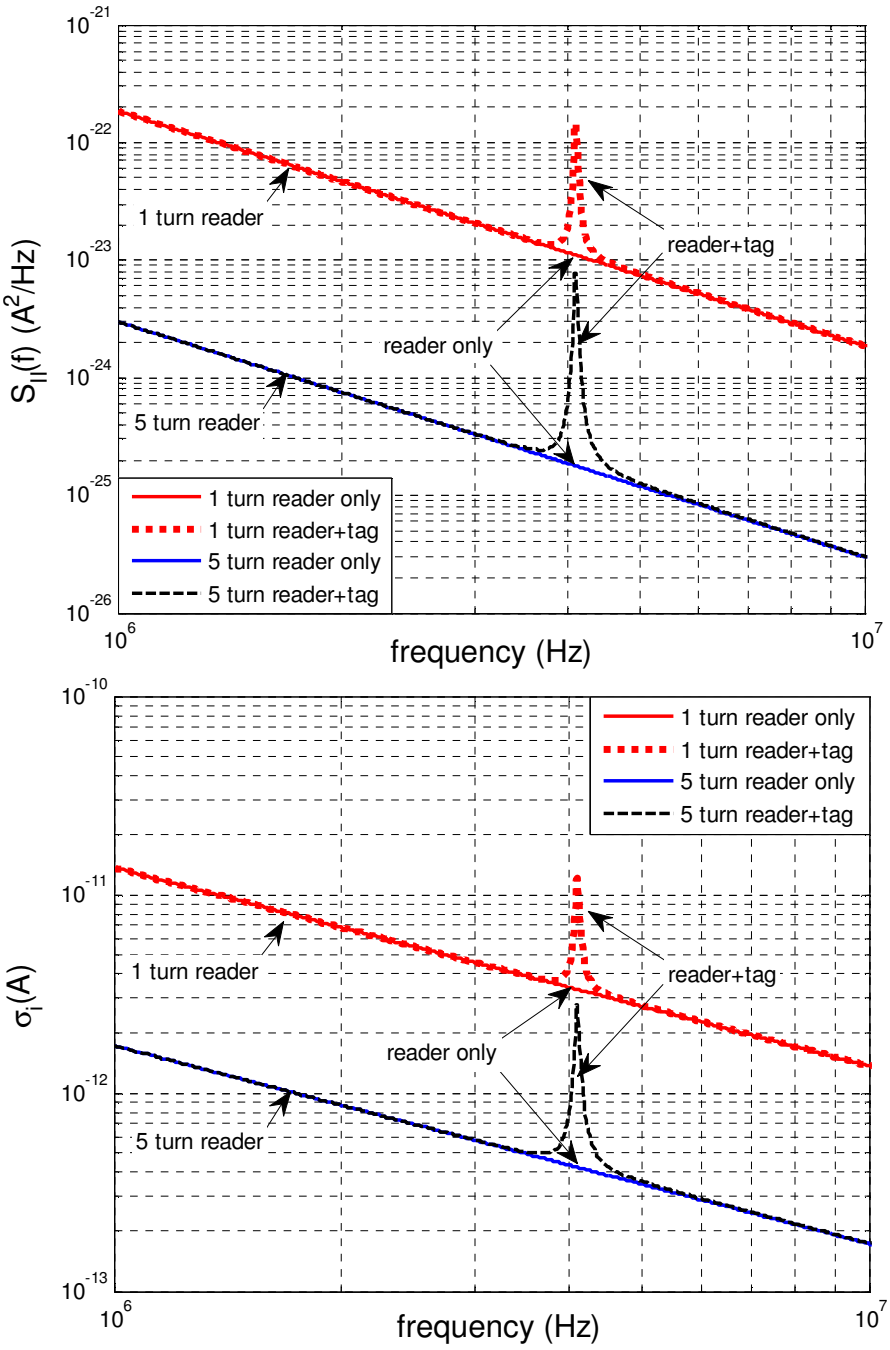

Figure 4.20 (top) The power spectral density ($S_{II}(f)$) of the noise current and (bottom) the r.m.s noise current (σ_i) calculated for a unit bandwidth in the presence and absence (baseline) of the tag when baseline is capacitive

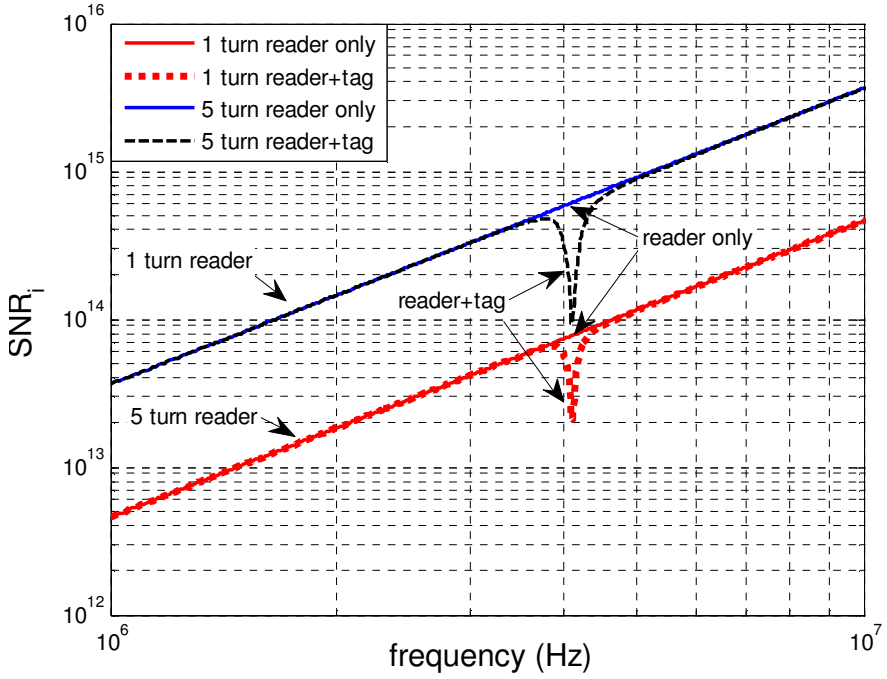

Figure 4.21 Signal-to-noise-ratio (SNR_i) of the current I_{in} calculated in the presence and absence (baseline) of the tag when baseline is capacitive.

The Figure 4.20 (top), is the power spectral density, $S_{II}(f)$, of the noise current and Figure 4.20 (bottom) is the r.m.s. noise current, σ_i. Both values are similar to that of the +90° baseline. However, contrary to the previous case, the signal to noise ratio SNR_i for the 5-turn reader is larger than that of the 1-turn reader (Figure 4.21). Since Z_{in} is dominated by the low value of Z_{C1}, the current drawn by the 1-turn and 5-turn readers are both negligible and roughly equal to each other. The equality of the currents in and the lower σ_i for the 5-turn reader explain its higher SNR_i. In spite of the larger SNR_i the estimated phase uncertainty σ_θ (Figure 4.22 (top)), is only slightly higher for the 1-turn case as than the 5-turn, which is because the baseline phase is ≈ -90° for both cases and σ_θ increases at extremities i.e. θ = 90/-90/0°. This same effect is observed (Figure4.22 (bottom)) in the graph of the uncertainty ($\sigma_{\Delta\theta}$) in measuring signal strength ($\Delta\theta$).

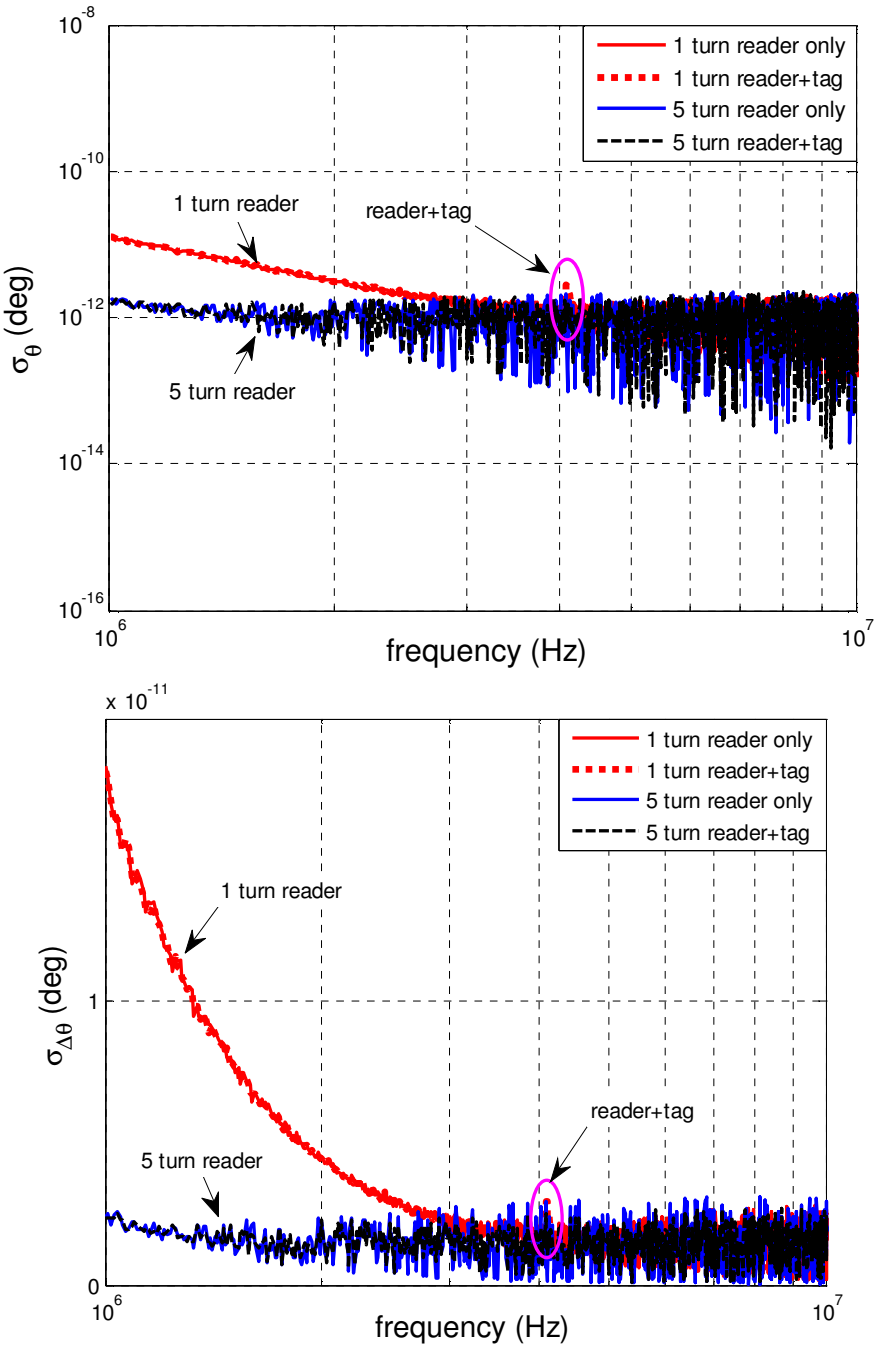

Figure 4.22 (top) The uncertainty (σ_θ) in estimating the phase response in the presence and absence (baseline) of the tag for a capacitive baseline. The variances add, resulting in the uncertainty ($\sigma_{\Delta\theta}$) in estimation of the signal ($\Delta\theta$), which sets the value of the minimum resolvable signal

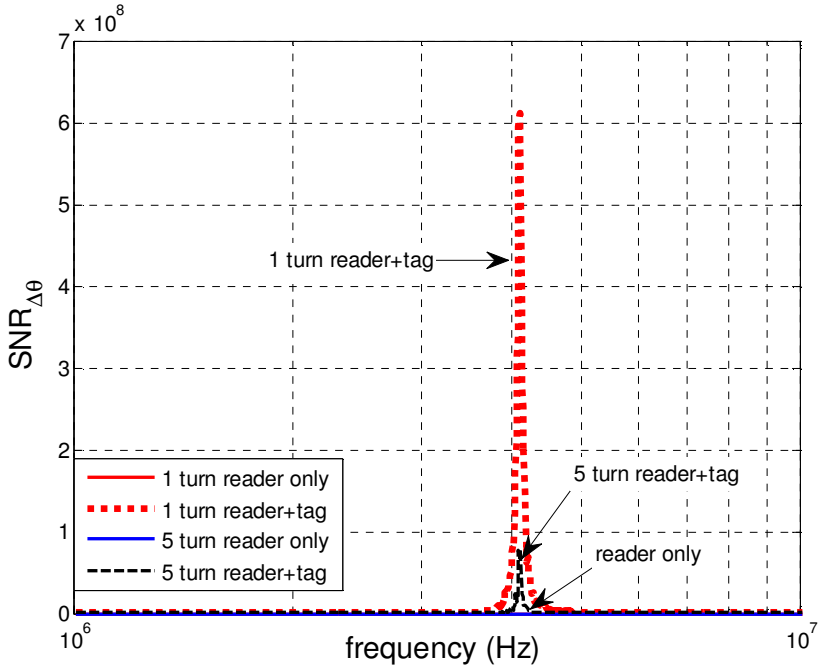

Figure 4.23 Signal-to-noise ratio $SNR_{\Delta\theta}$ is the ratio of phase change ($\Delta\theta$= signal) due to the presence of the tag to the uncertainty in its estimation ($\sigma_{\Delta\theta}$=noise)

The signal to noise ratio $SNR_{\Delta\theta}$ (Figure 4.23) is dominated by the comparatively larger difference in signal strengths $\Delta\theta$ for the 1- and 5-turn readers rather than the difference in uncertainty (noise). Once again, the extremely large value of $SNR_{\Delta\theta}$ ($\approx 10^8$) in spite of the small signal strength ($\Delta\theta \approx 1.7 m^o$) is due to the small value of the noise ($\sigma_{\Delta\theta} \approx 10^{-8}$) rather than larger signal. The $SNR_{\Delta\theta}$ plot suggests that for a given coupling factor, from a perspective of noise, the 1-turn reader performs better than the 5-turn reader even from a -90^o.

4.3.3 Resonant (0^o) Baseline

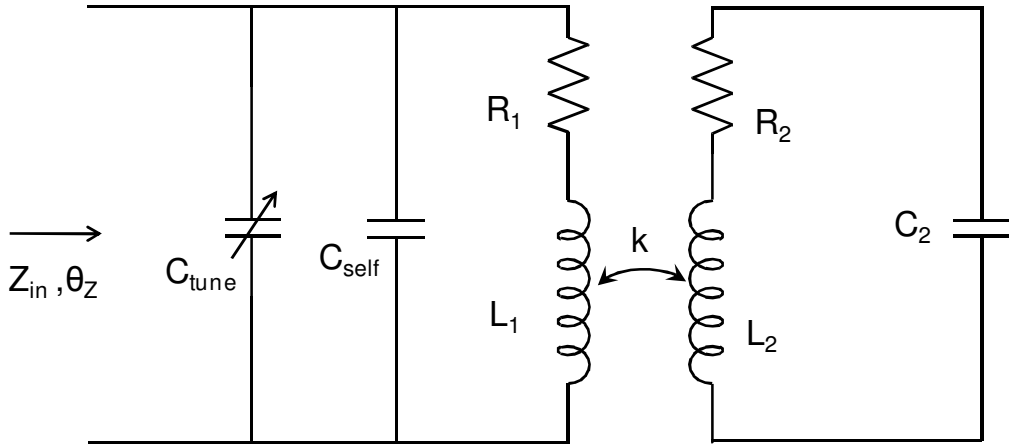

Figure 4.24 Equivalent circuit model used in the analysis of the resonant baseline case
The variable tuning capacitor C_{tune} is adjusted so that the reader is resonant at all source frequencies.

The resonant baseline is a unique case where an additional tuning capacitor placed in parallel with the reader (Figure 4.24). The value of this capacitor (C_{tune}) is adjusted so that the reader is tuned to be resonant at all source frequencies i.e $\omega_{0reader} = \omega_{source} = 1/\sqrt{L_1 C_1}$, where $C_1 = C_{tune} + C_{self}$ .The phase response (θ_Z), of the input impedance reader (Figure 4.25) shows that when the tag is absent, the phase is 0^o for all frequencies. The small error at low frequency is due to larger impact of the parasitic resistance in the 1-turn reader. When the tag is present, due to the finite width of its resonance, the detuning of the reader begins at $\omega < \omega_{0tag}$. Since inductance $L_{5N} > L_{1N}$, the 5-turn reader is detuned at a lower frequency than the 1-turn reader. The phase response is similar to that of a parallel RC circuit ($0 \rightarrow -90^o$) until $\omega \approx \omega_{0tag}$. Near ω_{0tag} the phase transitions from -90^o to $+90^o$, crossing 0^o at $\omega \approx \omega_{0tag}$. Since the tag coil is shorted by its capacitor, the reader coil is loaded by a shorted secondary (in the tag), and hence, the

effective inductance of the reader reduces. If R_2 and capacitive reactance X_{C2} are small, the effective reader inductance is by $L_{eff} = L_1(1-k^2)$, where k is the

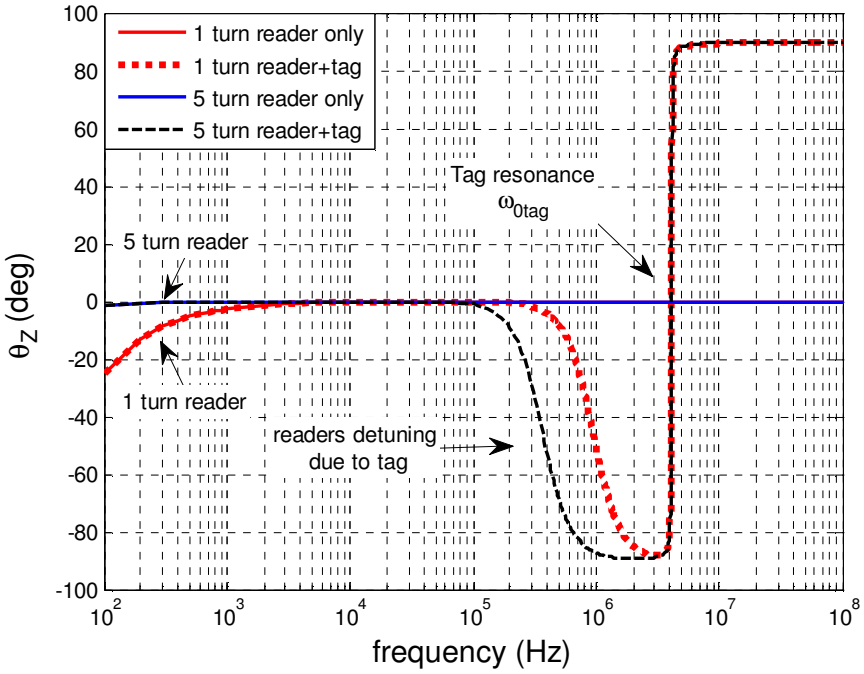

Figure 4.25 The calculated phase response (θ_Z) of input impedance is zero when tag is absent. The reader can be thought of as balanced arms of a bridge which are detuned by the tag.

coupling factor and L_1 is the reader's inductance. At $\omega > \omega_{0tag}$ the reader's resonant frequency is now $\omega_{0reader} = 1/\sqrt{L_{effective}C_1}$, while the source frequency is $\omega_{source} = 1/\sqrt{L_1C_1}$. Since $L_{effective} < L_1, \omega_{0reader} > \omega_{source}$, so the baseline stays at +90°.

Adjusting the frequency axis to 1-10MHz, we observe (Figure 4.25) that the phase response for both the 1- and 5- turn readers is identical for frequencies near and above ω_{0tag}. The signal strength $\Delta\theta$, is minimum at ω_{0tag}, but it is still larger than the previous baseline cases.

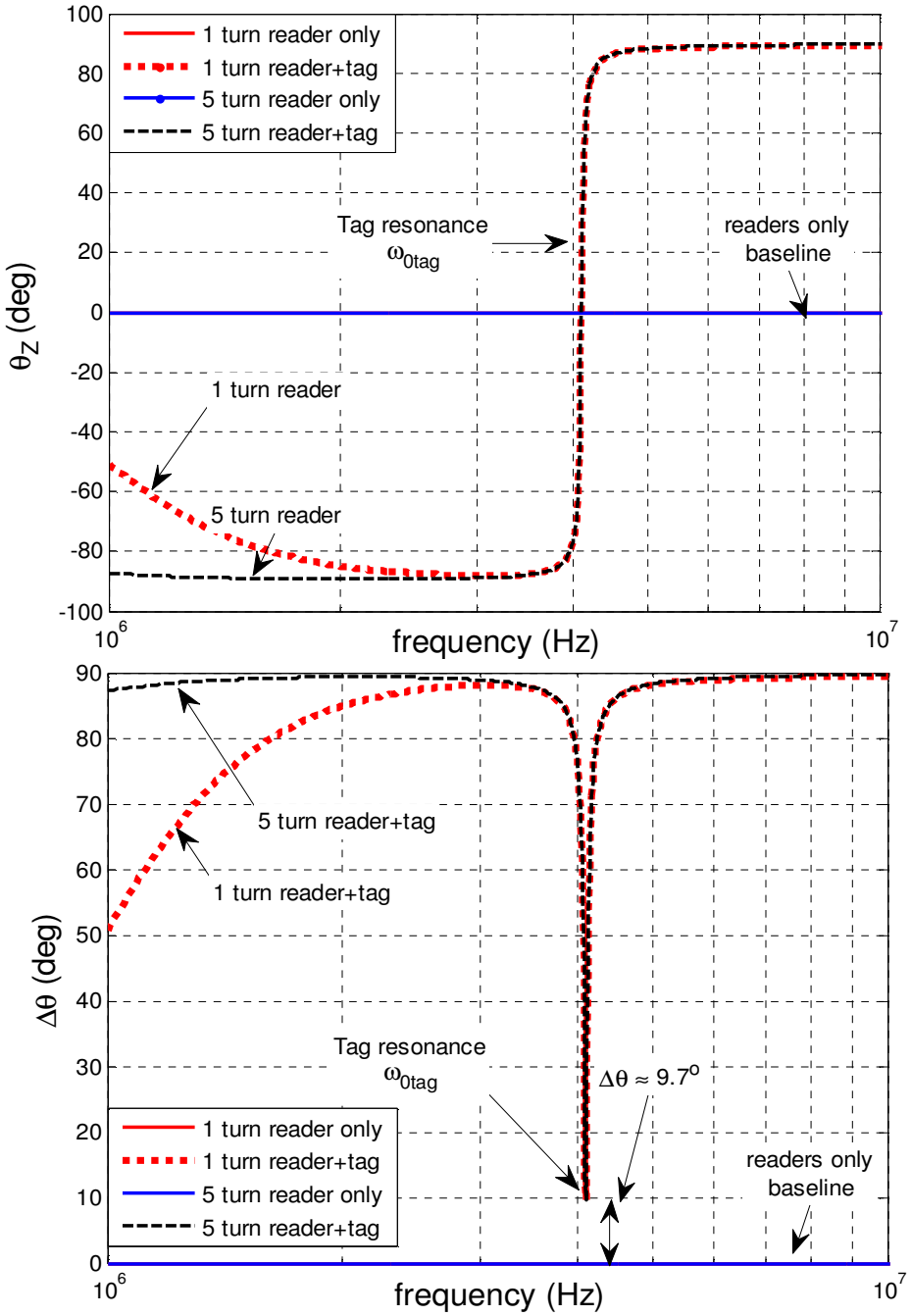

Figure 4.26 The phase response (θ_Z) with the frequency axis is adjusted (1-10MHz) to make the tag response more visible and (bottom) signal strength ($\Delta\theta$) which is the deviation of the phase from its baseline

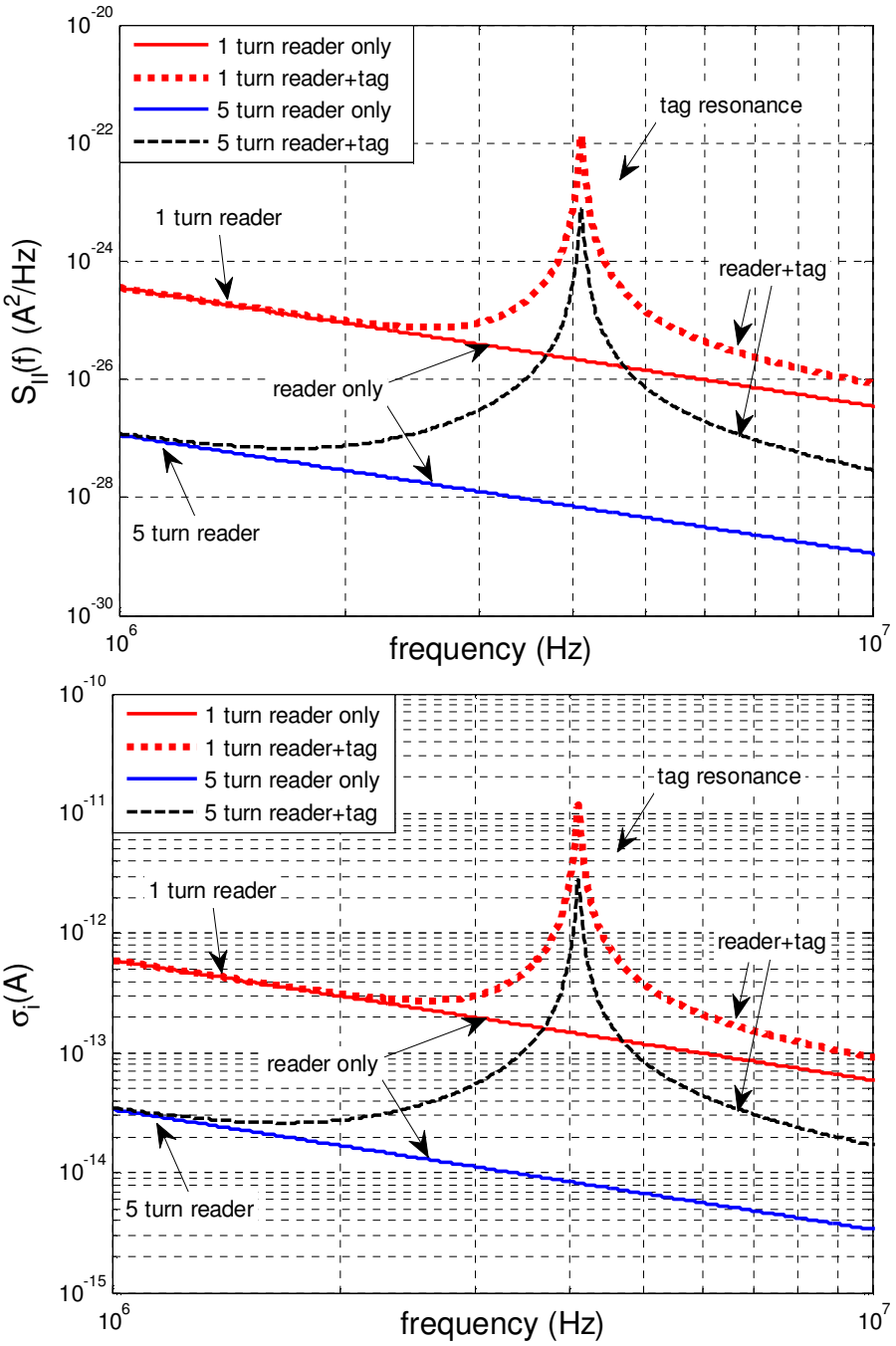

Figure 4.27 (top) The power spectral density ($S_{II}(f)$) of the noise current and (bottom) the r.m.s noise current (σ_i) calculated for a unit bandwidth in the presence and absence (baseline) of the tag for the tuned reader's resonant baseline

The PSD (Figure4.27 (top)), $S_{II}(f)$, of the noise current and the r.m.s. noise current (Figure 4.27(bottom)) σ_i, for the resonant reader are lower than that of the previous baselines. When the tag is present, the response is shaped by the resonance of the tag. Further, since the phase response (θ_Z) stays inductive at $\omega > \omega_{0tag}$ it contributes to the increase in PSD and σ_i compared to their baselines. Signal to noise ratio, SNR_i, of the current I_{in}, (Figure 4.28) when tag is absent is small because the reader presents a high Z_{in} at (parallel) resonance resulting in a small current I_{in}. Even so, similar to the $+90^o$ baseline case, since $Z_{in5N} > Z_{in1N}$, results in $I_{in5N} < I_{in1N}$, hence $SNR_{i5N} < SNR_{i1N}$. When the tag is present, at $\omega < \omega_{0tag}$, where the detuning is dominated by the parallel RC (θ_Z $0 \rightarrow -90^o$) and Z_{in} is dominated Z_{C1}, the $SNR_{i5N} \approx SNR_{i1N}$. Near and above ω_{0tag} we observe series RL behaviour and Z_{in} is dominated by $Z_{R+Leffective}$ hence $I_{in5N} < I_{in1N}$ and $SNR_{i5N} < SNR_{i1N}$.

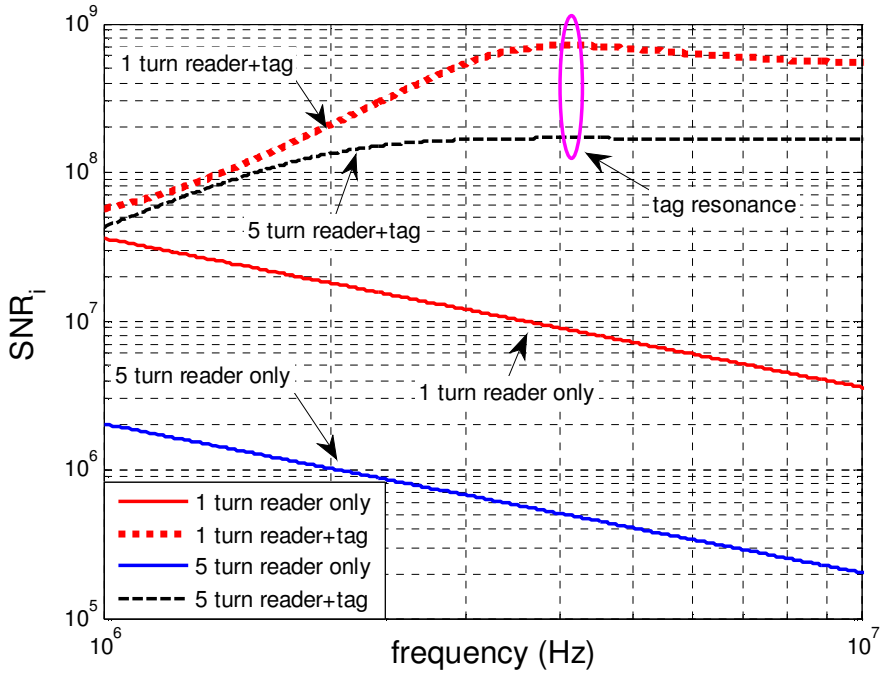

Figure 4.28 Signal to noise ratio (SNR_i) of the current I_{in} calculated in the presence and absence (baseline) of the tag for the tuned reader's resonant baseline.

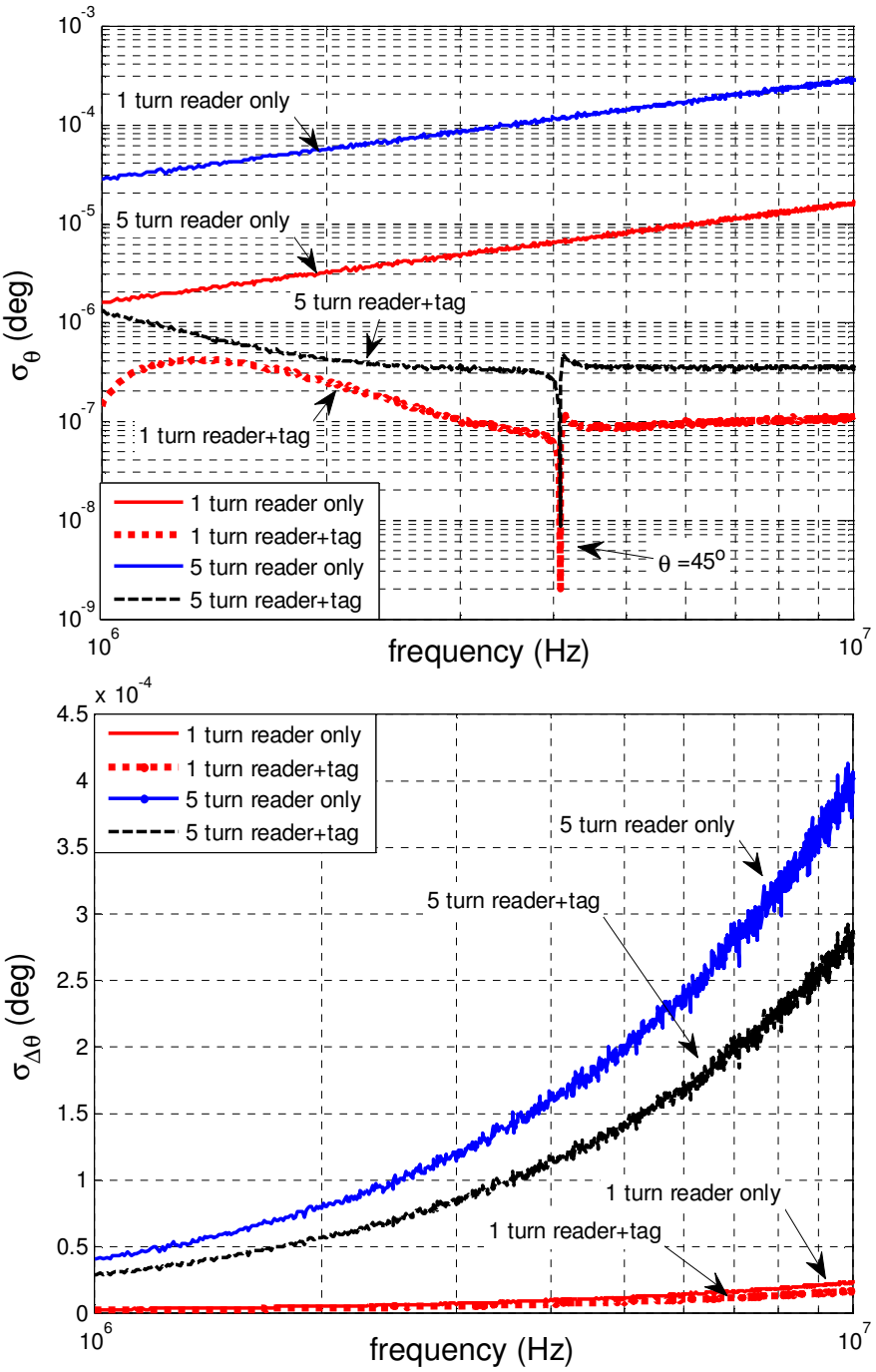

Figure 4.29 (top) The uncertainty (σ_θ) in estimating the phase response in the presence and absence (baseline) of the tag for a resonant baseline. The variances add resulting in the uncertainty ($\sigma_{\Delta\theta}$) in estimation of the signal ($\Delta\theta$) sets the value of the maximum resolvable signal

The phase uncertainty σ_θ (Figure 4.29(top)) is larger for the 5-turn reader which can be attributed to its smaller SNR_i. Also $\sigma_\theta|_{baseline} >> \sigma_\theta|_{tag\ absent}$ since the $SNRi|_{baseline} << SNRi|_{tag\ absent}$. The sharp dip in σ_θ occurs at a frequency near ω_{tag} where the phase, $\theta_Z \approx 45^o$, as it transitions from -90^o to $+90^o$. Both σ_θ and the uncertainty in the measured signal $\sigma_{\Delta\theta}$, are larger than in the previous baselines (Figure 4.29 (bottom)) . The larger signal strength ($\Delta\theta$) offsets some of the effects of larger $\sigma_{\Delta\theta}$(noise) leading to a small reduction in signal to noise ratio $SNR_{\Delta\theta}$ (Figure 4.30) relative to the previous baselines. Since $\sigma_{\Delta\theta 5N} > \sigma_{\Delta\theta 1N}$, the $SNR_{\Delta\theta 5N} < SNR_{\Delta\theta 1N}$ suggesting once again, that the 1-turn reader performs than the 5-turn reader. $SNR_{\Delta\theta}$ drops sharply at ω_{tag} since $\Delta\theta$ is minimum at ω_{tag}.

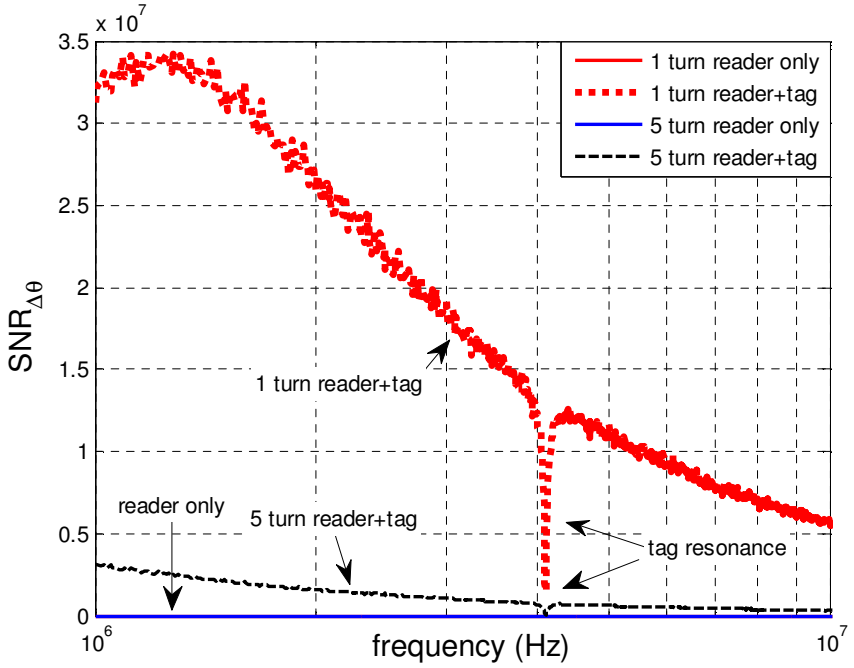

Figure 4.30 Signal to noise ratio $SNR_{\Delta\theta}$ is the ratio of phase change ($\Delta\theta$= signal) due to the presence of the tag to the uncertainty in its estimation ($\sigma_{\Delta\theta}$=noise)

4.4 MINIMUM DETECTION LIMIT

The quantity $\Delta\theta = \theta_Z\big|_{tag\ absent} - \theta_Z\big|_{tag\ present}$ measures of the difference between two phase responses at the resonant frequency of the tag ω_{0tag}. Our ability to resolve this difference dictates our ability to detect the presence of a tag from the phase response θ_Z. Our ability to resolve $\Delta\theta$ (signal) is influenced by the uncertainty in its measurement $\sigma_{\Delta\theta}$(noise). The value of $\sigma_{\Delta\theta}$ sets the minimum detection limit of the system. The smaller the value of $\sigma_{\Delta\theta}$ the better is our ability to resolve small phase changes $\Delta\theta$. The signal to noise ratio $SNR_{\Delta\theta}$ can be improved by either reducing $\sigma_{\Delta\theta}$ or increasing $\Delta\theta$.

The cases considered in the above analyses suggest that when measured with an ideal instrument and limited only by thermal noise, the performance of our typical ESS system using a 1-turn reader is better. This is true regardless of the baseline used to perform the measurement. While the signal $\Delta\theta$ was largest for the resonant reader (0^o) baseline, the $SNR_{\Delta\theta}$ was worse than the inductive ($+90^o$) and the capacitive ($+90^o$) baselines. The values $\sigma_{\Delta\theta}$ for the inductive $(10^{-8})^o$, capacitive $(10^{-11})^o$ and resistive $(10^{-4})^o$ baselines are informative only in assessing detection ability in the noise-limited case. The HP 4194A, impedance gain-phase analyzer which is the instrument commonly used in laboratory testing has a maximum phase resolution of 0.01^o [4194 Manual]. This phase resolution sets a lower bound for resolving $\Delta\theta$, so $\sigma_{\Delta\theta instr} = 0.01^o$. Although $\sigma_{\Delta\theta}$ and $\Delta\theta$ scale with component values and coupling factor, for all practical purposes, we will be limited by the instrument's resolution rather than the limit of thermal noise. The impact of finite $\sigma_{\Delta\theta}$ on the choice of coils, coupling factor and read range is considered next.

Chapter 5: Read Range

The presence of a finite detection limit affects the performance of the ESS system. The choice of circuit parameters used in the design our coupled reader and tag influences the signal strength that can be obtained. We begin by developing expressions that relate signal strength $\Delta\theta$ to the component/circuit parameters.

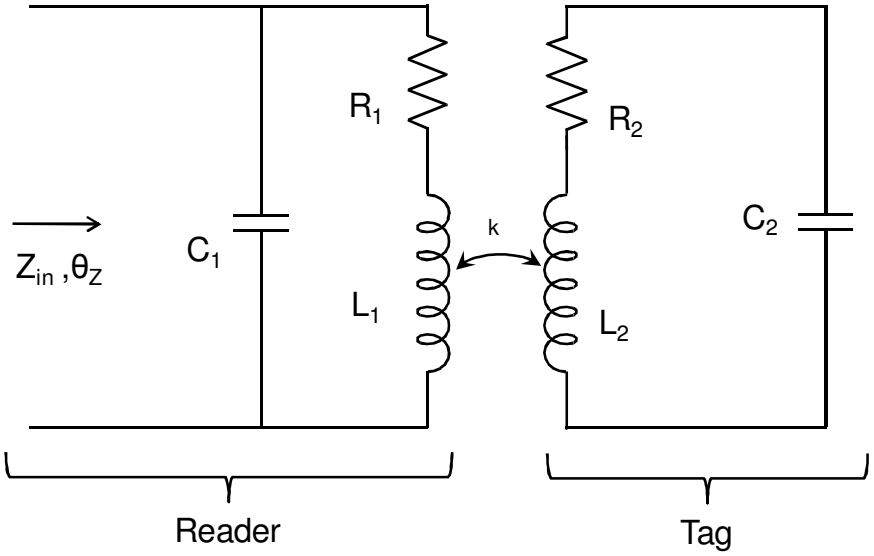

Figure 5.1 Equivalent circuit model of the reader and tag used in the derivation of expressions for signal strength $\Delta\theta$.

5.1 EXPRESSION FOR SIGNAL STRENGTH

In a coupled reader and tag system (Figure 5.1), the phase of input impedance θ_Z is a function of the circuit parameters of the reader (R_1, L_1, & C_1), the tag (R_2, L_2, & C_2), and coupling factor k between them. The signal strength is defined as $\Delta\theta = \theta_Z\big|_{tag\ absent} - \theta_Z\big|_{tag\ present}$, so it is also a function of the same circuit parameters. In

total there are 7 circuit parameters. Recall that the expression for input impedance Z_{in}, is given by:

$$Z_{in} = \frac{1}{j\omega C_1} \Bigg\| \left(R_1 + j\omega L_1 + \frac{\omega^2 M^2}{R_2 + j\omega L_2 - j\omega L_2} \right) \tag{5.1}$$

where $M=k\sqrt{L_1 L_2}$ is the mutual inductance between L_1 and L_2.

For convenience, we develop the expressions in two parts. Part 1 neglects capacitance C_1 , but Part 2 includes capacitance C_1.

5.1.1 Part 1 (excluding reader capacitance C_1)

Expressing the impedances as $Z_n = R_n + jX_n$ where R_n and X_n are the real and imaginary parts of a corresponding impedance Z_n, we have

input impedance when C_1 is absent :	$Z_{in\ reader\ no C1} = Z_4 = R_4 + jX_4$,
impedance of just the reader:	$Z_{reader\ no C1} = Z_1 = R_1 + jX_1$,
series equivalent impedance of the tag:	$Z_{series\ tag} = Z_2 = R_2 + jX_2$,
reflected impedance of the tag:	$Z_{reflected} = Z_3 = R_3 + jX_3$.

Now, since, $Z_{in\ reader\ no C1} = Z_{reader\ no C1} + Z_{reflected}$, $\Rightarrow Z_4 = Z_1 + Z_3$ hence,

$$R_4 + jX_4 = R_1 + jX_1 + R_3 + jX_3 . \tag{5.2}$$

Also since, $Z_{reflected} = \frac{\omega^2 M^2}{Z_{series\ tag}}$, we have

$$Z_3 = \frac{\omega^2 M^2}{Z_2} = \frac{\omega^2 M^2}{Z_2} \ , \tag{5.3}$$

or,

$$R_3 + jX_3 = \frac{\omega^2 M^2}{R_2 + jX_2} \tag{5.4}$$

The complex conjugate yields:

$$R_3 + jX_3 = \frac{\omega^2 M^2}{(R_2^2 + X_2^2)}(R_2 - jX_2) \tag{5.5}$$

Let $\alpha = \frac{\omega^2 M^2}{(R_2^2 + X_2^2)}$, substituting , we have,

$$R_3 = \alpha R_2 \text{ and } X_3 = -\alpha X_2 \tag{5.6}$$

If θ_3 is the phase angle of reflected impedance Z_3 then,

$$\tan\theta_3 = \frac{X_3}{R_3} = \frac{-\cancel{\alpha} X_2}{\cancel{\alpha} R_2} = \frac{-X_2}{R_2} \tag{5.7}$$

Similarly if θ_4 is the phase angle of impedance Z_4 then,

$$\tan\theta_4 = \frac{X_4}{R_4} \tag{5.8}$$

Also since, $R_4 + jX_4 = R_1 + jX_1 + R_3 + jX_3$, substituting from Equation 5.6 we have,

$$R_4 = (R_1 + \alpha R_2) \quad \& \quad X_4 = (X_1 - \alpha X_2)\,. \tag{5.9}$$

Hence,

$$\tan\theta_4 = \frac{X_4}{R_4} = \frac{(X_1 - \alpha X_2)}{(R_1 + \alpha R_2)} \tag{5.10}$$

Now, expanding the expression for R_4 and X_4 , we obtain

$$X_4 = X_1 - \frac{\omega^2 M^2}{(R_2^2 + X_2^2)}(X_2) \tag{5.11}$$

and

$$R_4 = R_1 + \frac{\omega^2 M^2}{(R_2^2 + X_2^2)}(R_2) \tag{5.12}$$

At the resonance frequency of the tag i.e $\omega = \omega_{0tag} = \omega_0 = \frac{1}{\sqrt{L_2 C_2}}$, since $X_2 = \omega L_2 - {}^{1}\!/\!_{\omega L_2} = 0$, substituting, the Equations 5.11 and 5.12 simplify to

$$X_4 = X_1 = \omega_0 L_1 \tag{5.13}$$

and

$$R_4 = R_1 + \frac{\omega_0^2 M^2}{R_2} \tag{5.14}$$

Further substituting $M = k\sqrt{L_1 L_2}$ we have,

$$R_4 = R_1 + \frac{\omega_0^2 k^2 L_1 L_2}{R_2} \tag{5.15}$$

Using Equation 5.10 and from Equation 5.13 and 5.15

$$\tan\theta_4\big|_{\omega_{0tag}} = \frac{X_4}{R_4} = \frac{\omega_0 L_1}{(R_1 + \frac{\omega_0^2 k^2 L_1 L_2}{R_2})} \tag{5.16}$$

The quality factor of the tag at its resonant frequency (ω_{0tag}) is,

$$Q_{02} = Q_2 = \frac{\omega_0 L_2}{R_2} \tag{5.17}$$

The quality factor of the reader at ω_{0tag} is,

$$Q_1\big|_{0tag} = Q_1 = \frac{\omega_0 L_1}{R_1} \tag{5.18}$$

The Equation 5.16 can be rearranged as follows,

$$\tan\theta_4 = \frac{X_4}{R_4} = \frac{\omega_0 L_1}{(R_1 + k^2 \underbrace{\langle \omega_0 L_1 \rangle}_{R_1 Q_1} \underbrace{\left\langle \frac{\omega_0 L_2}{R_2} \right\rangle}_{Q_2})} = \frac{\omega_0 L_1}{(R_1 + k^2 R_1 Q_1 Q_2)} = \frac{\overbrace{\omega_0 L_1}^{Q_1}}{R_1} \frac{1}{(1 + k^2 Q_1 Q_2)} \tag{5.19}$$

Hence,

$$\tan\theta_4 = \frac{X_4}{R_4} = \frac{Q_1}{(1 + k^2 Q_1 Q_2)}, \tag{5.20}$$

where, $Q_1 = \frac{\omega_0 L_1}{R_1}$, $Q_2 = \frac{\omega_0 L_2}{R_2}$, $\omega_0 = 1/\sqrt{L_2 C_2}$ and k is the coupling factor.

5.1.2 Part 2 (including reader capacitance C_1)

Including capacitance C_1 , if $X_5 = \frac{1}{\omega C_1}$ is its reactance then its impedance can be expressed as

$$Z_{readerselfcapC1} = Z_5 = -jX_5. \tag{5.21}$$

If input impedance $Z_{in} = Z_6 = R_6 + jX_6$, from Equation 5.2 and 5.21 we have,

$$Z_6 = R_6 + jX_6 = Z_5 \| Z_4 = \frac{Z_5 Z_4}{Z_5 + Z_4} \tag{5.22}$$

or

$$Z_6 = \frac{-jX_5(R_4 + jX_4)}{R_4 + jX_4 - jX_5}. \tag{5.23}$$

Taking the complex conjugate and simplifying, we have,

$$Z_6 = R_6 + jX_6 = \frac{X_5^2 R_4 + j(X_5^2 X_4 - X_5 X_4^2 - R_4^2 X_5)}{R_4^2 + (X_4 - X_5)^2}. \tag{5.24}$$

If θ_6 is the phase angle of the input impedance Z_6, then from Equation 5.24

$$\tan\theta_6 = \frac{X_6}{R_6} = \frac{X_5^2 X_4 - X_5 X_4^2 - R_4^2 X_5}{X_5^2 R_4}. \tag{5.25}$$

Rearranging the terms and from Equation 5.25 we get,

$$\tan\theta_6 = \left(\frac{X_4}{R_4} - \frac{X_4}{X_5}\frac{X_4}{R_4} - \frac{R_4}{X_5} \right) = \left(\tan\theta_4 - \frac{X_4}{X_5}\tan\theta_4 - \frac{R_4}{X_5} \right). \tag{5.26}$$

Recall that at resonant frequency of the tag, $\omega = \omega_{0tag} = \omega_0 = \frac{1}{\sqrt{L_2 C_2}}$ from Equations 5.13 and 5.15,

$$\begin{aligned} X_4 &= X_1 = \omega_0 L_1 \\ R_4 &= R_1 + \frac{k^2 \omega_0 L_1 \omega_0 L_2}{R_2}. \end{aligned} \tag{5.27}$$

Now consider the term $\frac{R_4}{X_5}$ at $\omega = \omega_0$,

$$\frac{R_4}{X_5} = \frac{R_1(1+k^2Q_1Q_2)}{1/\omega_0 C_1} = \omega_0 C_1 R_1 (1+k^2Q_1Q_2) \text{ .(5.28)}$$

If we define $Q_C = \dfrac{1}{\omega_0 C_1 R_1}$ as the quality factor of the R_1C_1 circuit at ω_0 then,

$$\frac{R_4}{X_5} = \frac{(1+k^2Q_1Q_2)}{Q_C}. \tag{5.29}$$

Similarly, $\dfrac{X_4}{X_5}$ can be simplified as follows:

$$\frac{X_4}{X_5} = \frac{X_1}{X_5} = \frac{\omega_0 L_1}{\omega_0 C_1} = \frac{\omega_0 L_1 R_1}{\omega_0 C_1 R_1} = \left\langle \frac{\omega_0 L_1}{R_1} \right\rangle \langle \omega_0 C_1 R_1 \rangle = \frac{Q_1}{Q_C}. \tag{5.30}$$

Substituting in 5.26, we have,

$$\tan\theta_6 = \frac{Q_1}{(1+k^2Q_1Q_2)} \left(1 - \frac{\left(1+k^2Q_1Q_2\right)^2}{Q_1Q_C} - \frac{Q_1}{Q_C} \right). \tag{5.31}$$

At the resonant frequency of the tag, the phase angle of input impedance $\theta_Z = \theta_6$. An inspection of Equation 5.31 indicates that in the weakly coupled limit (k <5%) for Q_1 and $Q_2 \geq 10$ and if $\dfrac{Q_c}{Q_1} \geq 10$, the error in estimating θ_Z using θ_4 (Equation 5.20) instead of θ_6 (Equation 5.31) is < 0.1%. This error reduces as Q_1, Q_2 and Q_C increase. Although Q_C is not the quality factor of the capacitor C_1 any intrinsic losses in the capacitor will further reduce the value of Q_c, Since capacitor dissipation factor (DF) or loss tangent (tanδ) is inversely proportional to its quality factor, the above analysis indicates that capacitors with low dissipation factors $\left(\text{DF} \leq \dfrac{0.1}{Q_1} \right)$ should be used. Such a low DF will

ensure that $\theta_Z \approx \theta_4$. Using this simplified form for θ_Z an expression for signal strength at resonance of tag is developed.

Signal strength is defined as $\Delta\theta = \theta_Z\big|_{tag\ absent} - \theta_Z\big|_{tag\ present}$ or $\Delta\theta = \theta_Z\big|_{k=0} - \theta_Z\big|_{k\neq 0}$.

Based on the preceding discussion, at the resonant frequency of the tag, where $\omega = \omega_{0tag} = \omega_0 = \dfrac{1}{\sqrt{L_2 C_2}}$. Therefore, we have $\Delta\theta = \Delta\theta\big|_{\omega_0} = \theta_4\big|_{k=0} - \theta_4\big|_{k\neq 0}$,

$$\tan\Delta\theta = \tan\left(\theta_4\big|_{k=0} - \theta_4\big|_{k\neq 0}\right). \tag{5.32}$$

Using the tan(A-B) expansion and substituting $\theta_4\big|_{k=0} = \tan^{-1}(Q_1)$ and $\theta_4\big|_{k\neq 0} = \tan^{-1}\left(\dfrac{Q_1}{1+k^2 Q_1 Q_2}\right)$, we have,

$$\Delta\theta = \tan^{-1}\left(\frac{k^2 Q_1^2 Q_2}{1+k^2 Q_1 Q_2 + Q_1^2}\right). \tag{5.33}$$

In the Equation 5.33 we get no signal (phase change) when tag is absent (k = 0, $\Delta\theta$ = 0) and a when tag is present, the signal is dependent on the strength of coupling k, the quality factor of the tag Q_2 and the quality factor of the reader, Q_1, at the resonant frequency of the tag.

5.2 EXPRESSION FOR K_{MIN}/ READ RANGE

Solving the Equation 5.33 for k gives us :

$$k^2 = \frac{\tan\Delta\theta\left(1 + Q_1^2\right)}{Q_1 Q_2\left(Q_1 - \tan\Delta\theta\right)}. \tag{5.34}$$

For the signal to be detectible, it should be larger than the minimum detectible limit i.e $\Delta\theta > \sigma_{\Delta\theta}$. By setting $\Delta\theta = \sigma_{\Delta\theta}$ ($SNR_{\Delta\theta}$ =1), in the Equation 4.26 , for a given set of $Q_1 = Q_{reader}$ and $Q_2 = Q_{tag}$ the value of coupling factor (k_{min}) obtained corresponds to the limit of the operating read range. To be able to "read" the tag, $k > k_{min}$. In other words, it gives us the value of k at which the signal will fall below the detection limit. It is also apparent that the value of k_{min} is also dependent on Q_{reader} and Q_{tag}.

The relationship between k_{min} required various values of Q_{reader} and Q_{tag} for a minimum detectible signal of 0.01^o ($\sigma_{\Delta\theta instr}$) is plotted (Figure 5.2). For a fixed value of Q_{tag}(Figure 5.2 (top)), k_{min} reduces almost linearly until Q_{reader} = 1. The slope decreases for 1< Q_{reader} < 10 and is constant (staurates) for Q_{reader}>10. For Q_{tag} > 10, the worst case k_{min} (≈5%) is in the weakly coupled limit even for Q_{reader} <1. The value at which k_{min} saturates reduces with increase in Q_{tag}. For a given Q_{reader}, k_{min} decreases as $\sqrt{Q_{tag}}$ (Figure 5.2 (bottom)) with increasing values of Q_{tag}. k_{min} saturates for Q_{reader} >10, and thereafter, further improvements in k_{min} can only be attained by increasing Q_{tag}. This saturation suggests that it is desirable to maximize both Q_{reader} and Q_{tag} and that the system can tolerate small values of either the Q_{reader} or Q_{tag} but not both at the same time. The curves also indicate that we encounter diminishing marginal returns if Q_{reader}>10, so it does not make sense to spend resources trying to make Q_{reader} arbitrarily high. Though increasing Q_{tag} continues to improve k_{min}, Q_{tag} is limited by transducer resistance--hence, when selecting a series resistive transducer, care should be taken to have a sufficiently small value so as not to limit read-range excessively.

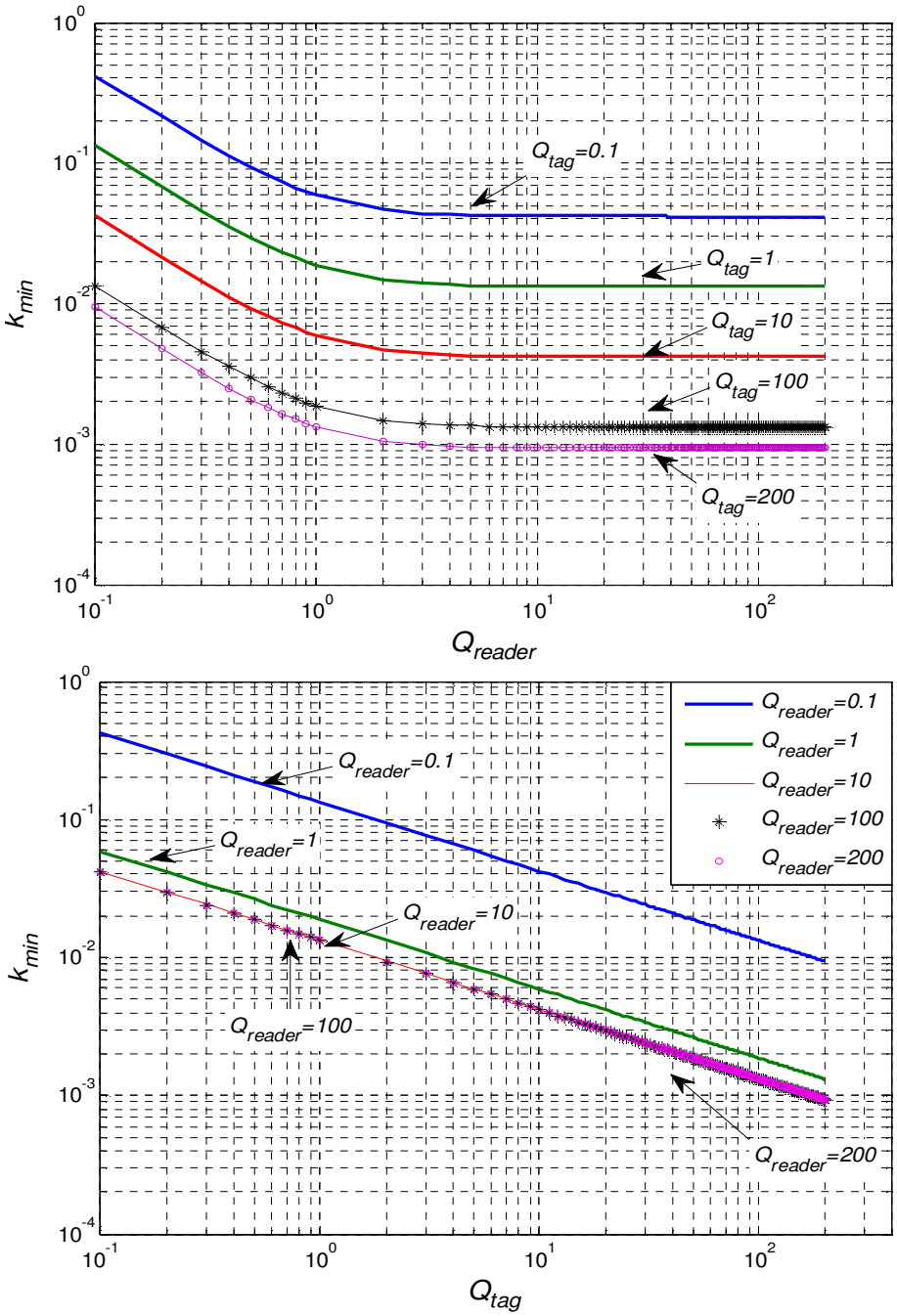

Figure 5.2 The relationship between $k_{\min}$ and required various values of Q_{reader} (top) and Q_{tag} (bottom) for a minimum detectible signal of 0.01^{o} ($\sigma_{\Delta\theta instr}$) is plotted. Note that k_{min} saturates for Q_{reader} values >10.

Q	$\Delta\theta_{min}$ (deg)	k_{min} (5-turn)	k_{min} (1-turn)	range (m) (5-turn)	range (m) (1-turn)
Q_{tag}=509	1e-8	5.85e-7	5.85e-7	3.51	3.31
$Q_{reader5N}$=573	0.001	1.85e-4	1.85e-4	0.51	0.48
$Q_{reader1N}$=153	0.01	5.85e-4	5.85e-4	0.345	0.325
	0.1	1.85e-3	1.85e-3	0.235	0.22
	0.5	4.14e-3	4.14e-3	0.17	0.16
	1.0	5.85e-3	5.85e-3	0.155	0.145
Q_{tag}=83	1e-8	1.44e-6	1.44e-6	2.6	2.455
$Q_{reader5N}$=155	0.001	4.55e-4	4.55e-4	0.38	0.355
$Q_{reader1N}$=10	0.01	1.44e-3	1.44e-3	0.255	0.24
	0.1	4.55e-3	4.55e-3	0.17	0.16
	0.5	0.10e-2	0.10e-2	0.12	0.115
	1.0	1.44e-2	1.44e-2	0.105	0.1

Table 5.1 The values of k_{min} and read range for the 5-turn reader, 1-turn reader and the tag for various minimum detection limits ($\Delta\theta_{min}$).

The values of k_{min} and read range for the 5-turn reader, 1-turn reader and the tag for various minimum detection limits ($\Delta\theta_{min}$) ranging from 10^{-8} degrees (thermal noise limit) to 1 degree (100 X instrument resolution) are tabulated in Table 5.1 The values are calculated for two cases of quality factors. The first case corresponds to the theoretical estimate of the Q for the readers and the tag where only the of finite d.c. resistance and skin effect at $\omega=\omega_{0tag}$ are considered (Table 5.2). The k_{min} is calculated using Equation 5.34. Once the k_{min} is computed, since the specifications of the coils are known, the distance corresponding to that k_{min} (read range) can be estimated graphically from the k

and distance plot (Figure 5.3). A combination of large Qs and small $\Delta\theta_{min}$ results in unrealistic read ranges for this case.

Specifictaion	RC_{1N}	RC_{5N}	Tag coil
Radius	5 cm	5 cm	3 cm
Wire gauge (AWG)	18	18	18
Turns (N)	1	5	5
Self inductance (L)	0.35 µH	6 µH	3.2 µH
$Rdc+Rskin\|_{\omega tag}$	53 mΩ	263 mΩ	158 mΩ
Quality factor $Q\|_{\omega_{0tag}}$	153	573	509

Table 5.2 Specifications of the four tags having a constant height wound with four different AWG and number of turns N_2.

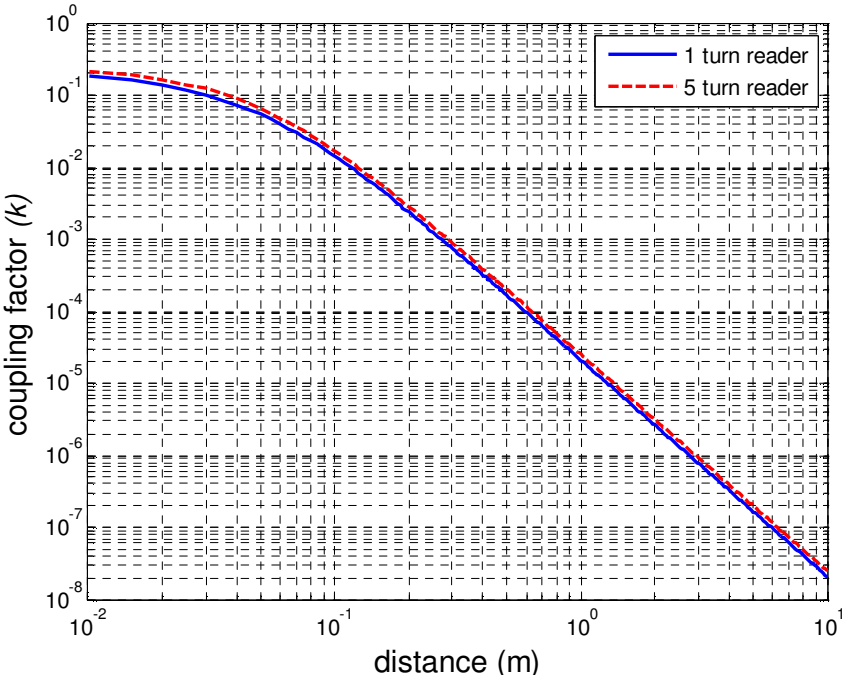

Figure 5.3 Coupling factor versus distance of coaxial separation between the 1-turn, 5-turn reader coils and the tag, used in estimating read range for Table 5.1 .

In the second case, the resistance of the readers and the tag is increased to 1Ω to account for the effect of resistance due to connectors and solder joints. The read range obtained for the noise limited case is practically unrealizable. The ranges (16-17cm ≈ 6") obtained when $\Delta\theta_{min} = 0.1^{o}$ for this case are more typical of what we observe in laboratory testing. The difference between the 1-turn and 5-turn read range is better observable at larger distances (lower k_{min}) which is can be attributed to its larger slope at distances > 0.1m (Figure 5.3).

Since the relationship between coupling factor and distance for a set of coils depends on their geometries, and because coupling v. distance curves determine read range, we now consider the effect of coil geometry

5.3 COIL GEOMETRY

We consider the case of where the reader and the tag are single layer cylindrical short solenoid coils since they are most commonly used in our application. The size of the tag coil is set by the end user. In our concrete corrosion monitoring application, we limit the sensor (cylindrical) size to a diameter of 3" and a height of ¾ -1" including the packaging. Thus tag coil size most commonly used has a radius (r_2)=3cm, wound using 18AWG enameled magnet wire. The form height is restricted to 1-1.5cm which can accommodate a maximum of 10-15-turns. Consider such a tag with a fixed diameter ($d_2=2r_2$) with a single turn $N_2=1$. Let the reader diameter be $d_1=2r_1$, where r_1 is the radius of the reader and X = distance separating the reader and the tag (Figure 5.4).

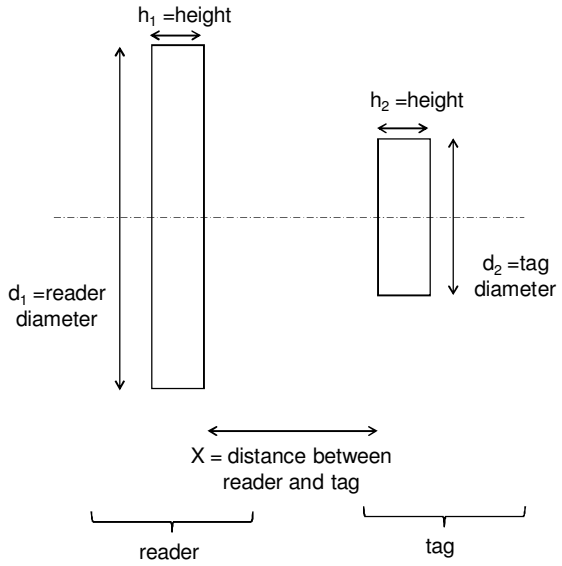

Figure 5.4 Schematic cross-sectional view representing dimensions of the reader, tag coils.

We define, $\alpha = \left(\frac{r_1}{r_2} \right)$ as the ratio of the radius of the reader to the radius of the tag and $\lambda = \left(\frac{X}{r_2} \right)$ as the ratio distance of the separation to the radius of the tag. Consider the Equation 3.10 obtained from the Neumann [23] form for the calculation of mutual inductance of between two coaxial circular loops,

$$M = N_{reader} N_{tag} \mu \sqrt{r_{reader} r_{tag}} \left[\left(\frac{2}{t} - t \right) \mathrm{K}(t) - \frac{2}{t} \mathrm{E}(t) \right] \tag{5.35}$$

where, $t^2 = \frac{4 r_{reader} r_{tag}}{d^2 + \left(r_{reader} + r_{tag} \right)^2}$, K($t$) and E($t$) are complete elliptic integrals of the first and second kind respectively and d is the distance of separation.

Substituting the values of r_1, r_2 and X in the expression for t^2, we have

$$t^2 = \frac{4r_1 r_2}{X^2 + (r_1 + r_2)^2}. \tag{5.36}$$

Substituting the geometry factors α and λ we obtain:

$$t^2 = \frac{4\alpha}{\lambda^2 + (1+\alpha)^2} \tag{5.37}$$

The above equations yield mutual inductance (M) for a tag of given radius r_2 for arbitrary values α and λ. For each of the values of α, the values of self inductance (L_1 and L_2) of the reader and tag are computed using Equation 3.8. Then, coupling factor k is calculated using $k = M / \sqrt{L_1 L_2}$. A surface of k values for a set of single turn reader and tag (N_1=N_2=1) and tag radius r_2 = 3cm is plotted (Figure 5.5) for various values of the geometry factors α and λ.

It is apparent that there exists an optimum radius at which coupling between the reader and tag is maximized. As expected, the value of k peaks when the distance of separation is very small. For λ<<1, the distance of separation approaches zero and coils of unequal radii will become coplanar. The maximum k occurs when $\text{reader}_{\text{radius}}$ is approximately equal to the distance between the reader and tag. To estimate the effect of varying reader and/or tag turns on coupling factor requires plotting as many surfaces as there are combinations of the number of turns. Instead, we plot contours at a fixed value of k for varying α, λ and turns (N_{tag} and N_{reader}), as shown in Figure 5.6.

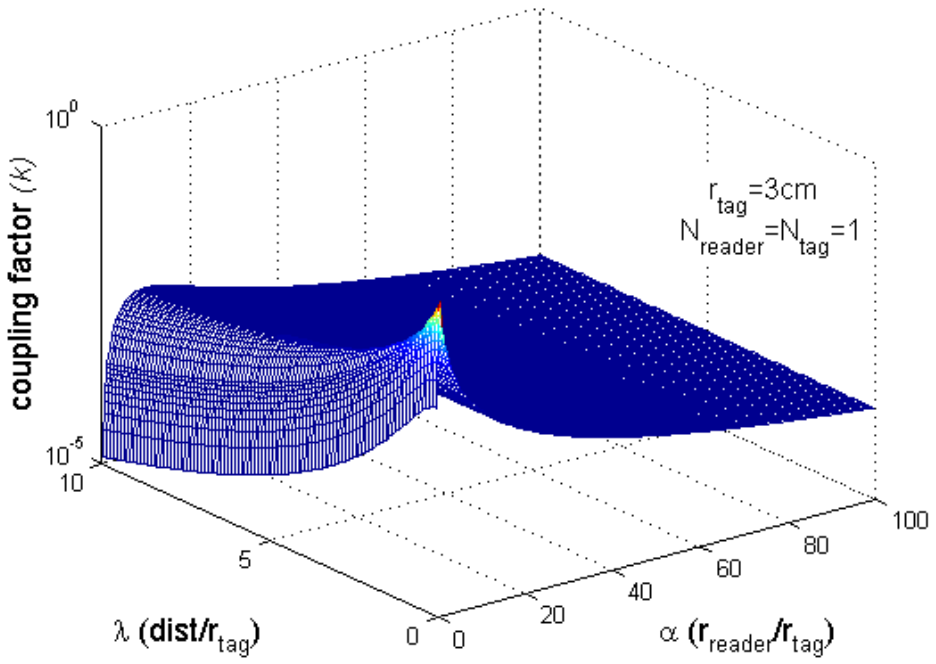

Figure 5.5 Coupling factor (k) for a tag with fixed radius as a function of varying reader radius and distance (range) of coaxial separation suggest that for maximum k occurs at an optimum reader radius = 90 to100% of the range.

Since we are at the detection limit typically at a coupling factor of ≈1%, the contours are generated for k=1% level. The maximum distance at which a set of coils can produce a coupling factor $k=k_{min}$ can be interpreted as its read range. For a single turn tag, and a fixed N_{reader}, as the $radius_{reader}$ ($radius_{reader}=r_1=\alpha r_2$) increases, the read range (distance = λr_2) reaches a maximum. Any further increase in $radius_{reader}$ reduces the flux between the reader and the tag resulting in decreasing read range. This suggests that for a fixed $radius_{tag}$ an optimum $radius_{reader}$ exists and it occurs when $radius_{reader} \approx$ 90-100% of the required read range. Also, in Figure 5.6(top) as N_{reader} increases, the maximum read range increases but the maximum read range occurs at the optimum $radius_{reader}$. The locus of maximum read range (distance, λ) versus $radius_{reader}$ (α) is a straight line with slope 0.9-1.

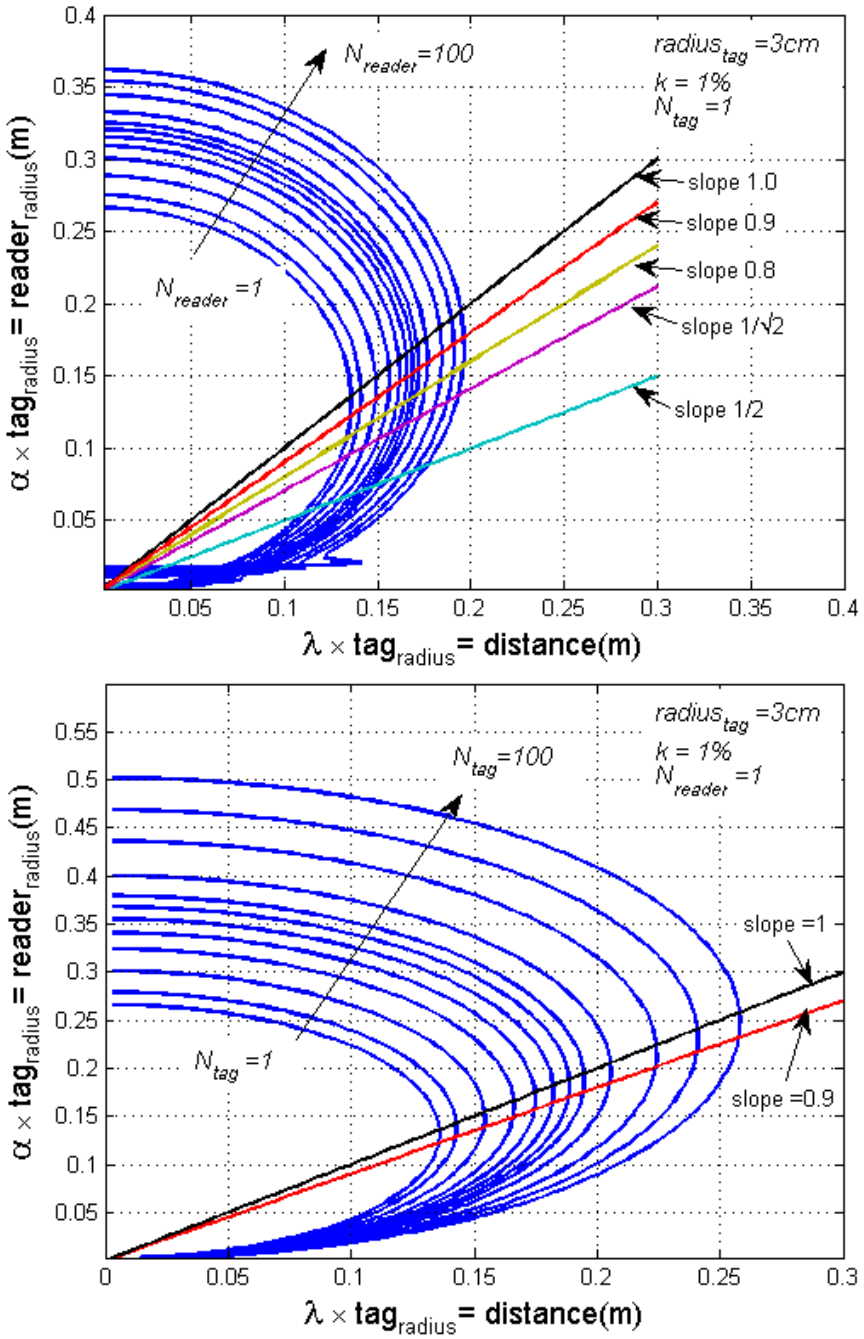

Figure 5.6 Contour plots at coupling factor k=1% as a function of number of turns of the reader (top) and number of turns of the tag (bottom) suggests that coupling factor could be increased by increasing the number of turns.

A similar relationship between $\text{radius}_{\text{reader}}$ and read range is observed in Figure 5.6 (bottom), for a single turn reader when N_{tag} is increased. Increased read range corresponds to an increase in coupling factor. This contradicts the fact that coupling factor is independent of the number of turns (since $k = M/\sqrt{L_{reader}L_{tag}}$, $M \propto N_{reader}N_{tag}$, $L_{reader} \propto N_{reader}^2$ and $L_{tag} \propto N_{tag}^2$ thus k is independent of N). The anomaly can be attributed to the fact that the Neumann form for calculating the mutual inductance of two circular loops is simply scaled by the number of turns. This does not account for the finite height changes of the coil as N increases. Thus M scales truly as N^2. In contrast, the formula for calculating the self inductance uses Nagaoka's short solenoid correction factor which accounts for the finite height of the coil as a result L does not scale as N^2. Figure 5.7 demonstrates the sub N^2 scaling of L_{reader} and L_{tag}. The dotted line corresponds to the ideal square law behavior and is provided for reference.

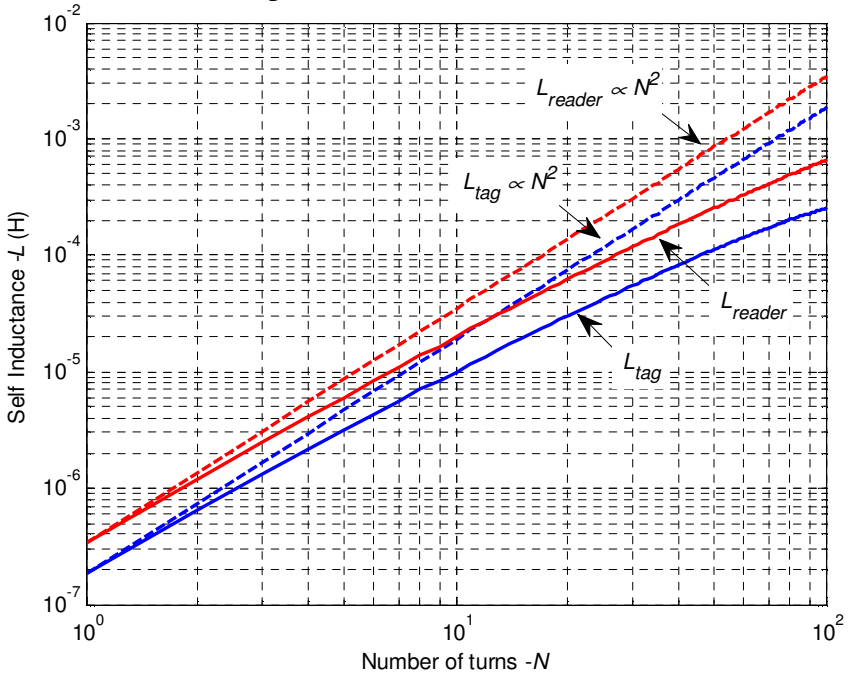

Figure 5.7 Non-ideal scaling of self inductance (L) of the reader and tag coils as a function of the number of turns (N) results from accounting for the effect of finite coil height in their calculation.

This difference in scaling of M and L is responsible for the increase in coupling factor. Since the reader coil has a larger radius, its short-solenoid correction factor does not increase as much as that of the tag. It should be pointed out that the increase in coupling factor is marginal. This is evident from the extremely weak dependence ($\propto N_{reader}^{1/14}$ and $\propto N_{tag}^{1/8}$) of the read range on number of turns. Using an alternate formula [22] to calculate mutual inductance including the effect of the finite coil height, we would expect the apparent increase in coupling factor to diminish even further. Thus, coupling remains largely independent of the number of turns, so increasing the number of turns does not increase read range.

The quality factor (Q) of a given coil depends on its resistance (R), the self inductance (L) and any tuning capacitance (C), which sets the resonant frequency (ω_0). . For a fixed minimum detection limit, increasing the Q_{tag} allows operation at smaller coupling factors $\left(k_{\min} \downarrow\right)$ resulting in larger read range. For a fixed coil shape, the Q is affected by the size of the coil, choice of wire gauge (AWG) the number of turns (N) and the tuning capacitance, if any. If no tuning capacitance is used, the above parameters also determine the self-resonant frequency (SRF) of the coil. The SRF of the reader coil is the highest frequency below which the reader is still inductive, and the tag's SRF sets its maximum possible operating frequency. Consider a single-layer cylindrical solenoid of fixed radius, its Q is determined by AWG, N and coil height. Increasing Q by increasing N is feasible only if the height of the solenoid is not restricted. In most applications the size of the tag has constraints. We now explore the effect of fixed height and radius on the design of our tag coils.

5.4 TAG COIL DESIGN

The tag-coil dimensions are determined by the end users application constraints. The coils used in our ESS application are single-layer cylindrical short solenoids. We limit the tag dimensions such that the radius of the tag coils $r_2 \leq 3$cm and its height $h_2 \leq$ 1.5cm so that the fully packaged sensor is not exceedingly large. In designing the tag coil we select the maximum permissible tag radius i.e r_2 = 3cm. For a fixed height h_2 = h_{2max}=1.5cm, the choice of wire gauge (AWG) determines wire thickness (t_{wire}) and the maximum number of turns N2max, that can be wound. Different combinations of AWG and N_{2max} result in different values of tag self inductance L_{tag} and tag self resistance R_{tag}. Lastly, for a fixed tag coil L_{tag}, its resonant frequency ω_{0tag} is determined the value of the tuning capacitor C_{tag}. We consider four tags of equal radius r_2=3cm and height h_2= 1.5cm wound with four widely spaced wire gauges and with their respective N_2= N_{2max}. These specifications and the calculated (Equation 3.8) value of L_{tag} are provided in Table 5.3.

Tag Label	r_2 (radius) (m)	h_{max} (m)	AWG tag	t_{wire} (m)	N_{2max}	L_{tag} (H)
Tag1	0.03	0.015	1	7.35E-03	2	3.49E-07
Tag2	0.03	0.015	10	2.59E-03	6	3.07E-06
Tag3	0.03	0.015	20	8.12E-04	18	2.83E-05
Tag4	0.03	0.015	30	2.55E-04	59	3.01E-04

Table 5.3 Specifications of the four tags having a constant height wound with four different AWG and number of turns N_2.

The value of C_{tag} can be chosen in three different ways:

1. C_{tag} is fixed ➔ ω_{0tag} or f_{0tag} is variable
2. C_{tag} is variable (tuned)➔ ω_{0tag} or f_{0tag} is constant
3. C_{tag} is the self capacitance of the tag coil ➔ ω_{0tag} or f_{0tag} is the tag's self resonant frequency

A C_{tag} of 470 pF was used for case 1 and the f_{0tag} is set to 4MHz for case 2. Since the short solenoid ratio β = 0.25 >0.05 for all four tags, the self capacitance was calculated using Medhurst's [ref] formula The specific values of C_{tag} and f_{0tag} for all three cases for the four tags is tabulated in Table 5.4

Tag Label	L_{tag} H	Case 1 C_{tag} (F)	Case 2 C_{tag} (F)	Case 3 C_{tag} (F)	Case 1 f_{0tag}(Hz)	Case 2 f_{0tag}(Hz)	Case 3 f_{0tag}(Hz)
Tag1	3.49E-07	4.70E-10	4.54E-09	3.92E-12	1.24E+07	4.00E+06	1.36E+08
Tag2	3.07E-06	4.70E-10	5.16E-10	3.84E-12	4.19E+06	4.00E+06	4.64E+07
Tag3	2.83E-05	4.70E-10	5.59E-11	3.93E-12	1.38E+06	4.00E+06	1.51E+07
Tag4	3.01E-04	4.70E-10	5.26E-12	3.89E-12	4.23E+05	4.00E+06	4.65E+06

Table 5.4 Values of tag capacitance C_{tag} and the corresponding resonant frequency f_{0tag} for the three cases for all four values of L_{tag}.

The intrinsic value of $R_{tag,}$ (i.e. no added R) is frequency dependent and is calculated (Equation 3.11) at the tag's resonant frequency for all tags and all three cases. The quality factor (Q_{tag}) of the tag at its resonant frequency can then be calculated using L_{tag}, R_{tag},*and* ω_{0tag} as $Q_{tag} = \frac{\omega_{0tag} L_{tag}}{R_{tag}}$. The calculated values of R_{tag} and Q_{tag} are tabulated in Table 5.5

Tag	L_{tag}	Case 1	Case 2	Case 3	Case 1	Case 2	Case 3

Label	H	R_{tag} (Ω)	R_{tag}(Ω)	R_{tag}(Ω)	Q_{tag}	Q_{tag}	Q_{tag}
Tag1	3.49E-07	1.50E-02	8.55E-03	4.97E-02	1.81E+03	1.03E+03	6.01E+03
Tag2	3.07E-06	7.51E-02	7.34E-02	2.48E-01	1.08E+03	1.05E+03	3.61E+03
Tag3	2.83E-05	4.37E-01	7.22E-01	1.38E+00	5.62E+02	9.86E+02	1.95E+03
Tag4	3.01E-04	3.94E+00	8.28E+00	8.80E+00	2.03E+02	9.14E+02	1.00E+03

Table 5.5 Values of tag resistance R_{tag} and the quality factor Q_{tag} calculated for the three cases for all four values of L_{tag} at their respective resonant frequency f_{0tag}

The signal strength produced by these tags at various read range (0.03m → 1m) is evaluated as follows. The reader coil is assumed to be a single turn wound with 18AWG wire. The radius of the reader is adjusted so that it equals the range at which the response is being computed. This ensures that the reader radius (r_1) is optimum for that read range. This is equivalent to measuring a given tag with as many reader coils as there are read ranges. The reader coil specifications and the calculated self inductance L_{reader} are shown in Table5.6

range (m)	r_1(radius) (m)	AWG reader	t_{wire} (m)	N_{reader}	L_{reader} (H)
0.03	0.03	18	1.02E-03	1	1.87E-07
0.09	0.09	18	1.02E-03	1	6.85E-07
0.15	0.15	18	1.02E-03	1	1.23E-06
0.2	0.2	18	1.02E-03	1	1.72E-06
0.25	0.25	18	1.02E-03	1	2.20E-06
0.3	0.3	18	1.02E-03	1	2.74E-06
0.4	0.4	18	1.02E-03	1	3.79E-06
0.5	0.5	18	1.02E-03	1	4.88E-06
0.6	0.6	18	1.02E-03	1	5.99E-06
1	1	18	1.02E-03	1	1.06E-05

Table 5.6 Range at which tag response is evaluated and the specifications of the corresponding optimum reader coil radius (r_1=range)

Since the resonant frequency of the tag is the operating frequency, the reader resistance R_{reader} and quality factor of the reader coil Q_{reader} are both calculated at f_{0tag}. Since the reader is single turn, its short solenoid ratio β<<0.05, so Medhurst's[24] formula cannot be used to calculate its self capacitance. However, it is a reasonable approximation that the 1-turn reader has negligible self capacitance, and the self-resonant frequency is primarily affected by the connector and cabling parasitics. Ignoring these parasitic effects, the 1-turn reader can be approximated as being inductive over all frequencies of interest, i.e $\omega_{0reader}$ always $\gg \omega_{0tag}$. Also, given that the reader and tag geometries are completely specified, assuming a coaxial orientation, we calculate the coupling factor k, at all ranges. Once Q_{redaer}, Q_{tag} and k are known, the signal strength $\Delta\theta$ can be calculated using Equation 5.33. Since the calculation is performed at the resonant frequency of the tag, signal strength $\Delta\theta=(\Delta\theta)_{max}$. The variation of $(\Delta\theta)$ as function of range for Tag1 Tag2, Tag3, and Tag4 are plotted for each of the three cases of C_{tag}.

For fixed C_{tag}, since $L_{tag1} < L_{tag2} < L_{tag3} < L_{tag4}$, thus, $\omega_{0tag1} > \omega_{0tag2} > \omega_{0tag3} > \omega_{0tag4}$. Also $R_{tag1} < R_{tag2} < R_{tag3} < R_{tag4}$, so $Q_{tag1} > Q_{tag2} > Q_{tag3} > Q_{tag4}$. The combination of a higher Q_{tag} and higher resonant frequency ω_{0tag} contributes to the higher signal strength (Figure 5.8 (top)).

For the case of constant resonant frequency ω_{0tag}, the ratio $\frac{L_{tag1}}{R_{tag1}} \approx \frac{L_{tag2}}{R_{tag2}} \approx \frac{L_{tag3}}{R_{tag3}} \approx \frac{L_{tag4}}{R_{tag4}}$, so $Q_{tag1} \approx Q_{tag2} \approx Q_{tag3} \approx Q_{tag4}$. All the tags can be considered to be the effectively the same and hence are indistinguishable from one another (Figure 5.8 (bottom)). The decrease in $\omega_{0tag1}, \omega_{0tag2}$ and ω_{0tag3} from previous case causes an overall decrease in the signal strength for Tag1, Tag2, and Tag3. At 1m, $\Delta\theta$ of Tag1 increases from 0.05^o in case1 to 0.02^o in case2. The signal strength for Tag4 increases since ω_{0tag4} is larger than in case1.

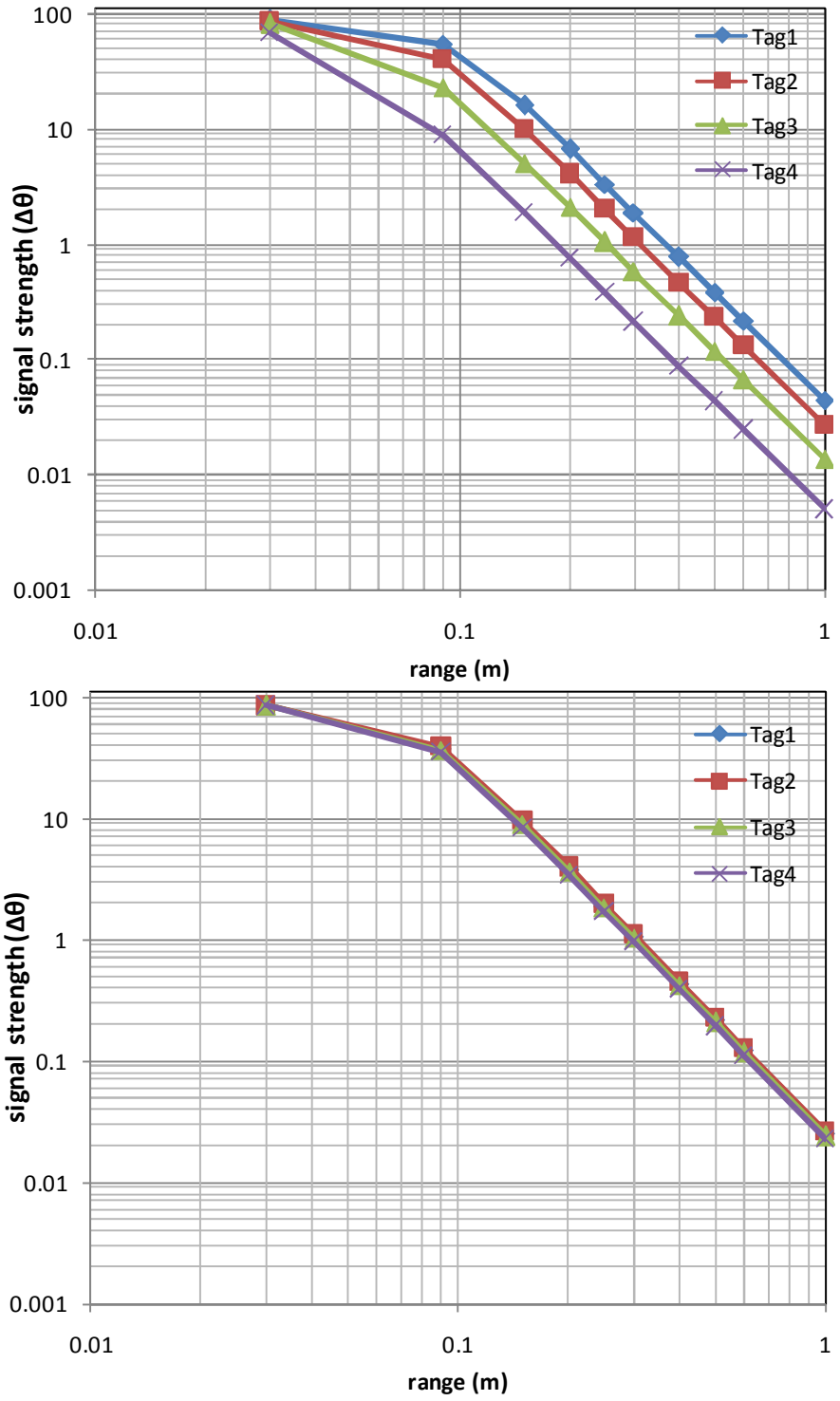

Figure 5.8 Variation of the signal strength as a function of range; (top) case of fixed C_{tag} (bottom) case of fixed ω_{0tag}. Overlapping curves identical Q_{tag}.

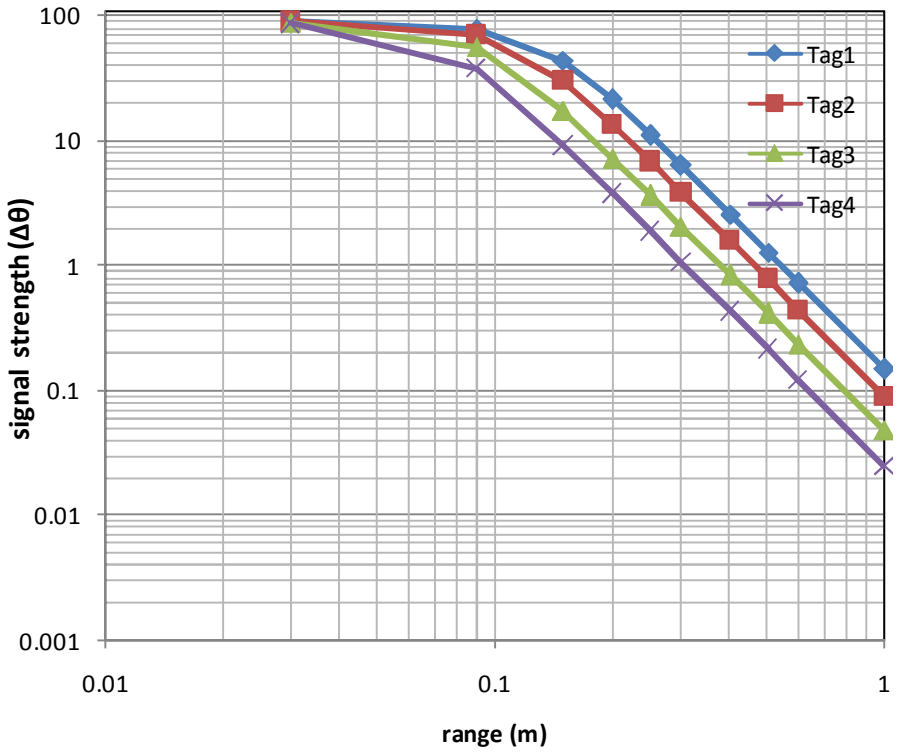

Figure 5.9 Variation of the signal strength as a function of range for the case of self resonant tag.

The highest resonant frequency ω_{0tag} of the tag is its self resonant frequency (SRF). Since Tag1 has the smallest wire gauges and number of turns, SRF Tag1 is the highest. The response (Figure 5.9) of signal strength is similar to the case with the fixed value of C_{tag}, but, since Q_{tag} and ω_{0tag} are comparatively much larger in this case, the values of minimum signal strength are much higher. At 1m Δθ Tag1 (0.05→ 0.15°).

In a manner similar to the 1-turn (1N) reader, the response signal strength versus range for all four tags and three cases of C_{tag} was recalculated using a set 5-turn (5N) reader whose radii are optimum for the range of measurement i.e radius = range. In addition, the effect of finite C_{reader} is also considered. All reader cases including the

previous (1N) case are tabulated for reference in table 5.7. For finite values of C_{reader}, signal strength is calculated using Equation 5.38 as follows:

$$\Delta\theta = \tan^{-1}\left(Q_1 - \frac{1}{Q_C} - \frac{Q_1^2}{Q_C}\right) - \tan^{-1}\left(\frac{Q_1}{(1+k^2Q_1Q_2)}\left(1 - \frac{\left(1+k^2Q_1Q_2\right)^2}{Q_1Q_C} - \frac{Q_1}{Q_C}\right)\right) \quad (5.38)$$

$$\text{Where } Q_1 = \frac{\omega_{0tag}L_{reader}}{R_{reader}},\ Q_2 = \frac{\omega_{0tag}L_{tag}}{R_{tag}},\ Q_C = \frac{1}{\omega_{0tag}C_{reader}R_{reader}},\ \omega_{0tag} = \frac{1}{\sqrt{L_{tag}C_{tag}}}$$

and k is the coupling factor at the range where $\Delta\theta$ is being calculated. Note that for C_{reader}=0, Equation 5.33 and 5.38 are equivalent.

Reader	C_{reader}	$\omega_{0reader}$	baseline	
1N	0	∞	always inductive	
5N	0	∞	always inductive	
1N	0.8 μF	<100 kHz	always capacitive	
5N	0.8 μF	<100 kHz	always capacitive	
5N	C_{self}	$\omega_{0selfreader}$	$\omega_{0tag}<\omega_{0reader}$ inductive	$\omega_{0tag}>\omega_{0reader}$ capacitive

Table 5.7 Range at which tag response is evaluated and the specifications of the corresponding optimum reader coil radius (r_1=range)

Due to the large radii used for the reader coils, the short solenoid ratio β <<0.05 for the reader coils, and thus, Medhurst's formula [24] cannot be used to estimate the self capacitance. At the same time, unlike the 1N readers the, self capacitance of the 5N readers cannot be ignored. The self capacitance of three 5N readers of radii 0.05, 0.11 and 0.15m were experimentally determined. The self capacitance for all other radii is

extrapolated from a linear regression of the measured data. This first-order approximation was sufficient for these analyses.

Tag1 and Tag4 are most widely separated in both their resonant frequencies and quality factors. For the case of fixed C_{tag} = 470pF, ω_{0Tag1} = 12.4MHz, ω_{0Tag4} =423 kHz, $Q_{Tag1} \approx 1800$ and $Q_{Tag4} \approx 200$. We consider the response (Figure 5.10) of signal strength versus range for these two cases when measured using the reader coil combinations specified in Table 5.7

The dotted lines in Figure 5.10 correspond to the cases when the reader's baseline is capacitive (i.e. $\omega_{0tag} > \omega_{0reader}$). The solid lines correspond to the cases when the reader's baseline is inductive (i.e. $\omega_{0tag} > \omega_{0reader}$).The following observations are made:

1. $\Delta\theta$ for 1N and 5N readers are indistinguishable
2. $\Delta\theta$ for inductive baseline always > $\Delta\theta$ for the capacitive baseline
3. For the inductive baseline, $\Delta\theta$ Tag1 > $\Delta\theta$ Tag4 suggests that higher Q_{tag} produces larger signal.
4. For the capacitive baseline, $\Delta\theta$ Tag1 < $\Delta\theta$ Tag4 suggests that higher Q_{tag} produces smaller signal.
5. For the case of the 5N reader with self capacitance (red curve), since $\omega_{0Tag1} > \omega_{0Tag4}$ it crosses into the reader's capacitive baseline resulting in smaller $\Delta\theta$. $\omega_{0reader}$ is always greater than ω_{0Tag4}, so the Tag4 response is exactly like that of the 1N and 5N inductive reader cases(overlapping curves blueΔ marker, green○ marker and pink□ marker).

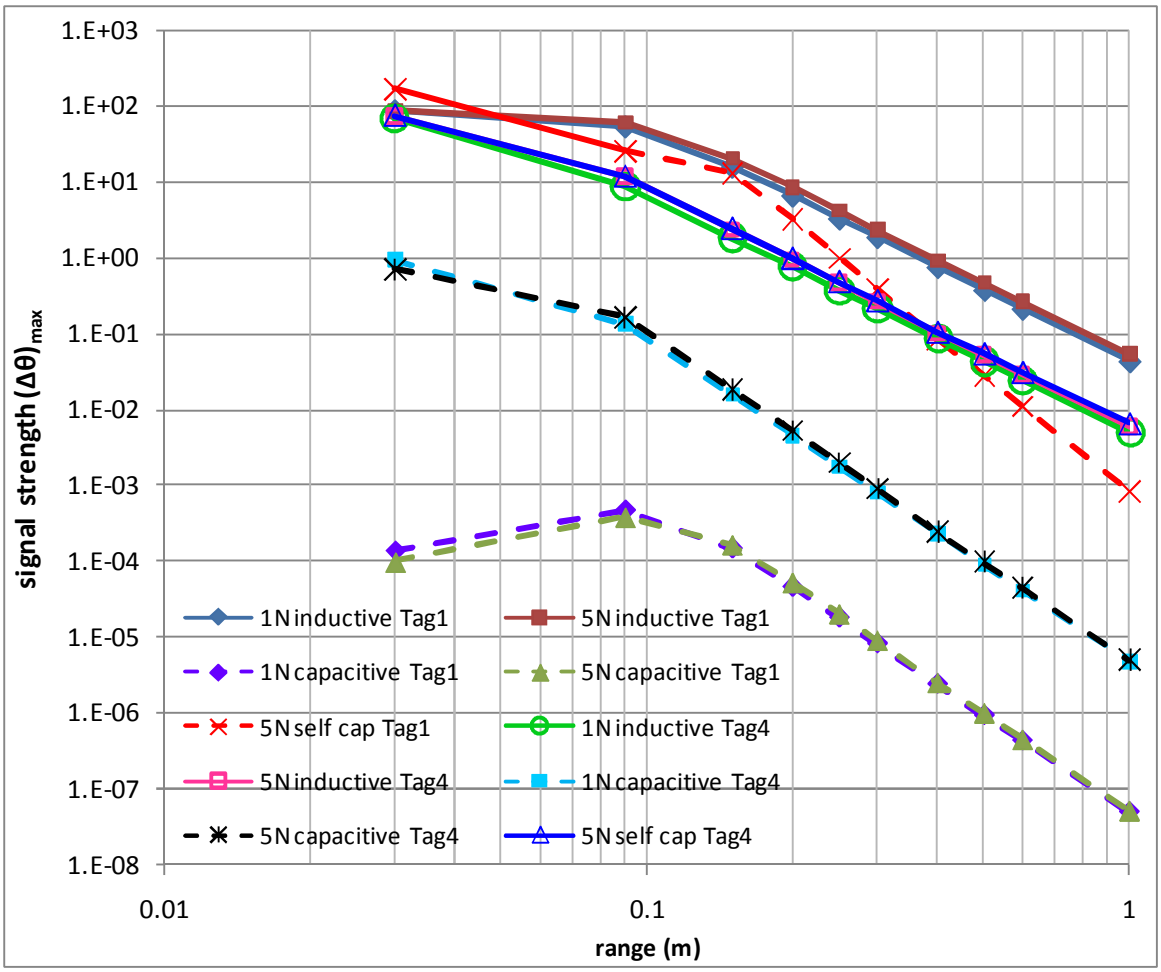

Figure 5.10 Variation of the signal strength as a function of range for Tag1 and Tag4 using a fixed value of C_{tag}= 470pF plotted as measured through the inductive and capacitive baselines of a 1turn (1N) and 5turn (5N) reader.

In the capacitive-baseline, the signal is weak because the reader coil is shorted by the reader capacitance, as discussed earlier in Chapter 3 section 3.3.1. Since the capacitive reactance is inversely proportional to frequency, once in the reader's capacitive baseline, the higher the resonant frequency of the tag, the smaller is the value of the shunt reactance across the reader. This effect explains the lower signal for Tag1 compared to Tag4 in the capacitive-baseline case despite Tag1's larger quality factor Q.

In addition to the tuning capacitance, since both the radius and the height of the tag coil are fixed, changing the turns (N) and wire gauge (AWG) modifies the tag coil's quality factor and operating frequency (ω_{0tag}). For a constant height coil, if N is doubled, the thickness of wire (t_{wire}) must be halved so that the product of N and t_{wire} is unchanged. In the low-frequency or d.c. current distribution limit, the resistance of the tag is dominated by the d.c resistance of the wire. Our tags operate at higher frequencies i.e.in the limit where the resistance is dominated by the skin effect, the tag resistance is given by

$$R_{tag}(\omega) = \sqrt{\frac{\omega\mu_o\rho}{2}}\frac{l_{wire}}{\pi t_{wire}}, \tag{5.39}$$

where μ_o is the permeability of air (H/m), ρ is the resistivity(Ω-m) of the metal wire used to wind the coil and ω is the frequency(rad/s), t_{wire} and l_{wire} are the thickness and length of wire used in winding the tag coil. The self inductance of the tag is given by

$$L_{tag} = \pi\frac{\mu_o}{2}r_{tag\_coil}\frac{N_{tag}^2}{\beta}K_N(\beta), \tag{5.40}$$

where N_{tag} is the number of turns of the tag coil, $\beta = h_{tag\_coil}/2r_{tag\_coil}$ is the short solenoid ratio, r_{tag_coil} and h_{tag_coil} are radius and the height of the coil in meters, and $K_N(\beta) = K_N\left(\frac{h_{coil}}{2r_{coil}}\right)$ is the Nagaoka correction factor. The quality factor (Q_{0tag}) of the tag at resonance when the tag operating in the high frequency limit can be expressed as:

$$Q_{0tag} = \frac{\omega_{0tag}L_{tag}}{R_{tag}(\omega_{0tag})} = \underbrace{\pi\sqrt{\frac{\mu_o}{2\rho}}r_{tag\_coil}K_N\left(\frac{h_{tag\_coil}}{2r_{tag\_coil}}\right)}_{G(h_{tag\_coil},r_{tag\_coil})}\sqrt{\omega_{0tag}}. \tag{5.41}$$

In the above equation since the radius and the height of the tag coil are fixed, $G(h_{tag\_coil}, r_{tag\_coil})$, is a constant, which implies that that for a fixed operating frequency (ω_{0tag}), the quality factor Q_{0tag} is independent of the number of turns.

The observations from Figure 5.10 suggest the use of a 1-turn reader, as it would provide the largest range of frequencies at which the tag can operate in the inductive baseline. From Equation 5.33 recall that signal strength $\Delta\theta$ for an inductive baseline is

$$\Delta\theta = \tan^{-1}\left(\frac{k^2 Q_1^2 Q_2}{1 + k^2 Q_1 Q_2 + Q_1^2}\right), \tag{5.42}$$

where, $Q_1 = \frac{\omega_{0tag} L_{reader}}{R_{reader}}$, $Q_2 = \frac{\omega_{0tag} L_{tag}}{R_{tag}}$, and $\omega_{0tag} = \frac{1}{\sqrt{L_{tag} C_{tag}}}$.

Since $k^2 Q_1 Q_2 \ll Q_1^2$ and $Q_1^2 \gg 1$, $\left(1 + k^2 Q_1 Q_2 + Q_1^2\right) \approx Q_1^2$. Hence,

$$\Delta\theta = \tan^{-1}\left(k^2 Q_2\right). \tag{5.43}$$

Substituting the above expressions for Q_2, we have

$$\Delta\theta = \tan^{-1}\left(\underbrace{\pi\sqrt{\frac{\mu_o}{2\rho}} r_{tag\_coil} K_N\left(\frac{h_{tag\_coil}}{2r_{tag\_coil}}\right)}_{G(h_{tag\_coil}, r_{tag\_coil})} k^2 \sqrt{\omega_{0tag}}\right). \tag{5.44}$$

Therefore, for a fixed volume and aspect ratio, signal strength can only be increased by increasing either the coupling factor (k) or the operating frequency (ω_{0tag}).

Chapter 6: Conclusions

6.1 MOTIVATION OF WORK

The objective of this research was to explore the interaction between the design and detection limits of the Electronic Structural Surveillance (ESS) system.

The ESS platform, developed at the University of Texas at Austin addresses the need for cost-effective, passive, battery-free, wireless sensors aimed at nondestructive Structural Health Monitoring (SHM) of reinforced concrete structures. The sensors (ESS tags) are passive resonant circuits and operate using inductive coupling between an embedded sensor, and an external reader. The inductively coupled reader coil is used to measure impedance response from which information pertaining to the state of the sensor is extracted.

ESS sensors targeting corrosion of steel reinforcement in concrete, have been developed in prior research. Estimating the changes in the tag from the inductively coupled impedance response is difficult. Specifically extending the range (distance) at which one can obtain a measureable signal in inductively coupled system poses a great challenge

The ability to detect the response of the tags is influenced the method of interrogation, the instrumentation used and the design of the reader and tag coils. The motivation for this work is to explore the interaction between design and detection limits of the ESS system in order to improve the performance of the ESS based sensors. To this end, the influence of finite noise and reader and tag coil on system performance is also explored and design rules for extending read range are developed.

6.2 SUMMARY OF WORK

6.2.1 Signal Strength and Detection Limit

Signal strength $\Delta\theta$ is a measure of the perturbation caused in the baseline phase response of the reader due to the presence of the tag. It is measured as the difference in the phase response when tag is absent and when the tag is present. $\Delta\theta = \theta_Z\big|_{tag\ absent} - \theta_Z\big|_{tag\ present}$.

The resonant frequency of the reader ($\omega_{0reader}$) relative to that of the tag (ω_{0tag}) determines the phase angle of the operating baseline. The three cases considered were:

1. Inductive Baseline: $+90^o$ → occurs when the $\omega_{0reader} > \omega_{0tag}$ –reader is inductive.
2. Capacitive Baseline: -90^o → occurs when the $\omega_{0reader} < \omega_{0tag}$ –reader is capacitive.
3. Resonant Baseline: 0^o → occurs when the $\omega_{0reader} = \omega_{source}$ –reader is tuned to be resonant at the source frequency.

The operating baseline response influences the ability to measure signal strength. Of the three baselines, the capacitive baseline provides the weakest signal since the inductively coupled reader is shunted by the low impedance of the reader capacitance (usually parasitic self capacitance). The resonant baseline provides the strongest signal since the reader behaves like a balanced bridge circuit. Hence, any perturbations due to the tag cause a large change in the measured phase response. In the inductive baseline, the measured phase response is dominated by the reader coil (inductor). Since the tag is coupled to this inductor, changes in the tag produce a measureable signal although it is not as strong as in the resonant baseline case. Although operating at the resonant baseline would provide the largest signal, this signal both the depth and width of resonance are

strong functions of coupling factor. So while this baseline is best suited for the purposes of detecting the presence or absence of the tag i.e. threshold measurements, it is unsuitable for measuring any analog sensors.

In addition to the difference in signal strength produced by operating at different baselines, the ability to measure signal (i.e. resolve small differences in phase) is influenced by the presence of finite noise. Since the ESS reader and tag form a passive network, the dominant noise considered was thermal noise. This noise causes uncertainty in the measurement of the phase response which in turn limits the resolution of $\Delta\theta$ that can be measured. The noise expressed in phase (degrees) produced by our typical ESS system is $\approx 10^{-8}$ for the inductive baseline, $\approx 10^{-11}$ for the capacitive baseline and $\approx 10^{-5}$ for the resonant baseline. These values are well below the detection limit of currently available instruments (HP4194A 0.01^{o}). Thus we are unlikely to be limited by the noise of the ESS system.

6.2.2 Circuit Design Considerations

The signal strength $\Delta\theta$ is a strong function of coupling factor, which, for coaxial coils, translates to a strong function of distance. The larger the $\Delta\theta$ the larger the potential range of the ESS system.

The components used in the design of the reader and the tag influence the signal strength. Analysis of the circuit of the tag and reader suggest the following design recommendations for larger signal strength.

- Increase the quality factor of the tag Q_{tag} .
- Increase the resonant frequency of the tag ω_{0tag}

  even at the expense of Q.
- Decrease the value of tag resistance R_{tag}.
- Decrease C_{tag} and L_{tag} corresponds to increase in ω_{0tag} .
- Increase quality factor of the reader Q_{reader} such that

$$Q_{reader}\big|_{\omega_{0tag}} > 1 \Rightarrow \frac{R_{reader}}{L_{reader}} < \frac{1}{\sqrt{L_{tag}C_{tag}}} < \frac{1}{\sqrt{L_{reader}C_{reader}}}$$

6.2.3 Geometry Design Considerations

The reader and tag coils are designed using physical parameters such as radius (r_{coil}) , height (h_{coil}), wire gauge (AWG) and number of turns (N). Thus, in addition to knowing what circuit/component values to target, it is important to evaluate the influence of coil geometry. Thus, various combinations of single layer cylindrical solenoids, used in our structural health monitoring application, were analyzed.

For such single layer cylindrical solenoids, it was fund that coupling factor k is maximized when the radius of the reader coil equals the distance (range) of coaxial separation between the reader and the tag coils.

Further the application constrains the size of the tag. For a given set of tag constraints i.e. maximum allowable height and radius, we should wind tags with the largest possible radius and use all the allotted height. Fixing the tag coil at this radius Since the height of the coil is fixed, the product of number of turns and wire thickness should be a constant. It is observed that that for such fixed radius and height constrained coils; the quality factor is independent of turns. It is also observed that coupling factor k, between the reader and the tags is largely independent of the number of turns (N). Thus

from Equation 5.44 , assuming that a size constrained tag coil is being interrogated by its optimum reader at a fixed coaxial separation, the only way to increase the signal strength is by increasing the operating frequency (ω_{0tag}).It is also observed that any increase in signal strength or range require increasing the coupling factor *k* and/or quality factor *Q* both of which cannot be effected without increasing the coil size.

Given that *k* is largely independent of number of turns, and the inductive baseline is the "preferred" baseline (works for both analog and threshold) for the measurement of the tag; a 1-turn reader should be used, as it would provide the largest range of frequencies at which the tag can operate in the inductive baseline.

Using the above the design rules developed in this work provide a clear and complete method to design efficient ESS systems. The expressions for minimum detectable limit Equations 5.33 and 5.38 involve dimensionless quantities if quality factors (*Q*) and coupling factor (*k*). If the equations to calculate circuit values are known, this method of analysis can be extended to many other shapes and sizes. The designer also has the flexibility to approach the ESS design problem at the circuit level or coil geometry level. Optimized coil design together with improved interrogation techniques can improve the read range and provide more information from the ESS sensor enabling their use as new sensors.

References

[1.] Pasupathy, P., D.P. Neikirk, and S.L. Wood. *Improved reading techniques for electronic structural surveillance tags*. in *Sensors and Smart Structures Technologies for Civil, Mechanical, and Aerospace Systems 2008*. 2008. San Diego, California, USA: SPIE.

[2.] Koch, G.H., et al., *Corrosion Cost and Preventive Strategies in the United States*, in *Office of Infrastructure Research and Development: Federal Highway Administration*, O.o.I.R.a.D.F.H. Administration, Editor. 2001.

[3.] Mietz, J. and B. Isecke, *Monitoring of concrete structures with respect to rebar corrosion.* Construction and Building Materials, 1996. **10**(5): p. 367-373.

[4.] Cady, P.D., *Corrosion of Reinforcing Steel in Concrete- A General Overview of the Problem*, in *Chloride Corrosion of Steel in Concrete Symposium*. 1977, American Society for Testing and Materials: Chicage, Illinois. p. 3-11.

[5.] Lee, S., K. P.D., and Y.P. Virmani, *Resisting Corrosion.* Public Roads, 2005. **68**(6).

[6.] Grizzle, K.M., *Development of a Wireless Sensor Used to Monitor Corrosion in Reinforced Concrete Structures*, in *Dept. of Civil Engineering*. 2003, University of Texas: Austin.

[7.] Grizzle, K.M., et al. *Wireless sensors for monitoring corrosion in reinforced concrete members,*. in *Smart Structures and Materials 2004 - Smart Systems and Nondestructive Evaluation for Civil Infrastructures*. 2004.

[8.] Novak, L.J., et al. *Development of state sensors for civil engineering structures*. in *Smart Structures and Materials 2003: Smart Systems and Nondestructive Evaluation for Civil Infrastructures*. 2003. San Diego, CA, USA: SPIE.

[9.] Andringa, M., *Development of a Passive Wireless Analog Resistance Sensor*, in *Dept. of Electrical and Computer Engineering*. 2003, University of Texas: Austin.

[10.] Andringa, M.M., *Unpowered Wireless Sensors for Structural Health Monitoring*, in *Dept. of Electrical and Computer Engineering*. 2006, University of Texas: Austin.

[11.] Andringa, M.M., et al. *In situ measurement of conductivity and temperature during concrete curing using passive wireless sensors*. in *Sensors and Smart Structures Technologies for Civil, Mechanical, and Aerospace Systems 2007*. 2007. San Diego, California, USA: SPIE.

[12.] Dickerson, N.P., et al. *Wireless threshold sensors for detecting corrosion in reinforced concrete structures*. 2006: SPIE.

[13.] Dickerson, N.P., et al. *Wireless low-cost corrosion sensors for reinforced concrete structures*. in *Smart Structures and Materials 2005: Sensors and Smart Structures Technologies for Civil, Mechanical, and Aerospace Systems*. 2005. San Diego, CA, USA: SPIE.

[14.] Nainani, P.R., *Optimization of Passive Wireless Concrete Corrosion Sensors Using the Genetic Algorithm*, in *Dept. of Electrical and Computer Engineering*. 2004, University of Texas: Austin.

[15.] Pasupathy, P., *Extraction of sensor state and range from electronic structural surveillance tags using an interrogation circuit model*, in *Dept. of Electrical and Computer Engineering*. 2008, University of Texas: Austin.

[16.] Simonen, J.T., et al. *Wireless sensors for monitoring corrosion in reinforced concrete members*. in *Smart Structures and Materials 2004: Sensors and Smart Structures Technologies for Civil, Mechanical, and Aerospace Systems*. 2004. San Diego, CA, USA: SPIE.

[17.] Terman, F.E., *Radio Engineering*. Third ed. 1947, New York: McGraw-Hill Book Company, Inc.

[18.] Park, Y.S., P. Pasupathy, and D.P. Neikirk. *Resonant chemical surveillance tags*. in *Electro-Optical Remote Sensing, Detection, and Photonic Technologies and Their Applications*. 2007. Florence, Italy: SPIE.

[19.] Kim, J.W., et al. *Measurement of liquid complex dielectric constants using non-contact sensors*. in *Sensors, 2009 IEEE*. 2009.

[20.] Pasupathy, P., et al. *Unpowered resonant wireless sensor nets for structural health monitoring*. in *Sensors, 2008 IEEE*. 2008.

[21.] Pasupathy, P., et al. *Versatile wireless sacrificial transducers for electronic structural surveillance sensors*. in *Sensors, 2009 IEEE*. 2009.

[22.] Grover, F., *Inductance Calculations: Working Formulas and Tables*. 1946, New York: D. Van Nostrand Company, Inc.

[23.] Ramo, S., J.R. Whinnery, and T. VanDuzer, *Fields and Waves in Communication Electronics*. 1965, New York: New York: John Wiley & Sons.

[24.] Medhurst, R.G., *H. F. Resistance and Self-Capacitance of Single-Layer Solenoids.* Wireless Engineer,, 1947(March).

[25.] Woo, A.Y. and A.C. Cangellaris, *Passive rational fitting of a network transfer function from its real part.* International Journal of RF and Microwave Computer-Aided Engineering, 2008. **18**(3): p. 209-218.

[26.] Miller, S.L. and D. Childers, *Probability and Random Processes: With Applications to Signal Processing and Communications*. 2nd ed. 2004, Burlington, MA: Academic Pres.

Vita

Praveenkumar Pasupathy was born in 1979 in Vellore, India, to Coimbatore S. Pasupathy and Geetha Pasupathy. He completed his higher secondary education graduating in May 1996. He completed his undergraduate engineering program at Vivekanand Education Society's Institute of Technology (Mumbai University). He graduated with his Bachelor of Engineering (Instrumentation) in the First Class in August of 2000. He worked at Endress+Houser India Branch Office (September 2000 to February 20001) and at BitMapper Integration Technologies Pvt. Ltd (March to July of 2001). He attended the graduate school at The University of Texas at Austin, between fall of 2001 and 2003. He joined Dr Dean P. Neikirk's research group at the Microelectronics Research Center in fall of 2002. After a leave of absence, he returned to graduate school in fall of 2004 to complete his Master of Science in Engineering and pursue his Doctor of Philosophy.

Permanent address : B/6 Banganga Cooperative Housing Society,
Govandi Station Road, Deonar, Mumbai-400088
Maharashtra, India.

This dissertation was typed by the author.